The immune system and inflammation in cardiac dysautonomia during hypertension

Thesis submitted for the degree of

Doctor of Philosophy

in

Cardiovascular Science

Oliver C. Neely

Magdalen College,

University of Oxford

Michaelmas Term 2021

Table of Contents

Acknowledgements

Phase 2 of 3 of my time in Oxford complete. Just the three years left to go of this marathon…

It has been said that undertaking a PhD/DPhil is similar to a neuronal action potential: a sharp depolarising impulse where everything seems to boom exponentially, followed by a just-as-sharp repolarising fall, until one feels they are below where they started. The job of the student's support network, is to take on the role of the sodium-potassium pump, restoring them to their baseline resting membrane potential. After four years following this little detour through the wilderness, off of the road between pre-clinical and clinical medical school, I find this phenomenon, described by Paterson (c.2017), to be highly accurate. I therefore wish to express my overwhelming gratitude to the wonderful people who guided me through the tough times, enjoyed with me the good times, and most importantly made wonderfully effective Na^+/K^+ ATPases.

First of all, thank you to the British Heart Foundation, for their enormously generous funding, which allowed me to undertake this DPhil. I hope the work I have carried out, along with the scientific training this has provided me, will contribute to their thankless task of ending heart disease.

To my supervisors Prof. David Paterson (cited above), and Prof. Ana Domingos for your mentorship, ideas and stability, all the while giving me enough independence to grow as a scientist.

To Dr Dan Li and Dr Chelsea Larabee, for their thorough technical teaching and unending patience.

To (now Dr) Harvey Davis, for your ever-reliable scientific advice, critical eye, and enjoyment of evenings discussing science and all else over beer at the Bear.

To Drs Tom, Perry and Niki for being excellent role models and really fun company throughout.

To all those I have taught, supervised or mentored over the course of this DPhil, for helping me become a better teacher, and asking interesting questions which made me consider something physiological in a different way.

To all the support staff in all departments in which I have worked, at DPAG, the William Dunn School of Pathology, and the Department of Biochemistry, you help keep all of us students on track.

To the team at the Oxford Biobank: Prof. Fredrick Karpe and Dr Matthew Neville for running the programme, and the highly efficient research nurse team of Jane Cheeseman (enjoy your well-deserved retirement) and Diane Mantripp for their supply of blood samples, and saint-like patience.

To my Transfer and Confirmation of Status examiners: Prof. Keith Channon and Prof. Pawel Swietach, thank you for your critical input during the course of my DPhil. To my final thesis examiners: Prof. Paul Leeson and Prof. Andre Ng, thank you for taking your time to read this thesis, exam my viva and suggest corrections.

To my family: my parents, parents Claire and Chris, my sister Imy, Granny & Tom, Grandma, Graham & Elaine thank you all so much for your endless support. Mum and Dad, thank you for being amazing parents, for your wonderful hotel service, and your ever-presence at the end of the phone to provide an ear. As a nurse and paramedic, I promise I'm finally getting on to clinical work now! Imy, thanks for a lot of shared laughs

every time we're home, and your ability to challenge me at any sport we pick, however little you've played!

To my friends. To George, Alex, Josh and James, for evenings spent chatting and laughing about nothing important, for playing with the felt, and messing about punting. To Matt, Jagir, Michael and Hari, for now 14 years of solid friendship! To Kiran and Charlie, for many hilarious afternoons spent trying to plot our way round a golf course. And to Peter, for encouraging me to run silly distances in the hills of Oxfordshire, and tolerating my antics during Lockdown III.

And finally to Freya - for being so lovely, caring, and supportive of everything I do. We always have the best time whenever we get to see each other, but you're also always there for me when we can't. You've made this inherently tough process so much easier. I promise we'll live in the same city at some point!

This thesis is also dedicated to the memory of our family dog Jude – the most lovely, beautiful and quirky black Labrador anyone could ever meet. His excitement was always the nicest welcome whenever I came home. We sadly lost him in June 2021, just as I was writing this thesis.

Publications

The following publications were produced during the course of this DPhil study:

Oliver C. Neely, Ana I. Domingos, David J. Paterson (2022) **Macrophages can drive sympathetic excitability in the early stages of hypertension. *Frontiers in Cardiovascular Medicine*, 8, 807904.

Emma N. Bardsley, Oliver C. Neely, David J. Paterson (2020) **Angiotensin peptide synthesis and cyclic nucleotide modulation in sympathetic stellate ganglia.** *Journal of Molecular and Cellular Cardiology,* 138, 234-243.

Chelsea M. Larabee, Oliver C. Neely, Ana I. Domingos (2020) **Obesity: a neuroimmunometabolic perspective. *Nature Reviews Endocrinology,* 16 (1), 30–43.

Gaia Calamera, Dan Li, Andrea Hembre Ulsund, Jeong Joo Kim, Oliver C. Neely, Lise Román Moltzau, Marianne Bjørnerem, David Paterson, Choel Kim, Finn Olav Levy, Kjetil Wessel Andressen (2019) **FRET-based cyclic GMP biosensors measure low cGMP concentrations in cardiomyocytes and neurons.** *Communications Biology,* 2, 394.

Kun Liu, Dan Li, Guoliang Hao, David McCaffary, Oliver Neely, Lavinia Woodward, Demetris Ioannides, Chieh-Ju Lu, Marcella Brescia, Manuela Zaccolo, Harikrishna Tandri, Olujimi A. Ajijola, Jeffrey L. Ardell, Kalyanam Shivkumar, and David J. Paterson (2018) **Phosphodiesterase 2A as a therapeutic target to restore cardiac neurotransmission during sympathetic hyperactivity**. *JCI Insight,* 3(9) pii: 98694.

** = directly associated with this thesis

Funding

This DPhil was funded by a 4-year British Heart Foundation Studentship awarded to me following application to the programme. After one year of laboratory rotations, I wrote a research proposal for the next 3 years of study, which was approved by the BHF.

Statement of Originality

The work presented in this thesis is entirely my own. Where necessary I received advice and teaching from peers, mentors and supervisors, as detailed here.

The hypotheses underlying this work were generated by myself, after reading the literature, and discussions with my supervisors Prof. David J. Paterson and Prof. Ana I. Domingos to hear their suggestions. I also discussed my ideas with my senior DPhil colleague Dr Harvey Davis, and my Transfer of Status and Confirmation of Status examiners Prof. Keith Channon and Prof. Pawel Swietach.

I received teaching with regard to carrying out specific laboratory techniques, but generated all data included in this thesis myself. Dr Dan Li taught me the principles of neuronal cell culture and real-time imaging. Dr Harvey Davis further helped me learn how to perform neuronal calcium imaging, as well as qPCR experiments. Dr Chelsea Larabee provided me training in flow cytometry and immunohistochemical staining, and the technique of cardiac perfusion. Michal Maj and Robert Hedley further trained me in flow cytometry and FACS. Dr Gareth Purvis taught me to culture bone marrow-derived macrophages. Finally, Dr Noelia Martínez-Sánchez showed me how to dissect superior cervical ganglia, and perform cardiac puncture. Other techniques such as coeliac ganglion dissection, leukocyte isolation, and co-culture, were self-taught with reference to available published material on these.

Abstract

Essential hypertension, along with a number of other cardiovascular diseases, is characterised by a state of hyperactivity of the sympathetic nervous system. This pathological phenomenon may contribute to the aetiology of hypertension itself, and causes end-organ damage. Elucidating the underlying cause of this dysautonomic phenotype could therefore provide a more effective means of therapeutic intervention to improve outcomes. Essential hypertension also features a state of low-grade systemic inflammation, which is hypothesised to drive peripheral sympathetic hyperactivity. This thesis examined this potential link in the Spontaneously Hypertensive Rat (SHR). The resident immune cells of the sympathetic ganglia, blood and kidneys of the SHR were first, examined using flow cytometry, and compared to those of the Wistar rat. The main finding was a systemic reduction in the classical-to-non classical monocyte-macrophage ratio. However, preliminary data suggest this is not replicated in blood samples taken from a small number of essential hypertension patients and matched controls, which may reflect low statistical power. Using qPCR analysis, no differences were found in the expression levels of a range of inflammatory or anti-inflammatory cytokines, macrophage polarisation markers or oxidative stress markers between SHR and Wistar stellate ganglia, except for a significantly higher expression of the chemokine *ccl2* in the SHR. Blood monocytes and bone-marrow derived macrophages (BMDMs) also did not show any inter-strain differences with regard to cytokines or polarisation markers. SHR stellate neurons were shown to exhibit greater $[Ca^{2+}]_i$ transients than those of Wistar rats in response to either nicotinic stimulation or high $[K^+]_o$-evoked depolarisation. When co-cultured with blood leukocytes, Wistar stellate neurons showed increased responsiveness to these stimuli, while SHR neurons did not. Interestingly, Wistar neuron $[Ca^{2+}]_i$

transients were enhanced by the presence of BMDMs, those from the SHR only increased in responsiveness with their own, and not Wistar, BMDMs. This BMDM-induced enhancement of Wistar neuron $[Ca^{2+}]_i$ transients were not affected by combined blockade of IL-1β, TNF-α, and IL-6, nor did IL-1β or TNF-α affect stellate neurons in mono-culture, suggesting these classical inflammatory cytokines are not involved in this effect. The results of this thesis suggest that SHR macrophages may play a role in driving stellate neuron hyperactivity in this model. Further elucidation of the role of this immune-neuronal axis may help uncover new pathophysiological nodes for effective therapeutic intervention in essential hypertension and other dysautonomic conditions.

CHAPTER I

Introduction

I.1 Hypertension and sympathetic dysautonomia: the clinical situation

The world faces a deadly and insidious pandemic. Hypertension, often defined as an arterial blood pressure ≥140/90 mmHg over a number of weeks, afflicts ~22% of the adult population worldwide (World Health Organization, 2014), and its complications are estimated as having led to 9.4 million deaths in 2010 (Lim et al., 2012), as the latest available yearly estimate. Most dangerously, this condition is usually asymptomatic until it produces its potentially lethal clinical sequelae, which include: heart disease, stroke, and other end organ damage. A recent study claimed that although diagnosis of hypertension has improved, as many as 20-60% of hypertensive individuals are unaware of this; a situation which is worse in lower income countries (Zhou et al., 2019; Geldsetzer et al., 2019).

Medicine is currently falling short in its fight against this disease; ~10% diagnoses may be termed "true resistant hypertension" in which blood pressure remains above target despite concurrent use of ≥3 anti-hypertensive medications of different classes, and do not fit the exclusion criteria of white coat hypertension[1] or non-adherence (Noubiap et al., 2019). In total at least 30% of treated hypertensive patients do not have adequate blood pressure control, suggesting that ~20% of patients exhibit either of the above exclusion criteria (Zhou et al., 2019; Geldsetzer et al., 2019). This group may still reflect some therapeutic inadequacy though. While patients with white coat hypertension do not actually have a higher risk of cardiovascular events or mortality (Cohen et al., 2019), poor compliance needs to be improved. Mutual planning and open discussion between physicians and patients will be necessary in order to achieve this (Hameed & Dasgupta,

[1] White coat hypertension is defined as an office-measured blood pressure in the hypertensive range on at least three occasions, while 24 hour ambulatory blood pressure is ≤135/85 mmHg (Mancia et al., 2007).

2019), but as side effects are a key contributor to non-adherence (Burnier & Egan, 2019), new therapeutics with different mechanisms of action may be of benefit here.

I.1.1 Sympathetic Dysautonomia

As will be later discussed, essential hypertension is a complex multi-factorial disease involving a number of systems, including the vasculature, kidneys and the sympathetic nervous system. Not only might sympathetic nervous system hyperactivity be causative of blood pressure elevation, it certainly contributes to a range of associated end-organ pathologies. Moreover, heightened sympathetic tone is present in a number of other cardiovascular diseases, including heart failure (Floras, 2009), post-MI (Graham et al., 2002; Moreira et al., 2017), and electrical storm (Tian et al., 2019). For this reason, study of hypertensive dysautonomia can serve as a potential model for the phenomenon in these conditions, and help improve treatments for this whole group of cardiovascular pathologies.

I.2 Physiological Control of Blood Pressure

The term *blood pressure* typically refers to that of the systemic arterial circulation, and it is measured as a pair of values: the pressure while the left ventricle is in systole (systolic), and that while it is in diastole (diastolic). The normal range for humans (in the form systolic/diastolic) is 90/60 to 120/80 mmHg. Mean arterial blood pressure (MAP) is directly dependent on two main variables: the volume of blood extruded by the left ventricle: cardiac output (CO), and the resistance of the arterial vessels, termed total peripheral resistance (TPR). This can be summarised in an equation, shown below, with central venous pressure (CVP) also incorporated, as it is the pressure difference between MAP and CVP which drives blood flow:

Equation 1: $MAP = CO \times TPR + CVP$

Changes in MAP can therefore be brought about by changing any of the variables on the right-hand side of this equation, although CVP is usually <6 mmHg and has very little direct influence on MAP. Examining the factors determining in turn controlling CO and SVR however, yields the following equations:

$$\underline{\text{Equation 2:}}\ CO = Heart\ rate\ (HR) \times Stroke\ Volume\ (SV)$$

$$\underline{\text{Equation 3:}}\ SVR = \frac{8 \times Blood\ viscosity\ (\mu) \times Vessel\ length\ (L)}{\pi \times Vessel\ radius\ (r)^4}$$

This reveals the ways in which MAP can be easily and rapidly controlled homeostatically: by modifying cardiac chronotropy (HR), inotropy (SV), or vasoconstriction/dilation (r). The latter is principally controlled by the smooth muscle-lined resistance vessels, the arterioles, and perhaps is able to exert the largest single influence on MAP, owing to its inverse power-of-4 relationship with SVR.

I.2.1 The Baroreflex

In the short-term, MAP is controlled by a neurovascular reflex known as the baroreflex, which is depicted in Figure 1, and aims to keep MAP constant in response to physiological challenges, such as orthostasis. Detection of a change in MAP by the baroreceptors leads to modulation of sympathetic output to the heart and vasculature, altering HR, SV and r, allowing effective control. The importance of this mechanism to daily blood pressure control was demonstrated in 1973 by Cowley Jr. et al., who denervated the carotid sinus of dogs, and found it caused a 2-fold increase in MAP standard deviation over a 24-hour period (Cowley et al., 1973).

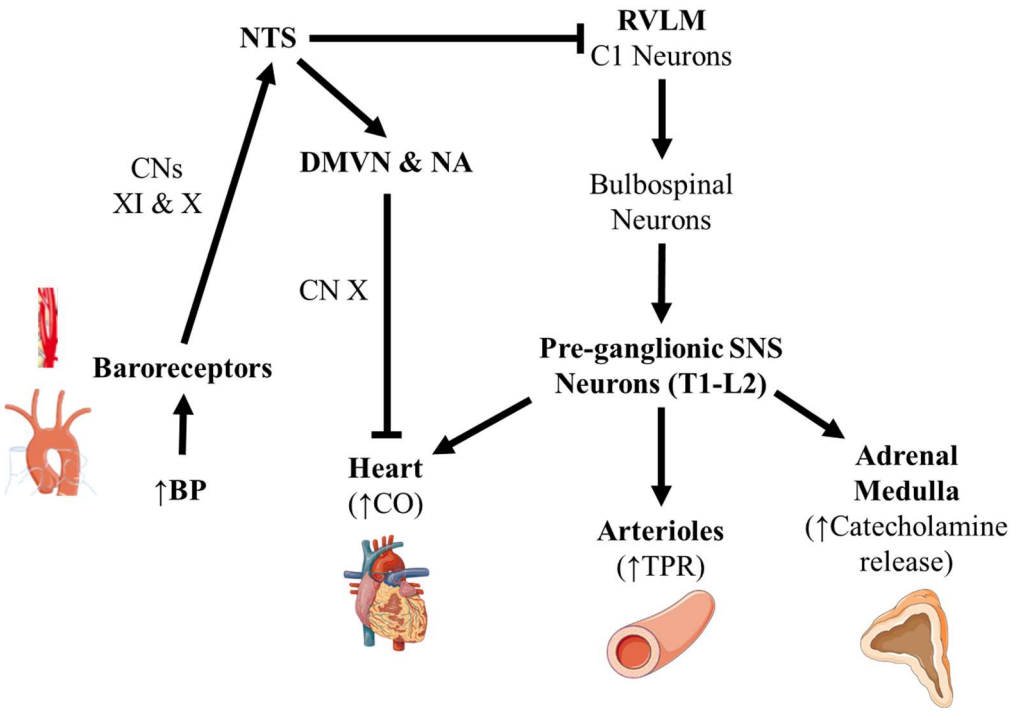

Figure 1| The Baroreflex. The SNS and CN X input to the heart are opposite but not equal; the SNS innervates most of the heart and increases chronotropy and inotropy, while the CN X parasympathetic input innervates almost only the sino-atrial node, thereby only substantially affecting chronotropy. Organ images are from Servier Medical Art (smart.servier.com) by Servier, and licensed under a Creative Commons Attribution 3.0 Unported License (https://creativecommons.org/licenses/by/3.0/). "Aorta" and "Head and neck arteries" images cropped.

BP = arterial blood pressure; CN = cranial nerve; CO = cardiac output; DMVN = dorsomotor vagal nucleus; NA = nucleus ambiguous; NTS = nucleus tractus solitarii; RVLM = rostral ventrolateral medulla; TPR = total peripheral resistance.

I.2.2 Long-term MAP Control

Control of MAP by autonomic nervous system input to the heart and vasculature relies on vasculature function as a closed system. As water and electrolytes can enter and leave the circulation, this is not strictly true, although as this happens slowly the model is sufficient in describing the acute regulation of MAP. In the longer term, changes in blood volume, controlled by the kidney, are also able to influence this parameter.

I.2.2.a Guyton's Curves

To appreciate renal blood pressure control, one must first understand the intrinsic physiological relationship between blood volume and MAP. A change in blood volume will correspondingly alter CVP, as the venous circulation functions as a reservoir for circulating fluid, due the greater compliance of its vessels. While CVP will only directly exert a minor influence on MAP, according to equation 1, it is also a key determinant of ventricular filling. According to the Frank-Starling Law of the heart (Patterson et al., 1914), an increased lengthening of the ventricular myocytes, brought about by increased diastolic filling, will increase the contractile force, thereby raising SV. For this reason,

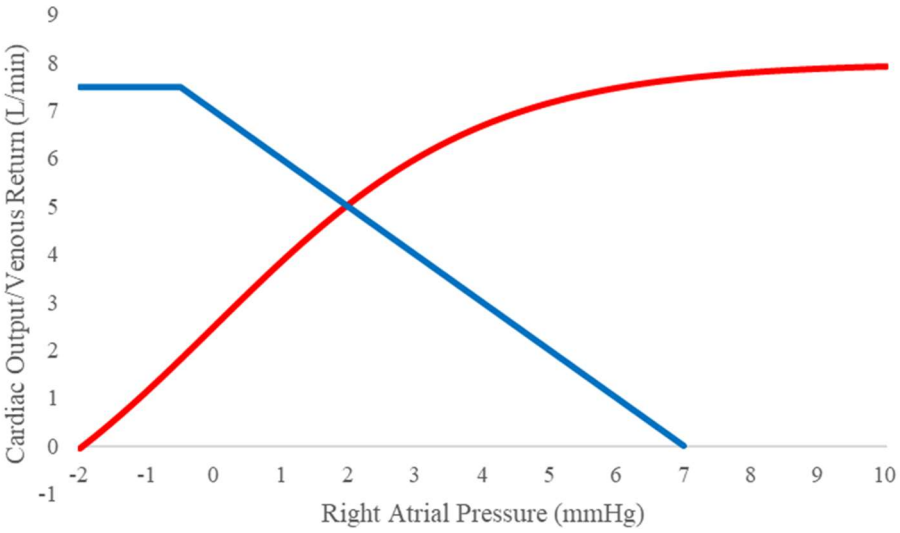

Figure 2| Guyton's curve. The red line is the Frank-Starling (or cardiac function) curve; as right arterial filling increases, so does stroke volume and thus cardiac output, until an eventual plateau (and eventual drop-off) where the myosin and actin filaments are optimally spaced. The blue line is venous return curve; as cardiac output increases, more blood is drawn out of the right atrium and venous system, thereby lowering right atrial pressure. Where the blue line crosses the x axis is the mean circulatory filling pressure: the pressure exerted of the circulation by the blood volume it contains. At high values of cardiac output, negative right atrial/venous pressure cause the vessels to collapse, limiting any further increase in venous return or cardiac output. (Guyton, 1955).

increasing blood volume increases SV which, as established above, is correspondingly changes MAP. This relationship is elegantly depicted in Figure 2, which is known as a Guyton curve, named for Arthur Guyton who first published the diagram (Guyton, 1955).

I.2.2.b Renal control of fluid volume

One of the roles of the kidney is fluid volume homeostasis, which it achieves by modulating excretion of Na^+ ions (the major extracellular electrolyte) and water. The main and simplest way in which this occurs is through pressure natriuresis; an intrinsic renal mechanism by which increased renal arterial pressure produces an increase in Na^+ excretion in the urine. This can be demonstrated in the isolated kidney (Kaloyanides et al., 1971), and occurs independently of glomerular filtration rate (Blake et al., 1950). The classic *in vivo* study of Hall et al. (1980) in dogs reveals the renal pressure natriuresis curve, summarised in Figure 3. There are a number of mechanisms proposed for this process, generally involving increase medullary blood flow and renal hydrostatic pressure, and subsequent release of paracrine signals such as NO and ATP which inhibit the action of various renal Na^+ transporters. This topic is reviewed in detail by Ivy & Bailey (2014).

Increased MAP, and through its influence on MAP, increased blood volume, can therefore stimulate Na^+ excretion by the kidney. A change in Na^+ handling is physiologically coupled to a change in water homeostasis; altering Na^+ excretion changes body fluid osmolarity, which stimulates/inhibits antidiuretic hormone (ADH) release by the posterior pituitary, thereby changing water excretion. In this way, the kidney can regulate blood volume and MAP.

This process will only be sufficient however if Na^+ loading remains constant. Na^+ balance has to be maintained in the body, but if it is coupled so tightly to MAP, the two become dependent on one another. This creates a problem, to which the solution is the renin-angiotensin-aldosterone system (RAAS; Figure 4), which serves to modify the pressure natriuresis relationship. (Hall et al., 1980) demonstrated this in the aforementioned

experiment, using an ACE-inhibitor or angiotensin II infusion, which were shown to shift the renal function curve (Figure 3). Activation of the RAAS is caused in general by a reduction in body fluid volume (Figure 4), which is related to bodily Na^+, and therefore the MAP operating point of the kidney is reset to a new appropriate level, which maintains normal MAP, while providing adequate Na^+ excretion.

Additionally, it seems that Na^+ can increase sympathetic nervous system activity through central nervous system effects (Farquhar et al., 2006; Gomes et al., 2017; Nomura et al., 2019), which in turn will promote RAAS activity, and Na^+ retention by the kidney. Recent data from our lab have also shown that Na^+ ions can directly act on peripheral sympathetic neurons to increase activity via actions on Na_X channels (Harvey Davis, personal communication), which is likely to be involved in this reflex.

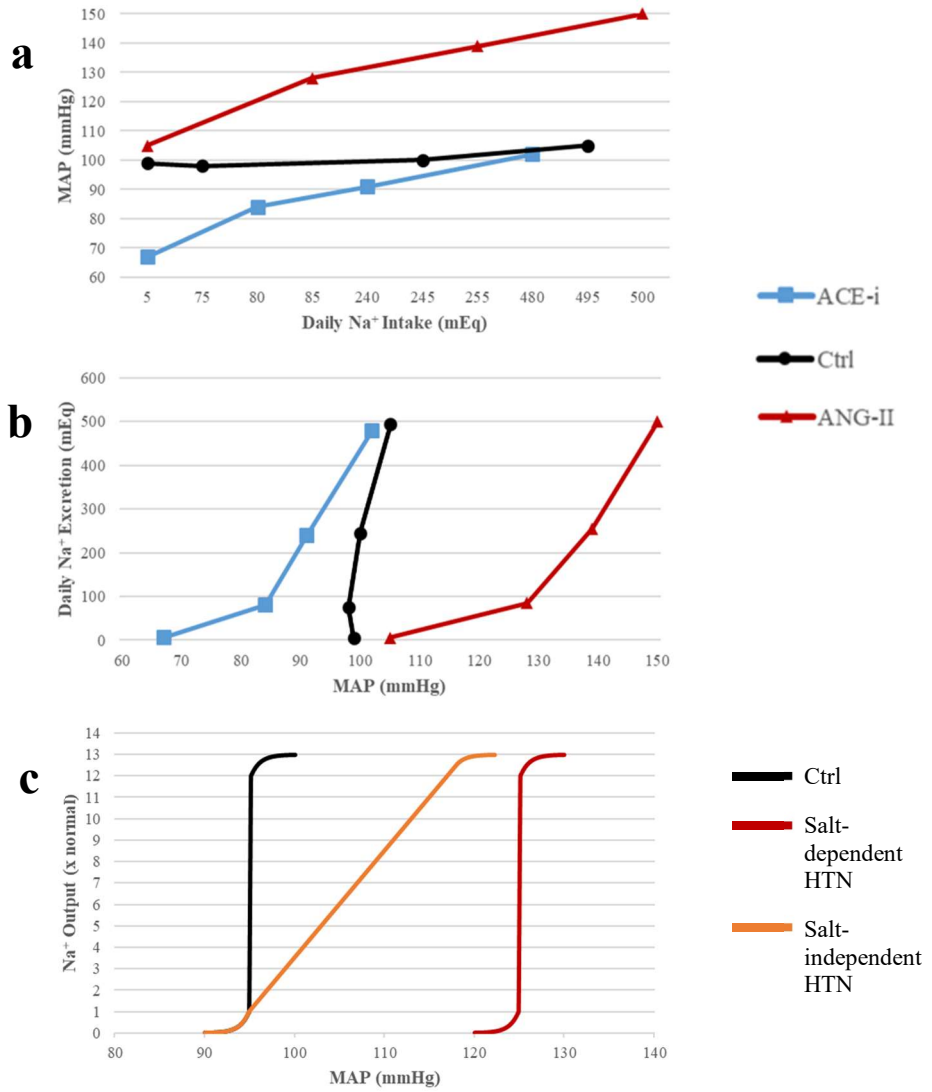

Figure 3| Renal pressure natriuresis. a) The effect of varying dietary Na^+ on MAP in dogs, compared between animals on ACE-inhibition, ANG-II infusion, or no other treatment Hall et al. (1980). Under physiological conditions MAP can be maintained at the homeostatic level up to ~12-fold the normal required daily Na^+ intake (black curve), due to the influence of the RAAS. When RAAS activity is inhibited (blue curve), or (effectively) clamped at a high level (red curve), MAP becomes dependent on Na^+ intake. As the RAAS acts to promote Na^+, and thus volume retention, the red curve reaches similar MAP values under low Na^+ loading, while the blue curve achieves this only at high Na^+ intake. b) Relationship between MAP and renal Na^+ excretion in the same animals. Na^+ excretion must equal Na^+ intake in order to maintain Na^+ and osmolarity homeostasis, and this experiment revealed this to be the case (data not shown). Therefore, the ACE-i curve (blue) reveals the inherent pressure natriuresis curve of the kidney; increasing MAP, increases Na^+ excretion. With clamped high ANG-II levels the curve is simply shifted rightwards (red). However, under the normal state, the ability to modulate RAAS activity based on [Na^+] allows the kidney to continually shift the curve along the x axis until the MAP set point for the required level of Na^+ (which balances out the intake) is the normal MAP value. The physiological black curve is the result of this. In this way, the RAAS allows Na^+ homeostasis to be modulated independently of MAP. c) Theoretical renal function curves under physiological conditions (black), salt-dependent hypertension (orange) and salt-independent hypertension (red).

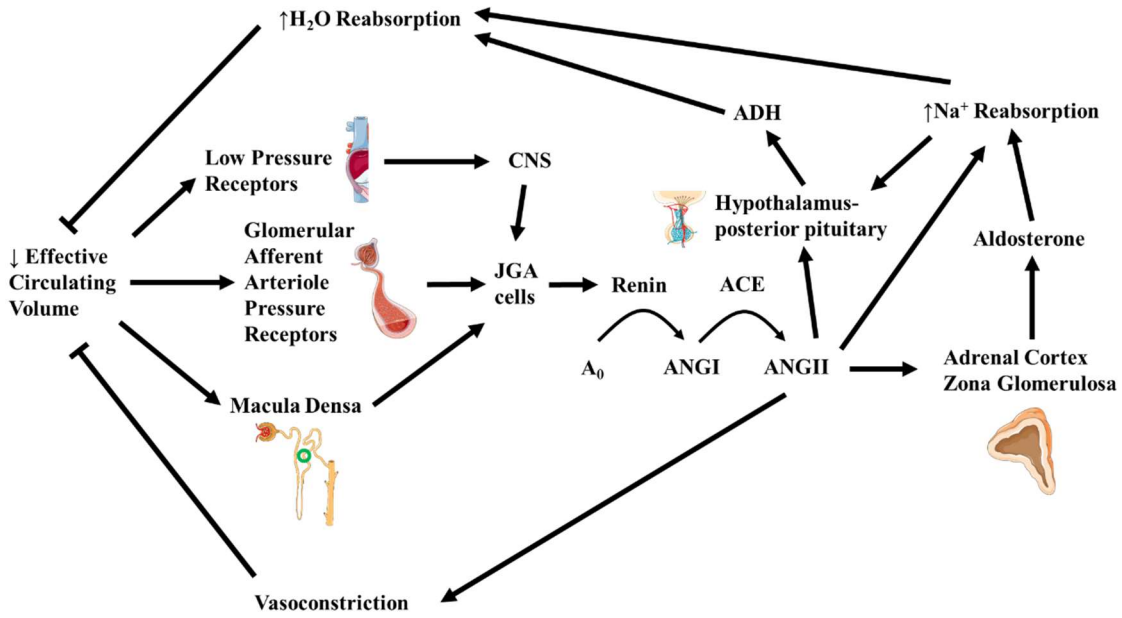

Figure 4| The Renin-Angiotensin-Aldosterone System (RAAS). Reduced effective circulating volume is detected by pressure receptors in the great veins and right atrium, and glomerular afferent arterioles, and by reduced flow of NaCl past the macula densa in the thick ascending limb of the loop of Henle. This is ultimately integrated by the juxtaglomerular apparatus, which releases renin. $\uparrow Na^+$ reabsorption directly increases H_2O retention through local osmotic effects in the nephron, but also generally raises body osmolarity, triggering ADH release. Organ images are from Servier Medical Art (smart.servier.com) by Servier, and licensed under a Creative Commons Attribution 3.0 Unported License (https://creativecommons.org/licenses/by/3.0/). "Heart" image cropped.

A_0 = angiotensinogen; ACE = angiotensin converting enzyme; ADH = anti-diuretic hormone; ANGI = angiotensin I; ANGII = angiotensin II; CNS = central nervous system; JGA = juxtaglomerular apparatus.

I.2.2.c Role of the baroreflex in long-term MAP control?

The baroreflex has long been regarded as a purely short-term controller of blood pressure, as it has been observed to adapt to chronic changes in MAP, resetting its homeostatic operating point; first described by McCubbin et al. (1956) in the dog. Denervation of the carotid sinus also produces only a transient increase in MAP, before returning to normal (Lohmeier et al., 2010). In a detailed review of the topic however, Lohmeier & Iliescu (2015) present evidence that the baroreflex at least does not completely reset in response

to a sustained change in MAP. In angiotensin II-induced canine hypertension, the baroreflex seems to chronically inhibit sympathetic outflow, and electrical baroreceptor stimulation leads to a sustained decrease in MAP. They argue that previous studies demonstrating baroreceptor resetting did not focus on sufficient long timescales. It is interesting, however that their electrical stimulation study did not produce at least a short term resetting (Lohmeier et al., 2010), as the older studies did (McCubbin et al., 1956). Electrical stimulation is far from the more physiological haemodynamic stimulus used by McCubbin et al. (1956), and perhaps its extreme level of activation has a slightly different effect. Additionally, the angiotensin II models which provide a substantial part of their evidence are not entirely reflective of human essential hypertension, which is a complex multi-factorial process that may involve higher levels of RAAS activity, but this is never the sole cause (this would be secondary hypertension, for example in hyperaldosteronism), and in many cases (such as older patients) it may not even be substantially involved. Moreover, even in these studies the baroreflex effect was is not sufficient to prevent MAP elevation. Overall, it seems likely that the baroreflex may contribute in part to long-term MAP control, and its stimulation certainly seems promising as a means to reduce blood pressure, but the extent of this contribution is unclear.

I.3 Classical hypotheses of hypertensive pathophysiology

Between 5 and 10% of hypertension cases are secondary to a discrete, known medical cause, for example: renal arterial stenosis, hyperaldosteronism or obstructive sleep apnoea (Rimoldi et al., 2014). Treatment for these (*secondary* hypertension) generally involves reversal of the causative underlying condition and therefore there is less need for development in this area. By contrast, *essential* hypertension, which makes up the

remaining 90-95% of patients, has a rather poorly understood aetiology involving a complex interplay of genetic and environmental factors, leading to an incompletely understood pathophysiology, for which there are many controversial hypotheses. No current treatment can therefore target its underlying cause, which could perhaps be a key clinical limitation.

I.3.1 Vessels or Kidneys?

The simplest and oldest explanation of hypertensive pathophysiology regards that the blood pressure elevation arises from an increase in SVR (Gull & Sutton, 1872; Folkow, 1987), and in turn, raised blood pressure induces vascular wall hypertrophy, further reducing their luminal volume and compliance, and producing a vicious cycle (Folkow, 1987). It is however, now fairly widely accepted that the final common node in hypertensive pathophysiology is the kidney (well-reviewed by Crowley & Coffman (2014)). In short, an increase in SVR cannot lead to sustained blood pressure elevation because the renal pressure natriuresis mechanisms will compensate; a decrease in the functional vascular volume will be offset by a reduction in circulating fluid volume. Evidence in support of this has been extensively reviewed previously, for example by Hall et al. (1990) and Cowley & Roman (1996), and includes the observations that: a) chronic vasoconstrictor application only causes a very weak sustained increase in arterial blood pressure in animal models[2], after an initial larger rise; b) all animal models of hypertension and human essential hypertensives seem to exhibit renal impairment and have shifted pressure-natriuresis curves; c) healthy renal transplants in animal models and human hypertension patients have been shown to normalise blood pressure, while

[2] In the case of many vasoconstrictors such as noradrenaline, anti-natriuretic effects and renal arteriole constriction may even account for some of this mild sustained increase in arterial blood pressure.

transplants from hypertensives to normotensive individuals increases blood pressure. Two important things to note though are that: first, increased vascular resistance can contribute to impaired pressure natriuresis if the renal vasculature is impeded (as is seen in renal arterial stenosis), and second, once renal impairment has occurred, any increase in SVR could, and probably does, then exacerbate this, worsening as vascular wall hypertrophy ensues. The original cause of renal dysfunction however, is unclear.

I.4 Dysautonomia

Essential hypertension is typically characterised by an autonomic nervous system phenotype comprising sympathetic hyperactivity (Grassi, 2009; Grassi et al.; 2010, Mancia & Grassi, 2014; Grassi et al., 2015) and impaired vagal tone (Mancia & Grassi, 2014). The sympathetic component of this 'dysautonomia' is seemingly the more important given its more widespread control over the systems relevant to hypertensive pathology, such as the kidneys and blood vessels, where the vagus nerve input seems less robust, and is also poorly studied in general. For these reasons, along with the fact that blocking a pathological process seems intuitively more achievable than activating a compensatory physiological one in terms of therapeutics, the sympathetic hyperactivity will be the focus of this thesis.

Sympathetic activity in humans can be measured mainly by muscle sympathetic nerve microneurography (Yamada et al., 1988; Floras & Hara, 1993; Grassi et al., 1998; Grassi et al., 2000; Smith et al., 2004), radio-labelled noradrenaline spillover (Esler et al., 1988; Esler et al., 1989; Ferrier et al., 1993) or plasma noradrenaline concentration (Ferrier et al., 1993; Masuo et al., 1997). This is present throughout all disease stages (Floras & Hara, 1993; Grassi et al., 1998; Grassi et al., 2000; Smith et al., 2004), correlates positively with disease severity (Grassi et al., 1998; Sakata et al., 1999), and even appears

to precede any actual arterial blood pressure elevation (Yamada et al., 1988; Ferrier et al., 1993; Masuo et al., 1997). From this it is tempting to suggest that this neural phenotype could potentially initiate disease itself, particularly as the sympathetic nervous system (SNS) influences the body in such a widespread manner. This hypothesis is also somewhat compatible with the idea of the kidney as the final common node of hypertensive pathophysiology; SNS input to this organ increases sodium and water retention and could also potentially constrict the renal vasculature (DiBona & Kopp, 1997). Moreover, once the kidneys are diseased, their afferent nerves signal to the CNS to further increase sympathetic input (Nishi et al., 2015). As the origin of renal dysfunction in hypertension is not entirely clear, could the hitherto elusive answer to hypertensive aetiology lie in the SNS itself?

I.4.1 A causative role in essential hypertension?

Sympathetic hyperactivity might not underlie every single case of essential hypertension; DiBona & Esler (2010) suggest that the phenomenon is responsible for haemodynamic disease in at least 50% of such patients. The authors conclude this in part from studies measuring [^{3}H]-noradrenaline spillover (Esler et al., 1988; Esler et al., 1989), which suggest some untreated essential hypertensives have similar levels of sympathetic outflow to normotensive controls. It could be argued however that this approach leads to an underestimation of the proportion of patients for whom sympathetic hyperactivity is a contributing pathology. First, even though the data from normo- and hypertensive individuals overlap (Esler et al., 1988; Esler et al., 1989), they have been shown statistically to be part of separate populations. Although some essential hypertensives may have sympathetic outflow values similar to those of normotensives (Esler et al., 1988; Esler et al., 1989), they may be elevated relative to their own baseline level. To

date no study has controlled recordings from hypertensive individuals to those before the developed the disease. Similarly, while some "normotensives" exhibit relatively high levels of sympathetic activity (Esler et al., 1988; Esler et al., 1989), these could potentially reflect a state of pre-hypertension, in which there is sympathetic overdrive, but not yet a sufficient blood pressure elevation to be clinically defined as hypertension. Second, a lot of the lack of sympathetic elevation in hypertension patients is accounted for by older individuals, in whom there is often no significant difference to age-matched controls (DiBona & Esler, 2010). It is possible that if these patients have had essential hypertension for some time perhaps the damage induced by excessive sympathetic drive may have already occurred. Additionally, in the normotensive population sympathetic activity seems to increase with age (Pfeifer et al., 1983), so it could be the case that normotensives start to catch up with their hypertensive counterparts, masking any differences. This increase in "normotensives" does appear to correlate with a slight (sub-threshold) blood pressure elevation, as commonly also occurs with age (Pfeifer et al., 1983).

Finally, both MSNA and radio-labelled noradrenaline spillover are measurements of a single time point and therefore might not pick up sympathetic hyperactivity in all patients; if possible it would be informative to measure these over a 24 h period, akin to those performed for blood pressure. DiBona & Esler (2010) also base their 50% estimate on the proportion of hypertensive patients who respond to anti-adrenergic drug therapy, although it is unclear to which studies this refers. Combined α_1 and β-adrenoreceptor blockade does effectively reduce blood pressure in hypertensives (Wofford et al., 2001). However, both of these are marginally less effective in this respect than other forms of antihypertensive drug, and are associated with worse mortality rates (Furberg et al., 2000;

Wiysonge et al., 2017). Of course, as Wiysonge et al. (2017) note, most of the trial data examining the efficacy of β-blockers for hypertension comes from study of atenolol. As newer β-antagonists with different properties are now available, further study is needed on their efficacy. The extent of reduction in blood pressure produced by clonidine (a central sympatholytic α_2 adrenoreceptor agonist) has been taken as the extent of sympathetic involvement in a given patient's hypertension (Grassi, 2016), although this approach ignores chronic changes which may occur following prolonged high stimulation of target organs by the SNS. Perhaps if given to pre-hypertensive patients, adrenergic blockade could reduce development of hypertension. At the very least therefore, sympathetic hyperactivity is likely a crucial initiator and driver of disease in a substantial proportion of essential hypertension cases, and possibly even more than this estimate.

I.4.2 A theragnostic marker?

Hypertensive dysautonomia leads to a range of other co-morbidities through over-stimulation of target organs, such as: cardiac hypertrophy (Burns et al., 2007; Levick et al., 2010), arrhythmia (Lown & Verrier, 1976), vascular dysfunction (Fisher et al., 2009), insulin resistance (Julius & Valentini, 1998) and inflammation (Singh et al., 2014), and may thus account for some of the end-organ damage of hypertension usually ascribed to the haemodynamic changes. In fact, it has been suggested that even in hypertensive patients with controlled blood pressure, persistent heightened sympathetic activity may still be associated with morbidity and mortality (Mancia & Grassi, 2014).

For this reason, dysautonomia might be describable as a 'theragnostic' marker for essential hypertension; providing a potential *thera*peutic target with scope to reduce blood pressure and end-organ damage, and giving a dia*gnostic* readout of disease severity. Measurement of sympathetic outflow could therefore be put to more use clinically, and

perhaps intervening at this stage in the hypertensive pathway could provide effective treatment by ameliorating the underlying cause. Additionally, this sympathetic hyperactivity may also be an exacerbating factor in a number of cases of secondary hypertension, where its inhibition could similarly be beneficial therapeutically.

I.4.3 Effects of hypertensive treatments on sympathetic activity

Most current frontline therapeutics do not substantially target the SNS. RAAS inhibitors such as ACE inhibitors, angiotensin receptor blockers and aldosterone antagonists do all produce an anti-sympathetic effect, although this is likely due to the sympatho-excitatory effects of angiotensin II and aldosterone respectively. These would therefore be less useful in most essential hypertensive patients for whom these mediators are not the main cause of their high blood pressure, and in whom angiotensin II and aldosterone levels may be normal.

Current calcium channel blockers tend if anything to produce a slight reflex increase in sympathetic outflow via the baroreflex. More modern drugs which can inhibit N- and T-type Ca^{2+} channels in addition to the L-type ones normally utilised by calcium channel inhibitor hypertension therapy, may reduce sympathetic outflow. However, these are seemingly rather weak effects (Grassi, 2016), which may help reverse deleterious sympathoexcitation caused by L-type Ca^{2+}channel inhibition, but will not likely sufficiently reduce it from baseline.

α_1 and β-adrenoreceptor antagonists are generally only used in certain cases of resistant hypertension, as a fourth drug, mainly owing to widespread side effects and poor mortality-reducing effects (Furberg et al., 2000; Wiysonge et al., 2017). While they do effectively lower blood pressure, as discussed above they tend to be weaker than other

drugs (Furberg et al., 2000; Wiysonge et al., 2017), and β-antagonists don't actually reduce central aortic pressure sufficiently, despite lowering the commonly-recorded peripheral arterial pressures (Williams et al., 2006). As noted previously, further study is needed of newer generation β-antagonists though.

This evidence presents a challenge to the neurogenic hypothesis of hypertension; if it is an SNS pathology in origin, why doesn't toning this down effectively reverse it? For these peripherally-acting α_1 and β-adrenoreceptor antagonists, it is very challenging to establish their level of functional sympathetic inhibition. α_1 antagonists act almost entirely post-synaptically on the arterial smooth muscle, and this vasodilation often produces a reflex sympathoexcition. β-blockers, while they similarly act on the end-organ, also act to a great extent on pre-synaptic receptors (Bardsley et al, 2018b). They do not consistently reduce MSNA (Grassi, 2016) and it is seemingly impossible to measure the level of neurotransmission between the sympathetic varicosities and post-synaptic target, making the level of functional SNS output seen by the end-organs impossible to quantify. It seems unlikely though that β-blockade could return a hypertensive individual's SNS output to normal, particularly due to reflex β-adrenergic supersensitivity which seems to contribute to β-blocker withdrawal syndrome. Additionally, β-blockade has been shown to increase ventricular sympathetic innervation, which may also blunt the effect (Clarke et al., 2010). To the best of the author's knowledge at the date of writing, measurement of hypertensive patient SNS activity on β-blockade compared to healthy controls has not been made, although for a number of other classes of drug, it has been shown that sympathetic hyperactivity in hypertensive patients is not returned to normal (Grassi, 2016). Of course as β-blockers are never given as a monotherapy for essential hypertension, this comparison is difficult.

Central sympatholytics, which often target the α_2 adrenoreceptor, are not often used due to their side effect profile, but produce an anti-hypertensive effect and reduce hypertension-associated organ damage (Vongpatanasin et al., 2011). Like with the peripheral-acting sympatholytics however, their effect on measured sympathetic outflow in hypertensives has also not been substantially measured, for similar reasons.

The archaic method of surgical sympathectomy was shown in the 1940s and 50s to produce a reduction in diastolic blood pressure >15 mmHg in almost all patients (Newcombe et al., 1959). In only 27% of cases was this sustained however, possibly owing to the surgical methods not producing complete sympathectomy[3] (which may have caused a rebound increase in the remaining sympathetic nerves; many patients developed Raynaud's phenomenon), or previous sympathetic hyperactivity may have already sufficiently damaged end-organs such that hypertension could be sustained even the absence of further sympathetic traffic. This approach is extreme, irreversible and all-or-none, and has potential to cause severe side effects, such as Horner's syndrome (Singh et al., 2006) (despite few sustained adverse effects being reported by Newcombe et al. (1959)) as the SNS is naturally a necessary physiological component. More recently, more focal renal denervation has been tested as a possible treatment for hypertension. Despite promising results in the two preliminary studies (Krum et al., 2009; Esler et al., 2010; Esler et al., 2012), the third SYMPLICITY (HTN-3) study, the first to be blinded and sham-controlled, showed no blood pressure benefit of radiofrequency renal sympathetic nerve ablation (Bhatt et al., 2014). However, it seems likely that this lack of effect was due in part to an insufficient extent of ablation, and the study was also confounded by a large proportion of medication changes investigation period (Kandzari

[3] For example, no patient had the full coeliac ganglion, which innervates the kidney, removed.

et al., 2015). In support of this, and providing renewed hope for the technique, both the SPYRAL HTN-ON MED (Kandzari et al., 2018) and -OFF MED (Bohm et al., 2020) trials have showed a significant, albeit <10 mmHg, reduction in systolic blood pressure compared to sham, utilising a more thorough surgical ablation procedure. While reducing blood pressure, this technique however is not able to tackle the systemic sympatho-excitation which occurs in hypertension, so would not be expected to reduce damage to other organs. Treating the underlying cause of hypertensive dysautonomia could reduce sympathetic activity in a more graded manner than surgical sympathectomy, and could safely do so systemically. Additional classes of hypertensive drugs could then be added in those whom end-organ, such as renal, damage is past the stage of complete reversibility.

In general, it seems that the above approaches to treating essential hypertension seem to fall short in terms of reversing SNS tone. A reason for this could be their broad mechanisms of action, and targeting pathways downstream of essential hypertensive aetiology. Medicine has need to reverse SNS pathology, which could potentially bring its activity back to baseline levels.

New experimental electrical nerve stimulation studies have shown it is possible to modulate sympathetic outflow and reduce blood pressure, using electrodes at one of a number of different sites. Deep brain stimulation at several brain nuclei (Ems et al., 2019), most notably the ventral periaqueductal grey matter (vPAG) (Green et al., 2005; 2007; 2010), reduces blood pressure, and a case report showed a marked sustained blood pressure decrease over a number of months on one patient with malignant hypertension (O'Callghan et al., 2017). Additionally, in the periphery, a recent study from the same

group as the vPAG studies showed that dorsal root ganglion stimulation was able to lower blood pressure (Sverrisdottir et al., 2020). While this study carried the caveat of being tested in chronic pain patients, in whom reducing pain is likely to lower blood pressure, the degree of MSNA reduction recorded poorly correlated with the extent of pain relief. Finally, another approach has been stimulation of the carotid sinus baroreceptors, in attempt to mimic the physiological response to high blood pressure. Some clinical trials have showed positive results using this method, causing sustained blood pressure reductions of more than 20/10 mmHg in resistant hypertensives over several months to years (Scheffers et al., 2010; Hoppe et al., 2012). However, given the reflex appears to adapt in hypertensives, it is not certain is this would be maintained in the longer term. All of these approaches serve to prove that reducing sympathetic tone can lower blood pressure. However, as none have been studied in the long term in hypertensive patients, it is unclear the extent to which these are substantially disease-modifying.

I.5 Inflammation in hypertension

Uncovering the root of hypertensive dysautonomia might require investigation of another bodily system. The immune system is widely implicated in hypertension; certain immune cell arms are essential for sustained blood pressure elevation in many animal models (including the SHR), and similarly immunomodulatory interventions can alter disease severity in many of these. These studies are extensively reviewed by Rodriguez-Iturbe et al. (2017). Crucially, a simple bone marrow transplant from SHR to Wistar rats increases blood pressure, while the converse decreases it (Santisteban et al., 2015), implying the SHR's immune system as a causative factor of the blood pressure phenotype. Clinically, higher levels of C-reactive protein (CRP, a common assessed marker of systemic inflammation) (Sesso et al., 2003; King et al., 2004; Lakoski et al., 2011; Jayedi et al.,

2019), or IL-6 (an inflammatory cytokine released along with CRP in the acute-phase response) (Lakoski et al., 2011; Jayedi et al., 2019) strongly predict future development of hypertension, and therefore both inflammation and sympathetic hyperexcitability seem to be co-features of a 'pre-hypertensive' state, before any overt cardiovascular disease is evident. Sympathetic overactivity seems to increase with progression of hypertensive disease, and it would be interesting to test whether the same is true of inflammation. Notably though, both these phenomena seem to increase with age (Pfeifer et al., 1983; Ong et al., 2018), a key risk factor for hypertension.

I.5.1 The immune system

Before full discussion of a potential role for the immune system in hypertension, it is first necessary to briefly review its basic functionality. This system has been historically divided into the innate and adaptive immune systems; the former involving detection of general damage or pathogen-related signals, while the latter relies on recognition of specific antigens, and subsequent immunological memory (Chaplin, 2010). The focus here will be on the cellular components of the immune system, as opposed to molecular effectors such as complement.

I.5.1.a Innate Immunity

The mammalian innate immune system involves a number of, generally myeloid, cells, and molecular mediators. Its activation is largely driven by the triggering of pattern recognition receptors (PRRs), which have evolved to recognise damage-associated molecular patterns (DAMPs) or pathogen-associated molecular patterns (PAMPs) (Akira et al., 2006). DAMPs are molecules commonly released during tissue injury, often intracellular molecules, for example ATP or S100 proteins, whose presence in the extracellular space thereby indicates damage. PAMPs are molecules not native to the

mammalian host body and specific to certain types of pathogen, notably lipopolysaccharide, or double-stranded RNA.

Activation of innate immune pathways leads to inflammation, which is characterised by its five cardinal signs of swelling, heat, redness, pain and loss of function. More specifically it involves localised vasodilation and increased extravasation of plasma into the tissue fluid (contributing to the swelling, heat, redness and loss of function), increased recruitment of immune cells to the inflamed site, and sensitisation of local pain fibres (causing pain, and reducing function). Essentially the purpose of this process is to allow recruitment of cells and mediators in order to resolve infection, and then promote tissue healing. Adaptive immune cells, fully described later on, are also recruited to sites of inflammation, typically following the innate components, and may further contribute to the reaction. Three main "types" of inflammation can be defined, based on the profile of cytokines (intercellular signal proteins) and cell types involved (Annunziato et al., 2015), although this is likely an oversimplification. The type of inflammation induced is dictated by more specific signals produced an invading pathogen.

The cells of the innate immune system play varied roles (Chaplin, 2010). Neutrophils are quickly recruited to sites of inflammation and are specialised for attacking pathogens, particularly extracellular bacteria and fungi, while eosinophils and basophils are specialised for anti-macroparasite immunity. Innate lymphoid cells (ILCs) are important producers of cytokines and are found in three varieties, one corresponding to each "type" of inflammation. A similar lineage to ILC-1s are known as natural killer T cells, which play a role in killing infected host cells.

Table 1| Types of inflammation (Annunziato et al., 2015).

Type	Main cells involved	Cytokines	Target
1	T_H1 cells, M1 macrophages, CD8 T cells, B cells, ILC-1s, NK cells	IFN-γ, TNF-α, IL-12	Viruses, intracellular bacteria, protozoa
2	T_H2 cells, eosinophils, basophils, B cells, ILC-2s, M2 macrophages	IL-3, IL-4, IL-5, IL-13	Macroparasites
3 (sometimes referred to as type 17)	T_H17 cells, Neutrophils, ILC-3s	IL-17A, IL-22	Extracellular bacteria, fungi

The results from Chapter III shift the focus of this thesis towards monocytes and macrophages, which therefore warrant a more detailed discussion in this introductory chapter. Macrophages are specialised phagocytic cells, with the capabilities of removing extracellular pathogens, dead or infected host cells, or clearing debris. These cells arise from two main origins: either embryonic macrophage progenitor cells, which form continually-replenishing tissue-resident populations, or adult bone-marrow derived monocytes, which circulate in the blood, and enter tissues where they subsequently differentiate into macrophages (Epelman et al., 2014).

Cytokine signals within the tissue can polarise the macrophages into a number of different phenotypes (Murray, 2017). Traditionally there a dichotomy has been ascribed to this: M1 macrophages, which are inflammatory, pathogen-killing cells and M2 macrophages,

which were thought to be pro-resolution effectors. In reality this is a substantial oversimplification, and more complex macrophage phenotypes are increasingly being observed. In particular, some M2-like macrophages appear to be involved in the type 2 inflammatory response. For this reason, some sources sub-categorise M2 macrophages into groups reflecting this (Roszer, 2015).

It is generally accepted that monocytes are found in two phenotypes within the mouse and rat circulations, based on surface marker expression: classical and non-classical, while the human has an additional intermediate type, and it appears the classical monocytes are the parent population of the others (Wolf et al., 2019). Attempts have been made to ascribe specific functions to each subset; classical monocytes generally being termed "inflammatory", while non-classical monocytes are often known as "resident" (Geissmann et al., 2003; Gordon & Taylor, 2005), with varied descriptions of the intermediate sub-type, many of which are inflammatory. However, many reports appear to conflict with this paradigm (Mukherjee et al., 2015; Narasimhan et al., 2019). Additionally, many inconsistencies exist in this simple functional categorisation into three subsets, and sources have suggested monocytes need to be sub-categorised in a more thorough way, and attempt to do so (Merah-Mourah et al., 2020). The exact significance of the extra sub-population of intermediate monocytes in the human is unclear, although a similar intermediate monocyte subset has also been reported in the mouse (Qu et al., 2004; Mildner et al., 2017). It may be the case that with further characterisation, a similar population may be delineated within the hitherto understudied rat monocytes.

I.5.1.b Adaptive Immunity

T and B lymphocytes are the principal components of the adaptive immune system, and work to produce specific responses tailored to a given antigen (Chaplin, 2010).

Professional antigen-presenting cells (APCs), predominantly dendritic cells (DCs), present fragments of invading antigens on major histocompatibility complex II molecules (MHC-II), which are then recognised by specific $CD4^+$ T-helper cells via their T cell receptors (TCRs). With additional co-stimulatory receptor binding between the T cell and APC, the lymphocyte is activated, and the local cytokine profile polarises the $CD4^+$ T cell towards a particular phenotype: T_H1, T_H2, T_H17, or a pro-resolution induced T regulatory cell (iTreg). T_H1, T_H2 and T_H17 cells then coordinate the immune reaction and help shape it towards a type 1, 2, or 3 response respectively, through release of cytokines and recruitment of other immune cells.

$CD8^+$ T cells are known as cytotoxic T cells, and are activated by binding of their TCRs to MHC-I complexes presenting antigen fragments. This molecular complex is expressed by virtually every cell in the body, and as most of these are non-phagocytic, it suggests cellular infection. $CD8^+$ T cells therefore use this as a signal to kill these cells.

B cells are the producers of antibodies, and mediate a humoral response to invading pathogens. These cells are also professional APCs, and upon presentation of antigen fragments on surface MHC-II complexes to specific T cells, they are activated and undergo a process of repeated proliferation, antibody recombination, and antibody specificity testing, to produce a large population of highly-specific B cell clones.

A classically-presented difference between these lymphocyte reactions and those of the innate immune system regards that the adaptive system also produces memory T and B cell clones, which continue to circulate post-resolution of inflammation. If these recognise the same antigen as in the primary adaptive response, a secondary response which is faster and stronger is initiated, allowing the pathogen to be eliminated often

before disease is caused. However, more recent study has revealed that the innate immune system does also have some capacity for memory, which is referred to as trained immunity (Netea et al., 2020).

I.5.2 Effect of anti-inflammatory cytokine therapies on blood pressure

Inflammation almost certainly promotes blood pressure elevation by actions on a variety of loci, such as the kidney and the vasculature (Solak et al., 2016); however, it seems likely this would also include the sympathetic ganglia, as the nervous system seems to be such a central and wide-reaching influencer of hypertension. Notably, in human patients, for example, infliximab anti-TNF-α antibody therapy can reduce blood pressure in rheumatoid arthritis patients (Klarenbeek et al., 2010; Sandoo et al., 2011; Yoshida et al., 2014), while concomitantly lowering plasma noradrenaline levels (Yoshida et al., 2014). Of course, this is potentially confounded by a simultaneous reduction in disease, and therefore pain, in these patients, which was shown to contribute to lowering blood pressure (Klarenbeek et al., 2010). However, infliximab seems to produce a blood pressure reduction beyond this (Klarenbeek et al., 2010).

There is though some suggestion that anti-TNF therapy can actually induce hypertension, and a recent meta-analysis finds a higher incidence in of hypertension in rheumatoid arthritis patients treated in clinical trials with anti-TNF, compared to placebo (Zhao et al., 2015). Interestingly though, this meta-analysis did not include the aforementioned infliximab studies, and only one drug individually (certolizumab pegol) significantly increased incidence of hypertension; the others, most notably infliximab, did not. In addition to being an inflammatory mediator, TNF-α also acts at the kidney to promote natriuresis, and therefore inhibiting this may lead to volume retention. However, in essential hypertensives, as there may be a large extent of inflammatory-driven blood

pressure increase, inhibiting TNF-α might still have a potentially net beneficial effect on blood pressure, the reduction of inflammation outweighing the reduced natriuresis. In support of this, in the studies showing a reduction in blood pressure, some of the patients studied had previously-existing hypertension (Sandoo et al., 2011; Yoshida et al., 2014), while in the clinical studies used for the meta-analysis, only new development of hypertension was recorded (Zhao et al., 2015). TNF-α acts via two receptors: TNFR1 and TNFR2, and the former seems to mediate the natriuretic effects, while the latter more readily exerts the pro-inflammatory effects, as many studies involving genetic knockouts have shown; reviewed by Mehaffey and Majid (2017). This could explain the clinical discrepancies and dichotomy of results, and specifically targeting the TNFR2 could perhaps more selectively reduce blood pressure.

Anti-TNFα therapy is by far the best studied anti-'proinflammatory cytokine' therapy with regard to blood pressure, but secondary analysis of the recent CANTOS trial showed no effect of anti-IL-1β drug canakinumab on blood pressure in patients with history of MI or pro-inflammatory disease (Rothman et al., 2020). Likewise, a trial using anti-CCL2 therapy on prostate cancer patients showed no blood pressure changes (Pienta et al., 2013; Kenneth Pienta, personal communication). Interestingly, IL-6 blockade produced a hypertensive side effect in 3/19 patients in one clinical trial (van Rhee et al., 2015). A wide range of other anti-cytokine therapy clinical trials have been carried out, but despite attempts to communicate with those in charge, the author was unable to receive any correspondence with regard to unpublished blood pressure changes. More analysis in these trials on patients with concomitant hypertension needs to be performed.

Table 2| Summary of clinical trials testing anti-cytokine therapy and which recorded arterial blood pressure.

Target	Drugs	Studies	Patient group	Effect	Notes
TNF-α	Infliximab	Klarenbeek et al. (2010)	RA (n=128)	Greater SBP and DBP reduction than for conventional therapy.	BP reduction associated with reduction in disease severity, but infliximab produced a reduction beyond this
		Sandoo et al. (2011)	RA (n=23)	↓7.7 mmHg SBP and ↓5.1 DBP over 3 months	Only SBP effect significant vs placebo
		Yoshida et al. (2014)	RA (n=16); 7 had existing hypertension	↓7.3 mmHg 24-ambulatory SBP over 2 weeks of treatment	↓Plasma noradrenaline, significantly correlating with SBP decrease
	Various	Zhao et al. (2015)	RA (meta-analysis)	Anti-TNFα therapy associated with hypertension development	
		Grossman et al. (2017)	Various inflammatory rheumatic diseases (n=16)	No change in 24-hour ambulatory blood pressure changes	
IL-1β	Canakinumab	Rothman et al. (2020)	Prior MI & CRP ≥2 mg/l (n=10,061)	No reduction in incidence of HTN nor reduction in BP	
IL-6	Siltuximab	van Rhee et al. (2015)	Multicentric Castleman's disease (n=19)	3 cases of hypertension	
CCL2	CNTO 888	Pienta et al. (2013)	Metastatic castration-resistant prostate cancer (n=46)	No effect on BP	Personal communication from Dr Kenneth Pienta

Any blood pressure reductions demonstrated by anti-TNFα therapy are small however, and it seems unlikely that inhibition of one single mediator could reverse a complex pathology. A combination therapy targeting multiple pathways would probably be required for an effective disease-modifying effect in any case.

I.5.3 Influence of inflammation on the SNS

How do inflammation and sympathetic activity interact? In the central nervous system inflammation can reportedly raise sympathetic outflow directly, which can experimentally induce hypertension in the rat, while inhibition of microglial activation with minocycline can stop this (Wu et al., 2012), and can also reduce sympathetic tone, inflammation and blood pressure in the SHR (Santisteban et al., 2015). It is also well established though that sympathetic hyperactivity occurs at the level of the peripheral ganglia themselves in the SHR, which exhibit greater stimulation-evoked noradrenaline release (Shanks et al., 2013b, Bardsley et al., 2018b), and show increased firing responsiveness to a given electrical stimulus (Davis et al., 2020). In neuropathic pain (Scholz and Woolf, 2007) and post-MI (Zhou et al., 2004; Hasan et al., 2006; Wernli et al., 2009), inflammatory reactions induce states of local peripheral neuronal activity, mediated by cytokines and other neuronal growth factors. Perhaps similar mechanisms could occur in sympathetic ganglia during hypertension. Interestingly, following sensory nerve injury, macrophage-released IL-6 contributes to the sprouting of sympathetic nerve fibres into the dorsal root ganglia (Ramer et al., 1998), suggesting this classic inflammatory mediator (which is positively associated with blood pressure in humans (Fernandez-Real et al., 2001)) could produce sympathetic hyperactivity. This is further supported by the observation that IL-6 signalling allows cultured sympathetic neurons to survive even in the absence of otherwise essential factor NGF, albeit this required

addition of a very potent protein conjugate of IL-6 and part of the soluble IL-6 receptor (Marz et al., 1998). NGF itself is also involved in sympathetic neuron sprouting in both neuropathic pain (Scholz and Woolf, 2007) and post-MI (Zhou et al., 2004; Hasan et al., 2006; Wernli et al., 2009), so could be another potential mediator involved in hypertensive sympathetic activity. In the pre-hypertensive SHR itself, NGF levels have been shown to be higher than age-matched WKY rats, although surprisingly not in the heart (Ueyama et al., 1992).

I.5.4 Role of oxidative stress

Aside from cytokines, oxidative stress (which is to say the toxic effects of excess free radicals, namely reactive oxygen (ROS) and reactive nitrogen (RNS) species), is strongly related to inflammation and may go hand in hand in producing a state of hypertensive dysautonomia. Studies on the SHR (Zalba et al., 2000; Cecilia Alvarez et al., 2008) and some on human hypertensive patients (Rodrigo et al., 2013) have demonstrated elevated oxidative stress; in the case of the former reversal of oxidative stress lowering blood pressure (Zalba et al., 2000). What is the cause of this? Oxidative stress reflects an imbalance in the production of free radicals and the cellular anti-oxidant mechanisms which act to remove these. This may result from: radiation, xenobiotic exposure, or inflammation (Gagné, 2014), which increase the load of oxidant species, or a reduction in anti-oxidant defences, which seems to occur during ageing (Jackson & McArdle, 2011), such that damage from physiological ROS production accumulates. This could help explain the positive relationship between ageing, hypertension and inflammation (Buford, 2016).

Inflammation and oxidative stress appear to mutually enforce one another; activated inflammatory cells such as macrophages and neutrophils produce reactive oxygen species

during the respiratory burst reaction, while reactive oxygen species appear to be themselves inflammatory stimuli, for example by activating the inflammasome (Zhou et al., 2011) or inducing protein modifications which produce immune-reactive neo-antigens (Kirabo et al., 2014). Oxidative stress can also elevate sympathetic tone; in the SHR ROS-induced mitochondrial dysfunction occurs in the rostral ventolateral medulla (RVLM; the main sympathetic outflow nucleus) (Chan et al., 2009), with a number of potential mechanisms suggested, including an increase in membrane calcium current (Annunziato et al., 2002). Moreover, induction of central nervous system inflammation with LPS induces RVLM oxidative stress, which leads to sympathetic hyperactivity and hypertension (Wu et al., 2012). A similar impairment of mitochondrial dysfunction is postulated to occur in the stellate ganglion (Li & Paterson, 2016), where it may impair sympatho-inhibitory nitric oxide signalling (Li et al., 2013); however, this causative role of oxidative stress remains to be confirmed.

I.5.5 Modulation of inflammatory processes by sympathetic input

In turn, the SNS influences inflammation, through direct inputs to lymphoid organs and the presence of adrenoreceptors on leukocytes. This neural output has influence on immune cells as it can produce a variety of immunomodulatory signals, of both pro- and anti-inflammatory natures, which depend to a great extent on the pre-existing immune status of the environment being innervation (Kenney & Ganta, 2014). In hypertension though, sympatho-immune interactions have been repeatedly shown to increase leukocyte production of inflammatory cytokines, and to promote mobilisation of these cells into target organs such as the kidney (Rodriguez-Iturbe et al., 2017). Most of this evidence comes from models of angiotensin II-induced hypertension though (Rodriguez-Iturbe et al., 2017), and this mediator is known to directly increase SNS activity, and therefore the

model may reflect more of a secondary hypertension. In the SHR, there are reportedly increased numbers of blood and bone marrow T cells (Zubcevic et al., 2014; Santisteban et al., 2015) and monocytes (Santisteban et al., 2015), and a concomitant lower number of endothelial progenitor cells (Zubcevic et al., 2014; Santisteban et al., 2015), compared to WKY rats. While this is associated with heightened sympathetic input to the SHR bone marrow, denervation does not substantially reverse this, whereas it does increase endothelial progenitor cell and decrease T cell numbers in the WKY (Zubcevic et al., 2014).

It would thus seem that the immune and SNSs are two key, mutually-reinforcing nodes in hypertensive pathophysiology, and therefore targeting their interaction could have a profoundly beneficial effect therapeutically. Ameliorating the inflammatory component in hypertension is likely to improve pathology in a variety of bodily loci; however, if it drives sympathetic hyperactivity, this may be the most important effect, particularly as this neural component influences the other loci so widely. Work on hypertensive neuroinflammation has hitherto focussed on the central nervous system, but repairing this source of heightened sympathetic outflow may prove futile if the downstream peripheral ganglia themselves are pathologically hyperactive. Therefore, immune interactions with sympathetic ganglia in hypertension are a crucial area of investigation, where if these produce pathological dysautonomia, therapeutic intervention could prove very effective.

In the SHR at 6 weeks of age in the study of Santisteban et al. (2015) it is possible that chronic bone marrow sympathetic activity has already altered the bone marrow inflammatory phenotype to the point of irreversibility, or it could be the case that the inherent difference between the strains originally arises within the bone marrow rather

than the nervous system. In support of this, bone marrow cross-transplants between SHR and WKY shift the leukocyte phenotype towards that of the donor (Santisteban et al., 2015). Furthermore, parasympathetic input to splenocytes seems to be anti-inflammatory in the WKY, whereas nicotine application instead promotes inflammatory cytokines responses in SHR splenocytes to toll-like receptor activation (Harwani et al., 2012). It would be interesting to examine whether their inflammatory response to adrenergic stimulation is enhanced. Regardless of where the SHR phenotype arises originally though, both the SNS and inflammation would seem to mutually enforce one another in hypertension, creating a vicious cycle which propagates the haemodynamic pathology.

I.6 Hypothesis and aims of this thesis

The main hypothesis was that a pathological immune system reaction within the sympathetic ganglia of pre-hypertensive animals drives local neuronal hyperactivity. This postulated aetiology of essential hypertension is summarised in Figure 5, along with the nodes at which therapeutics may intervene. The aims were thus as follows:

1. To investigate the immunological cellular and mediator environment of the SHR stellate ganglia.
2. If such an inflammatory phenotype exists, to identify the cause of this phenomenon.
3. To test whether local inflammation increases sympathetic neuron activity.

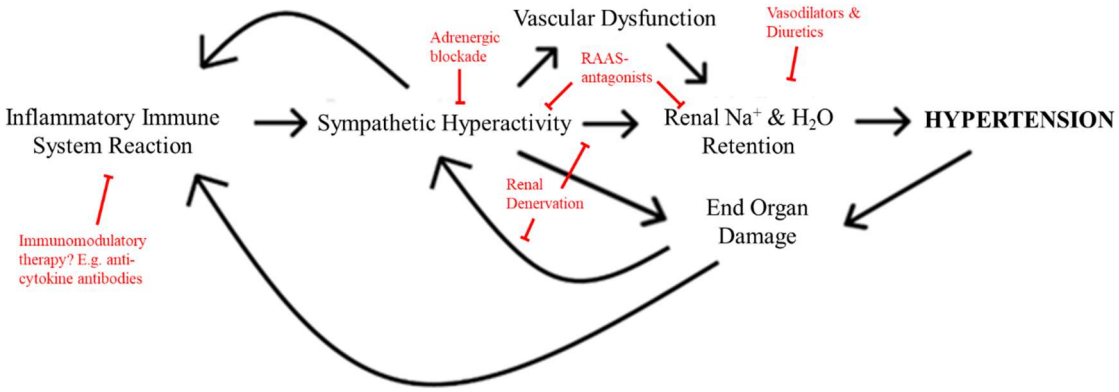

Figure 5| Hypothesised pathophysiology of essential hypertensive genesis, at least in a sizeable proportion of individuals. Areas of therapeutic intervention are shown in red, with pathways they inhibit indicated in each instance.

CHAPTER II

Methods & Materials

II.1 Animals

The sole laboratory animal species used in this work was the rat (*Rattus norvegicus*), the uses of which complied with the University of Oxford Local Ethical Guidelines and the Animals (Scientific Procedures) Act 1986 of the United Kingdom. These rats were purchased from Envigo, UK and housed in the local Biomedical Services Building or departmental holding room prior to experimental use. The keeping and use of these animals was covered by the UK Home Office Project Licence (PPL) of Prof. David J. Paterson: 30/3031 and P707EB251. The animals were housed in groups of approximately 2-6 in individually-ventilated cages (IVCs) under conditions of 20-24°C air temperature, 55% humidity, and a 24-hour day/night lighting cycle. The cages were supplied with standard rat chow and water (for the rats to consume *ad libitum*) in addition to woodchip, Sizzlenest, and an enrichment item.

Rats were principally used to provide a variety of tissues, on which *in vitro* experiments were later performed. These animals were culled in three main ways. One method was intra-peritoneal injection of an overdose of pentobarbital (under isoflurane anaesthesia), followed by exsanguination by jugular vein dissection, according to Schedule 1 of the Animals (Scientific Procedures) Act 1986 of the United Kingdom. For some experimental purposes, tissue manipulation was required to be carried out on the rats under terminal anaesthesia, before death occurred. One of two UK Home Office licensed procedures were performed to this effect, under protocol 19 (b) ii of the project licence P707EB251: "animals may be killed be perfusion fixation under terminal general anaesthesia (AC) at the designated establishment". In some animals the thoracic cavity was opened, a cut made in right cardiac atrium, and then 50-100 ml of cold PBS containing 10 U/ml heparin (as an anti-coagulant) was perfused via a needle into the ventricles, in order to flush blood

out of the vasculature. To obtain purer blood samples, for cell culture, in other rats the skin was removed from the thorax and a 23G needle, attached to a syringe containing ~100 µL anti-coagulant EDTA solution (100 mM), was inserted between the ribs and into the heart, and blood was withdrawn.

II.2 Animal models of sympathetic dysautonomia

A number of models can be used to study sympathetic dysautonomia, the advantages and limitations of these being listed in Table 1.

Table 1| Animal models of essential hypertension.

Model	Advantages	Limitations	References
Spontaneously hypertensive rat (SHR)	Wealth of literature published using this model, which seems to phenocopy human hypertensive dysautonomia	Genetic form of hypertension may be different to the human disease and occurs earlier in equivalent age, and SHRs also display attention deficit hyperactivity disorder (ADHD) (Sagvolden et al., 2009), a potential confounder	Okamoto & Aoki (1963)
Spontaneously hypertensive mouse	Mice are the most widely used laboratory mammal so reagents widely available, potential for further genetic manipulation	Genetic form of hypertension may be different to the human disease, and this model has not been widely studied	Schlager & Sides (1997); Davern et al. (2009)
Guizhou mini-pig	Larger mammal so closer to human and tissues easier to isolate, responsive to renal denervation	Relatively new so poorly studied, lacks wide accessibility	Li et al. (2016)

Transgenic mouse-lines such as: $\alpha2a^{-/-}$, $\alpha2c^{-/-}$, or α2b central nervous system overexpression	Mice are the most widely used laboratory mammal so reagents widely available, potential for further genetic manipulation	Sympathetic hyperactivity is mono-causal and different in mechanism to the human condition	$\alpha2a^{-/-}/\alpha2c^{-/-}$: Brum et al. (2002) α2b: Kintsurashvili et al. (2009)
Large mammal induced heart failure (multiple methods)	Larger mammal so closer to human	Technical difficulties, monocausal sympathetic hyperactivity and subject to rigorous ethical approval	Many
Large mammal induced myocardial infarction, for example porcine or ovine	Larger mammal so closer to human and tissues easier to isolate, myocardial infarction reflective of human post-MI dysautonomia	Technically challenging, expensive, and subject to rigorous ethical approval	Porcine: Vaseghi et al. (2017) Ovine: Jardine et al. (2005)
Human patients	Reflects the actual disease process	Heterogeneous population, ethical limitations on invasive study	Many

The spontaneously hypertensive rat (SHR) (Okamoto and Aoki, 1963) was chosen for use in this thesis because it is well-studied, recapitulates human dysautonomia and is a model of essential hypertension, the main focus of this study of sympathetic dysautonomia. These rats develop blood pressure elevation at approximately 4-6 weeks of age (Dickhout & Lee, 1998), though as this is before rat adulthood (Sengupta, 2013), it begins much earlier than tends to be the case for human essential hypertension, a potential limitation of the model.

SHRs were mainly used in this thesis at the age of 3-4 weeks, at which there are no haemodynamic changes (although sympathetic hyperactivity is already present (Dickhout and Lee, 1998, Li et al., 2012)) in order to avoid any confounding effects of systemic blood pressure elevation on the tissue under study. Such animals may thus be termed: pre-SHRs. A small number of 5-6 week old, and 12-18 week old SHRs were also studied to allow for findings to be confirmed in sustained hypertension (Dickhout & Lee, 1998) and early adulthood (Sengupta, 2013). SHR cells and tissue was compared to those of its background strain, the Wistar rat, at equivalent ages.

II.3 Human patients

Use of human blood was approved by the management team of the Oxford Biobank, whose work has received approval from the South Central - Oxford C Research Ethics Committee. Volunteers from the Oxford Biobank were recruited into two age-, sex- and BMI-matched groups:

A) Existing formal diagnosis of hypertension made by a doctor[4]
B) BP ≤120/80 mmHg on visit to clinic AND no previous clinical diagnosis of hypertension

These criteria were chosen to provide two distinct populations; one of which had existing hypertension, and the other which had evidence of pre-hypertension, to enable a more powerful comparison of hypertensive patients with controls. The blood pressure of these individuals was measured three times by a research nurse on their visit, after which they

[4] The NICE Guidelines use a clinic-measured blood pressure of ≥140/90 mmHg, and home or ambulatory blood pressure of ≥135/95 mmHg (NICE, 2019).

donated ~2 ml of blood. This was collected by venepuncture and anti-coagulated with heparin, before being stored on ice until processing.

II.4 Cell and tissue culture

II.4.1 Sympathetic ganglion dissection

Rat stellate ganglia were located bilaterally towards the posterior of the thoracic cavity, and the superior cervical ganglia (SCGs) were dissected from the separated heads of each animal, located in close apposition to the carotid bifurcation on each side. The paired coeliac ganglia were identified fused together along with the single superior mesenteric ganglion, encircling the coeliac arterial trunk. As these ganglia are fused and impossible to discern individually, the whole structure was excised and used experimentally, and therefore this is referred to as the coeliac/superior mesenteric ganglia (CG/SMGs). The anatomical organisation of all rat sympathetic ganglia is depicted in Figure 1.

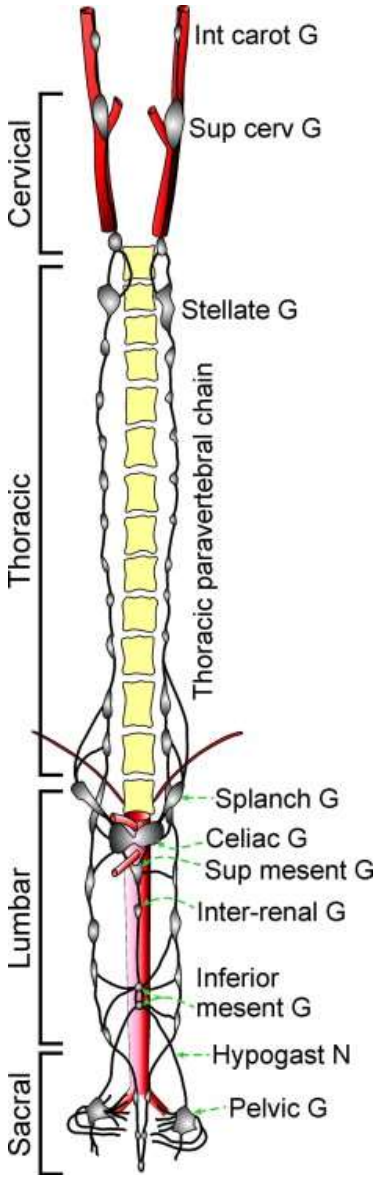

Figure 1| Anatomy of the rat sympathetic ganglia from Furness (2015); used with permission from Elsevier.

All ganglia were excised, placed into L-15 medium (Thermofisher or Merck, both US) on ice, and cleaned of all contaminating non-neuronal tissue, under a microscope. The thin layer of connective tissue which envelopes each one was carefully removed, using fine forceps, to as great an extent as possible.

II.4.2 Single neuron culture from sympathetic ganglia

Cleaned ganglia were cut into ~6 pieces each before enzymatic digestion in collagenase IV (1 mg/mL in L-15) for 25 min, followed by trypsin (2 mg/mL in Ca^{2+}- and Mg^{2+}-free Hank's Balanced Salt Solution; Merck or Thermofisher, both US) for 30 min; both at 37°C. Digested ganglia were then washed in blocking medium (Table 2) at room temperature, twice for 5 min each. Next, the ganglia were mechanically triturated in complete medium (Table 3) using two glass Pasteur pipettes in series, the second, fire-polished to narrow the opening. The resultant single-cell suspension was plated onto poly-D-lysine (0.1 mg/ml; Merck, US) and laminin- (0.048 mg/ml; Thermofisher, US) coated 6 mm glass coverslips in 4-well culture plates. These were incubated at 37°C under 5% CO2 for ~48 h prior to experimentation.

Table 2| Composition of blocking medium for stellate neuron culture.

Blocking Medium Component	**Concentration or percentage of total volume**
Neurobasal Plus (Thermofisher, US)	Base
Heat-Inactivated Foetal Bovine Serum (Thermofisher, US)	10%
Penicillin, Streptomycin (Thermofisher or Merck, US)	100 U/ml, 100 µg/ml

Table 3| Composition of complete medium for stellate neuron culture.

Complete Neuronal Medium Component	**Concentration or percentage of total volume**
Neurobasal Plus	Base
B-27 Plus Supplement (Thermofisher, US)	2%
GlutaMAX (Thermofisher, US)	1.5 mM[5]
2.5S NGF (Merck, US)	5 ng/ml
Penicillin/Streptomycin	50 U/ml, 50 µg/ml

II.4.3 Whole stellate ganglion explants

The culture of whole rat stellate ganglia was performed using a protocol adapted from that used by Pirzgalska et al. (2017) for mice. Cleaned ganglia were placed into sterilisation medium (Table 4), to reduce the chance of bacterial contamination, before being plated onto 8-well tissue culture chambers previously coated with poly-D-lysine (0.1 mg/ml). Next, 10 µL of Matrigel (Corning Life Sciences, US) was layered on top of the ganglia, covering them completely, and the plates were incubated at 37°C for 7 min. Finally, 1 mL of stellate explant culture medium (Table 5) was added to each well. The concentration of NGF used is the minimum required to sustain sympathetic neuron survival (Greene, 1977), to enable the effects of additional stimulatory treatments on neuronal activity to clearly be observed. The ganglia were returned to an incubator at 37°C under 5% CO_2 and left for ~48 hours before being used for experiments.

[5] The B27 Plus supplement at 2% provides an overall concentration of 0.5 mM Glutamax; so additional Glutamax was added to provide a final concentration of 2 mM.

Table 4| Composition of sterilisation medium for blood co-culture with stellate explants and neurons.

Sterilisation Medium Component	**Concentration or percentage of total volume**
Dulbecco's Modified Eagles Medium (Thermofisher, US)	Base
Heat-Inactivated Foetal Bovine Serum	10%
Penicillin, Streptomycin	100 U/ml, 100 µg/ml

Table 5| Composition of culture medium for stellate explants.

Stellate Explant Culture Medium	**Concentration or percentage of total volume**
Dulbecco's Modified Eagles Medium, without phenol red (Thermofisher, US)	Base
Heat-Inactivated Foetal Bovine Serum	10%
GlutaMAX	2 mM
2.5S NGF	5 ng/ml
Penicillin, Streptomycin	50 U/ml, 50 µg/ml

For some experiments ganglia were co-cultured with blood-derived leukocytes. These were prepared from blood samples taken from 3-4 week old Wistar rats and SHRs by transthoracic cardiac puncture, as detailed in Chapter II.1. Using this method, 1-2 ml of fresh blood could be obtained per 3-4 week old animal. 1 mL of each sample was added to 10 ml of eBioscience red blood cell lysis buffer (Thermofisher, US) as per the manufacturer's instructions, and incubated at room temperature for 10 min on a shaker. To arrest the reaction, 10 ml of DMEM containing 10% FBS was added to each sample

and the suspensions were centrifuged at 400 rcf for 4 min to obtain a pellet. Blood cell suspensions were then either depleted of monocytes using clodronate liposomes, according to a protocol developed by Claassen et al. (1990), or incubated with PBS-containing liposomes as a control. The pellets were resuspended in the ganglionic culture medium containing either 100 µl Clodrosomes, or the same concentration of the control liposomes, and incubated at 37°C for 1-2 h. After this the cells were pelleted and resuspended in fresh ganglionic culture medium and this suspension was used to culture the ganglionic explants. The products of each original 1 ml blood sample were resuspended in 2 ml of such medium; this being split across two ganglia so that each ganglion received approximately the number of leukocytes derived from 0.5 mL of rat blood. SHR blood may contain a higher concentration of leukocytes than that of Wistar rats (Burba-Anczewska, 1978, Schmidschonbein et al., 1991, Reed and Hendley, 1994), so this difference would therefore be incorporated in the culture conditions of ganglia treated with blood from each respective strain.

II.4.4 Bone marrow-derived macrophages (BMDMs)

The following protocol was adapted from Muschter et al. (2015) and a laboratory protocol of the Greaves group, University of Oxford, for mouse BMDM culture. Tibiae and femurae were extracted from 3-4 week old Wistar rats, cleaned of soft tissue and stored in PBS at 4°C for up to 24 hours. These were then sprayed with 70% ethanol and one at a time the ends of each bone were cut off with a scalpel. A syringe and 25 G needle were used to flush out the bone marrow into a petri dish, using ~6 ml cold PBS. The combined effluent from all bones was then passed through a 70 µm filter and collected in a 50 ml falcon tube, before being centrifuged at 300 rpm for 5 min. The cell pellet was resuspended in complete BMDM media (4 ml/bone, Table 6). The cells were plated on

10 cm petri dishes, 8 ml per dish, and incubated at 37°C/5% CO2. Four days later half the media was removed and replaced with fresh BMDM. Two days after this, all media was removed and the plates washed with PBS, before ~4 ml TrypLE (Thermofisher, US), or EDTA (2 mM in PBS; Merck, US where cells were being processed for flow cytometry) was added to each. After 3-4 min once the cells had detached the suspension was removed and combined with an equal volume of α-MEM + 10% FBS media, and this was then centrifuged at 300 rpm for 5 min. Cells were then plated onto the required format, for example, 6 mm glass coverslips, re-suspended and prepared for flow cytometry, or washed in PBS before being once again pelleted and flash-frozen in liquid N_2 prior to RNA extraction.

Table 6| Composition of complete BMDM medium.

BMDM Medium Component	**Concentration or percentage of total volume**
Alpha-Minimum Essential Medium, nucleosides (Thermofisher, US)	Base
Heat-Inactivated Foetal Bovine Serum	10%
Recombinant Rat M-CSF (Abcam, UK)	20 ng/ml
Penicillin, Streptomycin	100 U/ml, 100 µg/ml

II.4.5 Sympathetic neuron co-cultures

Co-cultures of stellate neurons and blood leukocytes or BMDMs were prepared on 6 mm poly-D-lysine/laminin-coated coverslips. For leukocyte co-culture, stellate neurons were prepared in the same way as for their solitary culture, but in half the normal volume of medium. Blood leukocytes, prepared in the same way as described above for culture with whole ganglia, with either clodronate or PBS-filled liposomes (Encapsula Nanosciences,

US), were then added to the neurons in an equal volume of neuronal culture medium. To separate these cells from the liposomes, after the incubation 10 mL of Neurobasal plus containing 21.5% Optiprep (Merck, US) was added to each mL of cell suspension, and the mixture centrifuged at 400 g for 15 min with no brake. The liposomes floated to the top while the cells formed a pellet at the bottom. These were resuspended in neuronal culture medium. Each mL of blood provided leukocytes for three wells of four 6 mm coverslips.

In the case of BMDM co-culture, the neurons were once again plated in half the normal volume of culture medium, and day 6 harvested BMDMs were added to this in the same volume of media, but containing 40 ng/ml M-CSF, to produce a final concentration of 20 ng/ml (Table 7). These BMDMs had been previously cultured in 10 cm dishes at a density of 2 bones per dish, and were plated at an approximately equivalent density, adjusting for well surface area.

All co-culture preparations were incubated at 37°C, 5% CO_2 for 48 hours before imaging.

Table 7| Composition of neuronal BMDM co-culture medium.

Sympathetic Neuron-BMDM Co-Culture Medium Component	**Concentration or percentage of total volume**
Neurobasal Plus	Base
B-27 Plus Supplement	2%
GlutaMAX	1.5 mM
2.5S NGF	5 ng/ml
Penicillin, Streptomycin	50 U, 50 µg/ml
Macrophage Colony Stimulating Factor	20 ng/ml

II.5 Flow cytometry and cell sorting

Flow cytometry is a technique whereby lasers are used to measure physical properties of cells (generally, although other small particles, such as liposomes, may be used) in a high-throughput manner (Shapiro, 2003). A flow cytometer machine pumps a suspension of cells into the centre of a surrounding, faster-moving stream of 'sheath fluid', which is used to channel the cellular suspension into a single-file stream; a process known as hydrodynamic focussing. The stream is then passed in front of one or multiple lasers, allowing each cell to be analysed individually. The scattering of light by each cell is recorded in both the forward direction (forward-scatter; FSC), providing an index of cell size, and at 90° to this (side-scatter; SSC), giving an index of cell granularity/complexity. The fluorescent emission of each cell, at a variety of chosen wavelengths, after excitation by a selection of lasers, is also able to be recorded, the use of specific antibodies or dyes thus allowing determination of antigen expression or other biological properties of a cell.

Each time a particle passes in front of the lasers, its desired parameters are recorded, as an 'event'. The most commonly-used method of recording is a photomultiplier tube (PMT) which converts the scattered or emitted photons into a proportional voltage pulse. This proportionality is adjusted such that the recorded voltages fall within an optimal range of sensitivity.

II.5.1 Compensation

Even though flow cytometry uses lasers at specific excitation wavelengths, and filters defining a small range of emission wavelengths, fluorophores display relatively broad spectra of emission/excitation light. For this reason, a source of noise is introduced when one uses multiple fluorophores in a flow cytometry panel; fluorophores may be excited slightly by a different laser, or may emit light that passes through other filters. While this

can be reduced by selecting fluorophores at opposite ends of the excitation/emission spectra, a small amount of overlap may still exist, and when using a large number of fluorophores, spacing between spectra becomes impossible, especially when there are limitations on those commercially available.

To remove the influence of this multi-channel spill-over, a process known as ‘compensation’ must be performed. Briefly, this involves measuring the percentage of overlap between every pair of fluorophores in a panel, then performing a computational algorithm to make adjustments for this in the subsequent analysis. To do this, samples each labelled with only one of the fluorophores in the panel (single-colour compensation controls) are run through the flow cytometer one-by-one, under the same settings as the experimental samples, to record spill-over into every other channel. For this purpose, purposefully-designed antibody-binding compensation beads are commercially available. Naturally compensation is most accurate when there is minimal fluorophore overlap, so antibody panels are designed to leave as must space as possible, and those channels on the same laser or similar filter sets are set to the same voltage. Single-colour compensation is illustrated in Figure 2 and elegantly reviewed by Roederer (2002).

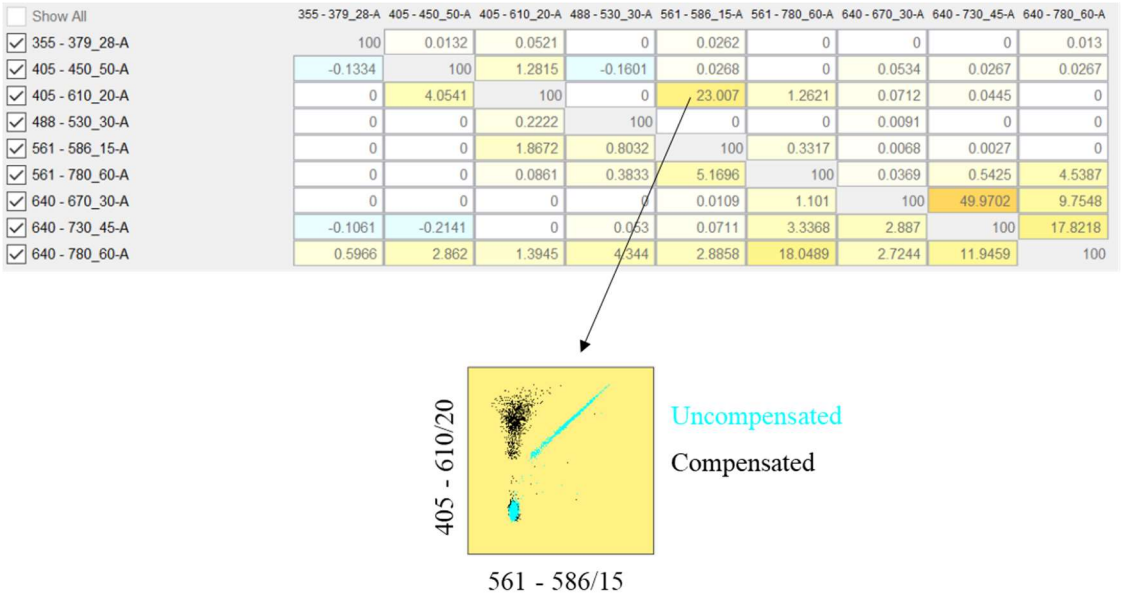

Figure 2| Process of single-colour compensation. The upper panel display the matrix formed by the percentage spill-over between each possible pair of fluorophores. The plot for the single-stained 405 - 610/20 compensation sample showing intensity in the 405 - 610/20 and 561 - 586/15 channels is shown as an example; with the uncompensated and compensated data overlaid. This single colour compensation sample only expresses the fluorophore of the 405 - 610/20 channel, but the uncompensated data show positivity in the 561 – 586/15 channel. This shows the characteristic positive correlation relationship; as an event's positivity in the original channel increases, so does its intensity in the other, suggestive of spill-over. The compensated plot shows little-to-no positivity in the 561 - 586/15 channel.

II.5.2 Gating

Examining the recorded values for each event within the desired parameter, one can attempt to identify distinct populations of cells from a heterogeneous mixture. The voltages produced by each event however lie on a continuous scale, so in order to fit these to discrete populations of cells, thresholds must be defined around a range of desired values; these are known as 'gates'. To reduce the degree of subjective arbitration, unstained samples may be used to first define negative populations, with anything having a higher intensity defined as positive. In many cases these 'unstained' samples are incubated instead with an isotype control antibody, which matches all properties of the

staining antibody, except that it is specific to an antigen not expressed by the population in question. This helps control for non-specific binding.

An improvement on this approach however, is the use of fluorescent-minus-one (FMO) controls. Although compensation greatly reduces the influence of one fluorophore over another, due to fundamental and unavoidable limitations in the mathematical method, a small impact of fluorescent spill-over remains. Originally, two uncompensated channels will have a linear relationship; an increased intensity in one, will lead to a proportional increase in that of the other due to spill-over. The compensation algorithm is only able to reduce the linear relationship occurring between two channels, x and y: $y = mx$, where m is the constant of proportionality, into a relationship to $y = m\sqrt{x}$. By recording data from samples stained with every fluorophore except a given one, an FMO control, one can control for this remaining spill-over; the population of events recorded in a given channel's FMO control is the true negative for that channel in the context of a particular experiment (Figure 3). Put simply an FMO control is a stricter negative control as it has fewer differences to the fully-stained experimental sample, than does an unstained one (Roederer 2002).

Finally, another general gate essential for any cellular flow cytometry is one for doublet-discrimination. Two (or theoretically more) cells may occasionally pass in front of the laser overlapping, producing a combined voltage peak. This joint event does not provide useful information as any positivity of one cell will produce positivity, possibly incorrectly, for the pair. In order to remove these, one must make a comparison between two of the: area, height or width of the voltage pulse for FSC or SSC of each event. Doublets will have an increased width relative to the area or height of their voltage pulse,

allowing these to be gated out. In this thesis, doublet discrimination was performed using FSC-A/FSC-H plots, as shown in Figure 4.

II.5.3 Fluorescence-activated cell sorting

A technical extension of flow cytometry is its use to physically separate out and collect cells falling into defined populations in real time: known as fluorescence-activated cell sorting (FACS). The process begins with simple flow cytometry, but electrical charges are applied to selected populations, allowing them to be deflected differentially by electrostatic plates into separate collection tubes.

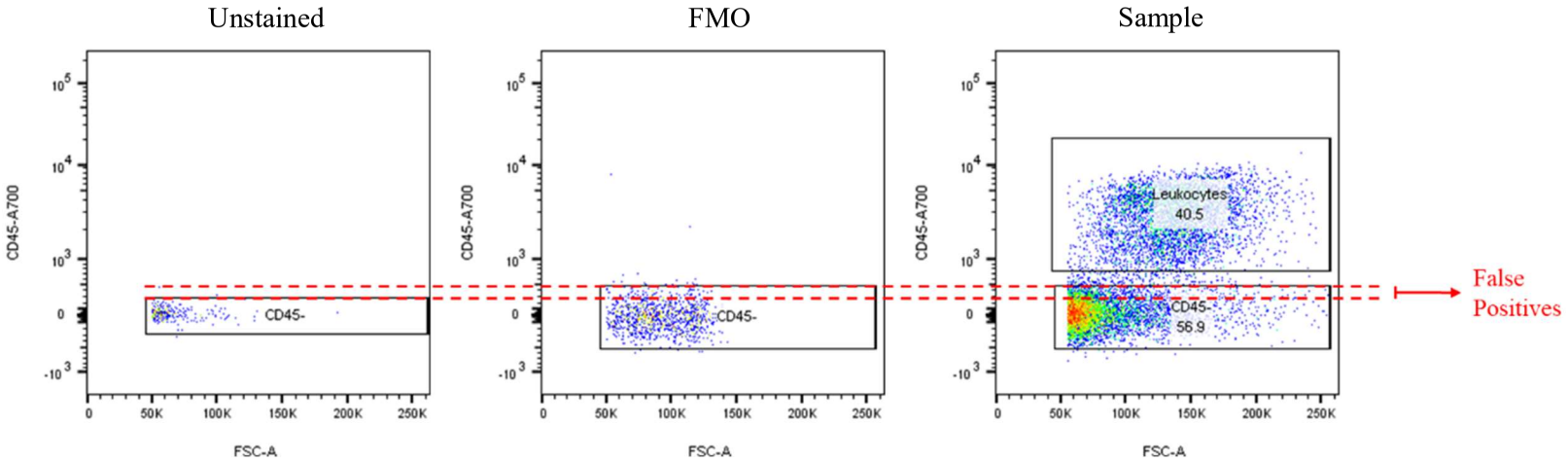

Figure 3| Principle of using fluorescent minus one (FMO) controls for gating. Using the negative gate of the unstained sample leaves an interval of false positives which are excluded by the gate drawn using the FMO control.

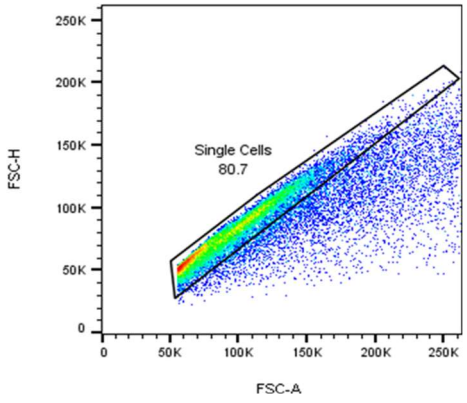

Figure 4| Doublet discrimination gating using FSC-A versus FSC-H. The single cells form a band around approximately the line y=x; doublets appear below this line as they express a larger FSC-W (the other component of FSC-A) for a similar FSC-H.

II.5.4 Methodology

II.5.4.a Sample Preparation

All rat tissue samples were first prepared for subsequent staining and flow cytometric analysis or sorting. In the case of sympathetic ganglia, the cut ganglion pieces underwent simultaneous enzymatic digestion in HBSS with hyaluronidase (1000 U/ml), collagenase II (1 mg/ml) and DNase I (5 U/ml) for 30 min at 37°C. Subsequently these were centrifuged at 400 rcf for 4 min, the supernatant was discarded, and then the tissue was mechanically triturated in 1 ml PBS using two glass Pasteur pipettes in series, the second fire-polished to narrow the opening.

Heparinised blood samples, obtained during cardiac perfusion, were passed through a 70 μm filter and centrifuged at 400 rcf for 4 min. Next these were resuspended in ~10 ml red blood cell lysis buffer and left at room temperature for 10-15 min, before the reaction was stopped by addition of an equal volume of FACS buffer, and the whole suspension was centrifuged again at the same settings as before. The pellet was then resuspended in PBS, spun down at 400 rcf for 4 min once more, before a final resuspension in fresh PBS. For experiments in which monocyte-macrophages were to be isolated by FACS, blood samples were instead obtained from rats by cardiac puncture under terminal anaesthesia, with EDTA used as the anti-coagulant; described above (Chapter II.1). These samples were otherwise processed in the same way as those obtain from cardiac perfusion.

Renal tissue was prepared for flow cytometry using a protocol adapted from Rubio-Navarro et al. (2016). Pairs of kidneys were stripped of their capsules by hand, the hila were removed. The remaining renal tissue was finely cut up using scissors and then pushed through a 40 μm filter using the plunger from a 10 ml syringe, the resultant pulp being washed through with 15 ml of FACS buffer. The filtered suspension was

centrifuged at 400 rcf for 4 min and resuspended in ~15 ml red blood cell lysis buffer, which was left at room temperature for 90 s, before lysis was terminated by dilution with 15 ml of FACS buffer. The solution was centrifuged under the same settings as before, resuspended in 10 ml PBS, and 1 ml of this was taken forward for analysis.

BMDMs were prepared for flow cytometry after their harvest on day 6 of their culture protocol. Harvested cells were washed once in PBS, before the staining process commenced.

Human blood samples, obtained via the Oxford Biobank, first treated with red blood cell lysis buffer; 1 ml of the heparinised blood was added to 10 ml of buffer and incubated for 15 min. The solution was then passed through a 70 μm filter, combined with an equal volume of FACS buffer, and centrifuged at 400 rcf for 4 min, before washing and resuspension in PBS. The PBS cell suspension was then diluted 1:2 in more PBS, and 1 ml PBS containing half the total quantity of cells was taken forward for staining.

II.5.4.b Staining

The resultant single-cell suspensions were stained with 0.5 μL eBioscience™ Fixable Viability Dye eFluor™ 780 (Thermofisher, US) for 30 min at 4°C, and then 1 ml of FACS buffer was added, and the suspension centrifuged at 400 rcf for 4 min to wash off the dye. The cells were next incubated for 10 min in anti-rat CD32 (1:100 in FACS buffer) at 4°C to prevent FcR-mediated antibody binding, prior to incubation for 30 min in appropriate panel of fluorescently-tagged flow cytometry antibodies.

In the case of human blood samples, these were fixed after the 30 min antibody staining, to minimise their potential infectious risk. The cells were washed once in FACS buffer,

once in PBS, then resuspended in 200 µL 2% PFA (in PBS) for 15 min, before washing and resuspension in FACS buffer once more.

II.5.4.c Cytometry and Sorting

For simple flow cytometry, a BD LSRFortessa™ X-20 was used, equipped with 5 lasers, and a total of 18 filter sets, each corresponding to an emission wavelength on a specific laser (Figure 5). For FACS of classical and non-classical monocytes from rat stellate ganglia and blood, the samples were run through a BD FACSAria™ III Cell Sorter. Single colour controls were prepared using compensation beads according to the manufacturer's instructions, and FMO controls were also used for each antibody panel to aid gating. Data were later processed using FlowJo 10 software.

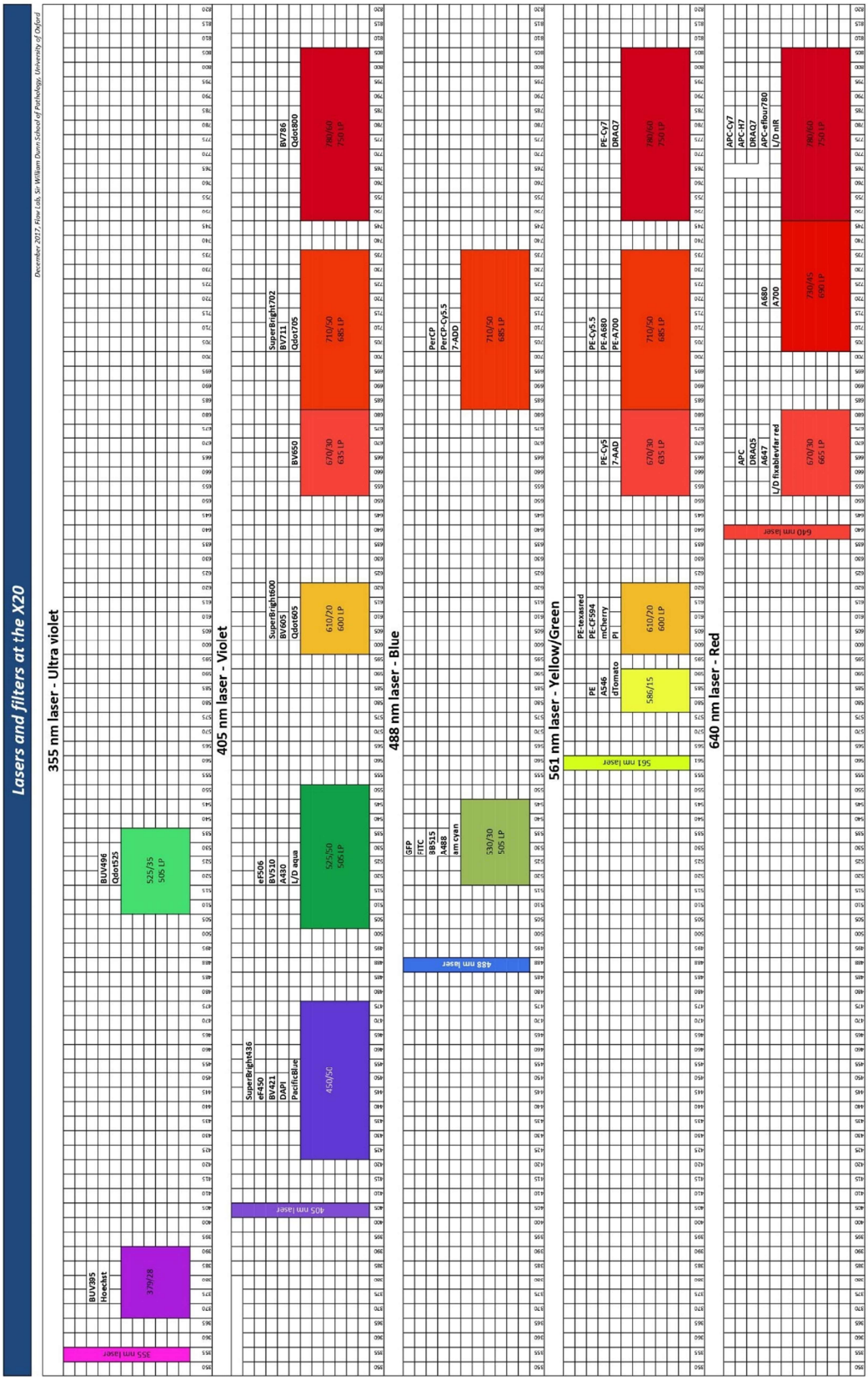

Figure 5| Lasers and filter sets of the BD LSR Fortessa X20 used for flow cytometry experiments in this thesis. Image credit to Michal Maj, Flow Cytometry Facility, Sir William Dunn School of Pathology, University of Oxford.

II.6 Immunohisto-/immunocytochemistry

The terms immunohistochemistry and immunocytochemistry essential refer to the same process (Figure 6), except that the former is performed on pieces of tissue (*histo-* = tissue), while the later refers to individual cells (*cyto-* = cells), for example in culture[6]. Both of these involve using labelled antibodies to detect the presence (or absence) of a target antigen within a tissue/cellular sample, and the principle was first demonstrated in 1942 by Coons et al. (1942). This study used a fluorescently conjugated antibodies to recognise *pneumococci* bacteria, which may be referred to as *direct* immunocytochemistry, as the primary antibody is conjugated to the stain. *Indirect* immunocytochemistry, which involves an unstained primary antibody against the target, and subsequent detection of this by a conjugated secondary anti-immunoglobin antibody, is now more commonly used, due to the amplification of signal as multiple labelled secondary antibodies can bind to each bound primary one.

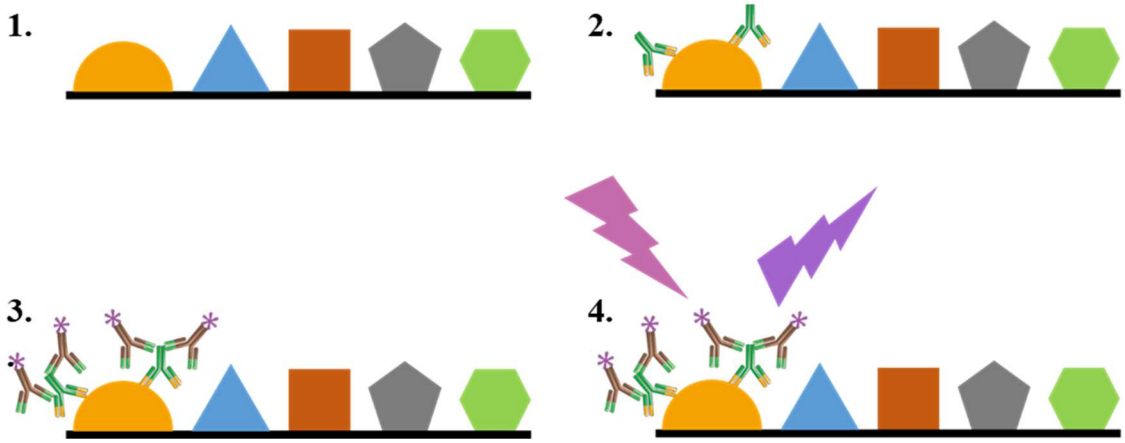

Figure 6| The principle of immunocytochemistry. 1. Different antigens are present in a sample. 2. Specific primary antibodies bind to the desired antigen. 3. Secondary antibodies recognise the primaries. 4. Conjugate of secondary antibody reveals the presence of the antigen; in this case a fluorophore is depicted. (Brandtzaeg, 1998). Antibody images are re-coloured versions of "Labeled Antibody" from Servier Medical Art (smart.servier.com) by Servier, which is licensed under a Creative Commons Attribution 3.0 Unported License (https://creativecommons.org/licenses/by/3.0/).

[6] In the remainder of this section (Chapter II.5), for brevity, the term *immunocytochemistry* will be used to cover both terms.

In preparation for staining, tissues or cells need to be fixed in order to stabilise the biological architecture of the sample, particularly if they are to be later permeabilised. Tissues are then sectioned, which is generally performed either when embedded in paraffin, or a specific cryosectioning medium. Intracellular antigens necessitate permeabilisation of the cells or tissues with a detergent to disrupt the plasma membrane. Finally, serum or bovine serum albumin is used to *block* the sample and reduce later non-specific binding of the primary antibody.

II.6.1 Methodology

Clean stellates were immersed in cold 4% PFA (Alfa Aesar, US) and stored at room temperature on a rotator for ~1-2 h; spleens were incubated in the same solution overnight. For cryoprotection, the tissues were transferred to 15% sucrose (Merck, US) in PBS solution for ~6-12 h, or until the tissue had sunk, and subsequently put into 30% sucrose for the effect. The tissue was then embedded in OCT and stored at -20°C as required. 20 µm sections were cut on a cryostat, transferred to microscope slides, and returned to -20°C for further storage. In the case of cell culture staining, neuron and macrophage co-cultures were plated directly onto 35 mm glass-bottomed dishes, before fixation for 15 min in 2% PFA.

For staining, microscope slides were thawed in room temperature PBS and then the tissue circled with a PAP pen. The sections or cell-containing dishes were then incubated in a PBS-based blocking and permeabilisation solution (Table 8), for 1 hr, before incubation in primary antibody solution overnight at 4°C in a humid box. The following day the stained slides/dishes were washed three times each for 5 min in PBS and then incubated in secondary antibody and DAPI for 1 hr at room temperature. Finally, the samples were washed three times for 5 min in PBS once again, prior to mounting using ProLong™ Gold

Antifade Mountant (Thermofisher, US). Imaging was carried out on a confocal microscope within a day of mounting, and the recorded images processed using ImageJ software.

Table 8| Composition of blocking solution for immunohistochemistry.

Blocking and permeabilisation solution component	**% of total volume**
PBS (Merck, US)	Base
Goat serum (Merck, US)	2
BSA (Merck, US)	3
Triton X-100 (Thermofisher, US)	1
NaN_3 (Merck, US)	0.1

II.7 Quantitative Reverse Transcription PCR (RT-qPCR)

The polymerase chain reaction (PCR) is the repeated copying of a section of DNA by a polymerase enzyme. To analyse mRNA expression, a sample of cell or tissue RNA is first reverse-transcribed into *complementary* (c)DNA, before the reaction takes place. For quantification, primers specific to genes of interest are used for the PCR, equipped with fluorescent probes, which increase in intensity with every replication cycle. The number of cycles taken for the fluorescent signal to cross a determined threshold, the Ct value, gives an index of relative gene expression (Figure 7). In order to control for differences in overall RNA, some ubiquitously expressed genes are analysed and the target genes normalised to these as a control. In this thesis *b2m* was used as it has been shown not to be differentially expressed by the Wistar and SHR stellate ganglia (Bardsley et al., 2018a; Davis et al., 2018).

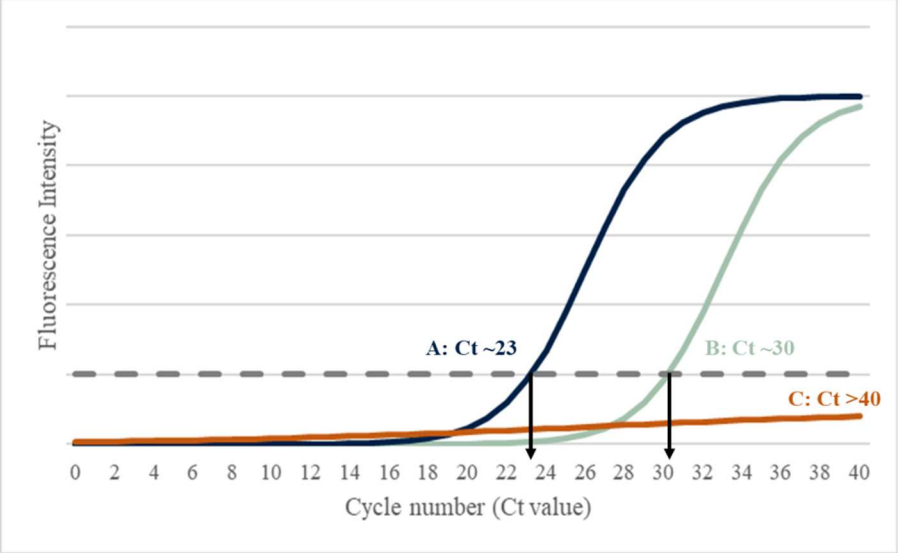

Figure 7| Example qPCR assay for expression of three genes: A, B and C. The cycle number at which each gene assay crosses the threshold (grey dotted line) is the Ct number and gives an index of relative gene expression. It took ~7 cycles longer for gene B to cross the threshold than gene A and as each cycle is a doubling of cDNA, this means gene A is expressed 2^7 times as much as gene B.

II.7.1 Methodology

Clean stellate ganglia were snap frozen and temporarily stored in liquid nitrogen immediately following connective tissue removal. Cultured BMDMs were collected from their petri dishes, resuspended in PBS and centrifuged at 400 rcf for 4 min for washing, and then the supernatant was removed and the cell pellet also snap frozen in liquid nitrogen. Sorted monocyte-macrophages were placed onto dry ice immediately following separation, and then transferred to liquid nitrogen as soon as possible.

RNA was extracted from ganglia and cells using an RNeasy mini kit, according to the manufacturer's instructions and these samples stored at -80°C if required. In the case of monocyte-macrophages FAC-sorted from stellate ganglia, RNA amplification was then attempted using a MessageBOOSTER™ cDNA Synthesis Kit (Lucigen, US), according to the manufacturer's instructions, which additionally converts the amplified RNA to cDNA, ready for qPCR. In the case of non-amplified RNA samples, contaminating DNA was digested by DNase at 37°C, before the RNA was converted to cDNA using

Superscript IV Vilo with UNG. cDNA samples were stored at -20°C and gene expression quantified using a Taqman gene expression assays, within a week of synthesis.

Data were collected on an ABI Prism 7000 real time PCR machine, processed using 7000 system software, and analysed using the delta Ct method.

II.8 Real-time Ca^{2+} imaging

Fluorescent calcium indicator dyes are molecules which bind Ca^{2+} ions and whose bound and unbound states have different excitability or emission spectra. Single-wavelength dyes are fluorescent in one of these states, but not (or only weakly) in the other, and therefore the intensity of emission at their peak emission wavelength gives an index of $[Ca^{2+}]$. Emission intensity is dependent not only on Ca^{2+} but also on factors such as the concentration of dye and its viability, so changes in these factors leakage from cells or photobleaching will affect the measured $[Ca^{2+}]$. Ratiometric dyes circumvent this limitation by being fluorescent in both bound and unbound states, except that the emission or excitation peaks are different in each state (Figure 8). One must alternate the excitation or recorded emission wavelengths and the *ratio* of the dual wavelengths thereby indicates the relative $[Ca^{2+}]$, and as both of these would be similarly affected by changes to factors affecting intensity, the ratio remains relatively constant. However, due to having to excite at or record from two wavelengths sequentially, these have poorer temporal resolution.

Most dyes contain charged carboxylate groups, making them unable to permeate cell membranes. To allow recording of intracellular Ca^{2+} they would therefore need to be injected, which is very technically challenging and inefficient. Alternatively, they can be introduced to the cells as an acetoxymethyl (AM) ester derivative, which is uncharged, and therefore can cross the plasma membrane. Once inside the cells this is cleaved by

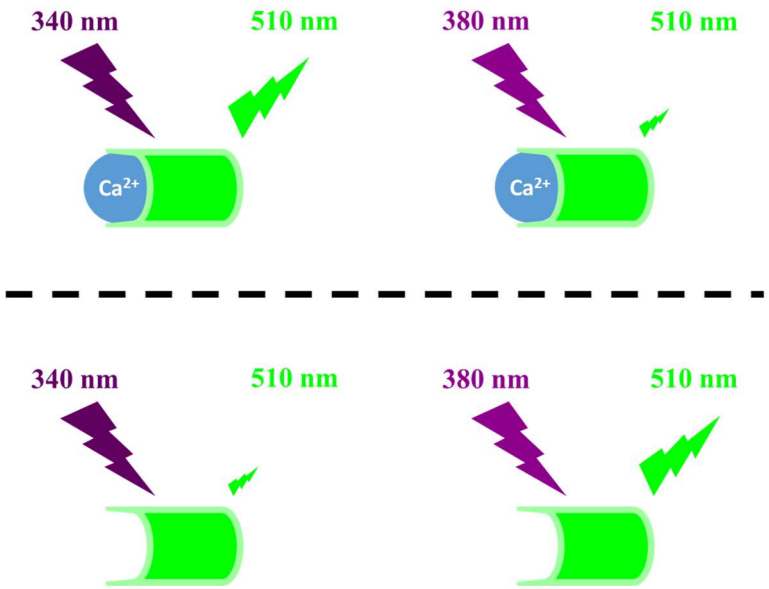

Figure 8| The principle of Fura-2 imaging. Fura-2 always has an emission peak at ~510 nm, but its excitation peak is ~340 nm when bound to Ca^{2+} and ~380 nm when not (Grynkiewicz *et al.*, 1985). The $[Ca^{2+}]$ can then be calculated using the following equation:

$$[Ca^{2+}] = \frac{R - R_{mi}}{(R_{max} - R) \times Sf \times Kd}$$

where R is the 340/380 ratio at a given time, R_{min} is the ratio where $[Ca^{2+}] = 0$ (commonly calibrated using a chelator), R_{max} is the 340/380 ratio where Fura-2 is saturated with Ca^{2+} (often calibrated using ionomycin to expose the cytosol to the mM levels of extracellular $[Ca^{2+}]$, Sf is a scaling factor, and Kd is the dissociation constant for Fura-2. In the experiments of this thesis relative changes in $[Ca^{2+}]$ were compared between conditions or rat strains, and therefore there was no need to calibrate and calculate exact $[Ca^{2+}]$ values.

cytoplasmic esterase enzymes, restoring the charged groups, and effectively trapping the dye inside the cell (Tsien, 1981). The Ca^{2+} imaging experiments of this thesis used Fura-2 to record cytosolic Ca^{2+} due to its ratiometric property (Grynkiewicz et al., 1985) and technical ease.

II.8.1 Methodology

Stellate neurons were plated onto 6 mm laminin and poly-D-Lysine coated glass coverslips as described in Chapter II.3. Prior to imaging, these were incubated in culture medium containing 2 µM Fura-2 AM, at 37°C for 30 min, before being washed with Tyrode's solution (Table 9) three times for 5 min each. The coverslips were then imaged

in a 100 µL, gravity-fed perfusion chamber, in 37°C Tyrode's solution at a flow rate of ~3-4 ml/min. An inverted Nikon microscope, with a 40x oil-immersion objective, was used to obtain the images, which were captured by QICLICK digital CCD camera, using Optofluor QICLICK software.

Table 9| Composition of Tyrode's solution used for stellate neuron Ca^{2+} imaging.

Neuronal $Ca2^{+}$ imaging Tyrode's Solution	**Concentration (mM)**
NaCl (Merck, US)	135
KCl (Merck, US)	4.5
HEPES (Merck, US)	20
Glucose (Merck, US)	11
$CaCl_2$	2
$MgCl_2$	1

Neurons were identified by their large size and thick borders, as compared to other cells present on the coverslips, and only those which appeared healthy, showing no obvious signs of damage or blebbing, were selected for imaging. Images were captured every 2 s, during which the coverslips were excited sequentially at wavelengths of 355[7] and 380 nm, and the emission intensities at 510 nm recorded. Background 510 nm emissions were subtracted from that of the cells for both excitation wavelengths in each image, and the resultant values used to calculate the 355/380 ratio. This was then normalised to a baseline

[7] While the peak excitation wavelength for Ca^{2+}-bound Fura-2 is at 340 nm, the LED system available to our laboratory uses 355 nm instead. This is close enough to 340 to serve the same purpose, and even though 355 nm will have greater spillover into the 380 nm channel, this is acceptable if this is held constant for comparisons between datasets.

ratio for each cell, which was taken as the average of the final 5 images prior to addition of the first treatment. Cells underwent the pharmacological protocol shown in Figure 9.

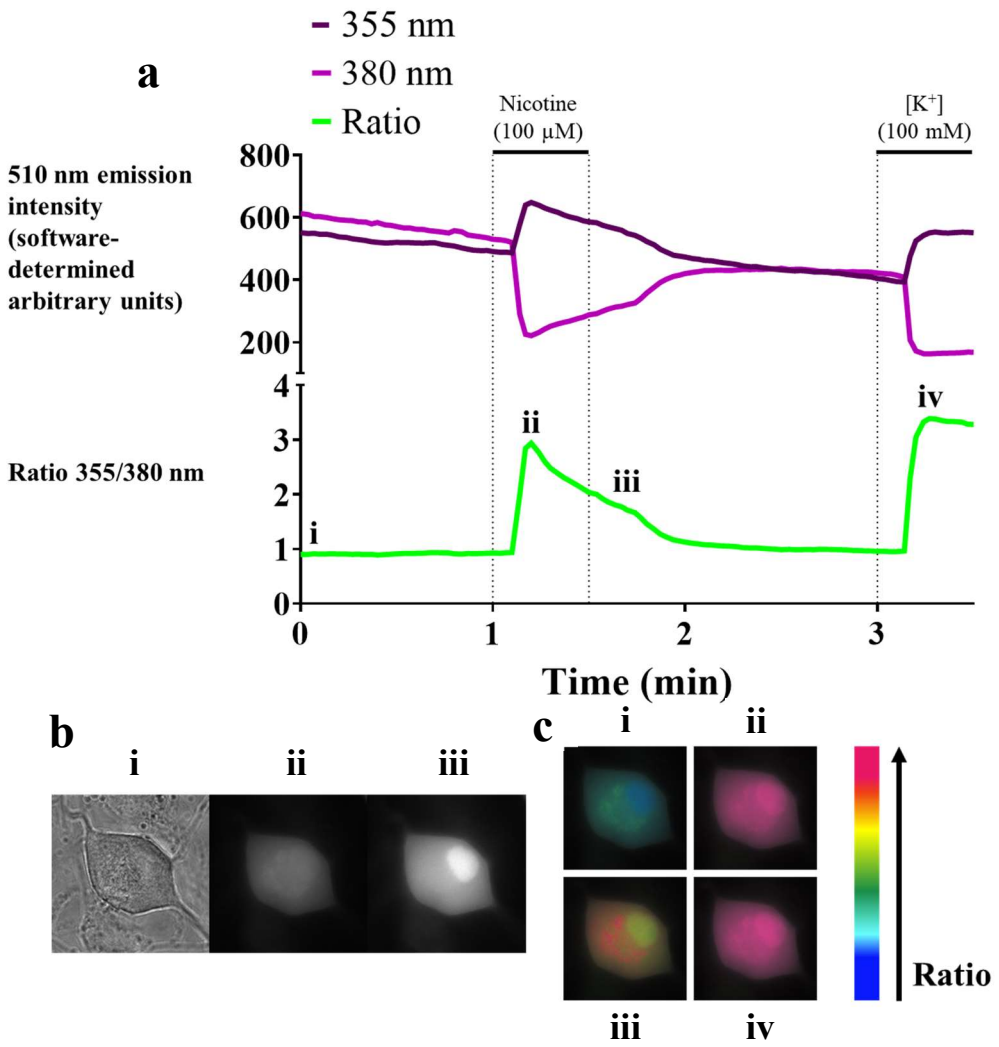

Figure 9| Exemplar stellate neuron Fura-2 Ca^{2+} imaging experiment. a) Changes in Fura-2 fluorescent properties during the course of an experiment in which a neuron is stimulated sequentially with nicotine and high $[K^+]_o$ and the 510 nm light emission is recorded every 2 s upon illumination with 355 and 380 nm light. The evoked $[Ca^{2+}]_i$ transients correspond to an increase in emission in response to light at the 355 nm wavelength, but a decrease in this respect for 380 nm light; thereby increasing the 355/380 nm ratio. Note also, in the 355 and 380 nm traces, the gradual decline in fluorescence during the experiment, caused by a combination of dye leakage and photo-bleaching. However, as a ratiometric dye, this does not substantially affect the signal. b) Images of the neuron from which the recording was taken at the start of the experiment under: (i) bright-field, (ii) 355 nm light, and (iii) 380 nm light. c) 355/380 nm ratio images at the time points indicated in a).

I.9 Whole stellate ganglion noradrenaline release experiments

Physiologically, post-ganglionic sympathetic neurons receive stimulation by acetylcholine (ACh) released from pre-ganglionic neurons. This acts on nicotinic ACh receptors, leading to depolarisation and triggers a post-synaptic action potential. Travelling down the axon to the noradrenaline-containing varicosities, this voltage stimulus opens N-type voltage-gated Ca^{2+} channels, leading to Ca^{2+} ion entry, which triggers vesicular noradrenaline release. The cholinergic neurotransmitter signal is difficult to reproduce in culture because prolonged stimulation would be necessary to release detectable noradrenaline, but nicotinic receptors desensitise rapidly (Giniatullin et al., 2005), and it would be extremely technically difficult to repeatedly apply puffs of acetylcholine or nicotine at the same frequency as they are released from pre-synaptic neurons *in vivo*. For this reason, a model system used to examine ganglionic activity *in vitro* is electrical stimulation (Figure 10); this mimics the depolarisation of the post-ganglionic neurons and thereby similarly produces noradrenaline release. This method has been previously published by our lab, where it was shown that the SHR exhibits greater release of noradrenaline, compared to the Wistar rat (Bardsley et al., 2018b), suggesting this is a good model to study SHR sympathetic dysfunction. This study then used high-performance liquid chromatography to analyse the noradrenaline content of the ganglia and supernatant. Unfortunately, this gold-standard technique was not available for use within this thesis, so an ELISA was instead used, use of this being previously published by the Domingos lab (Pirzgalska et al., 2017).

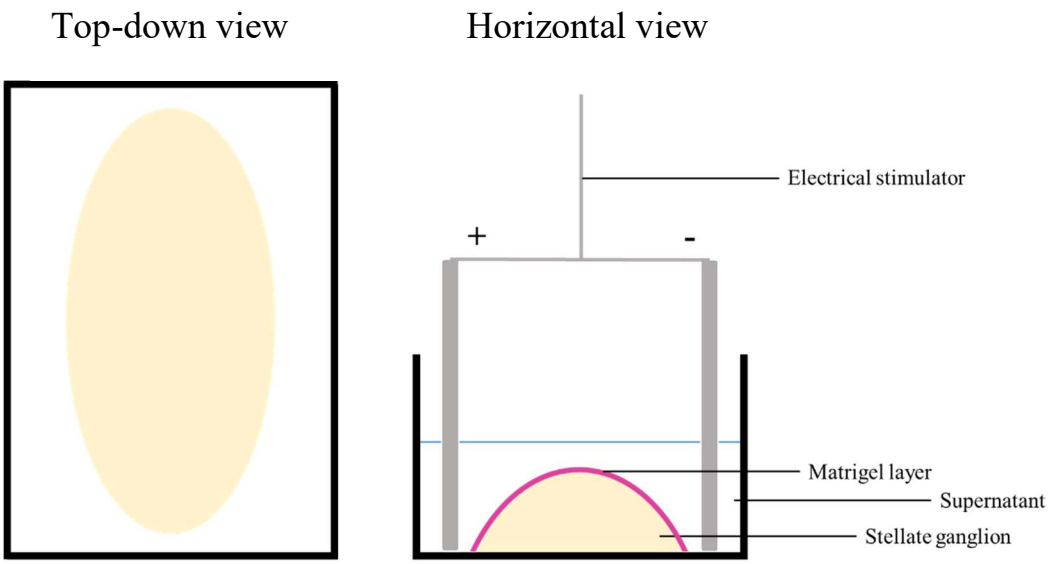

Figure 10| Experimental set-up of stellate ganglion noradrenaline release experiments.

II.9.1 Methodology

The protocol used in this thesis was adapted from the aforementioned publication of Bardsley et al. (2018b). Culture medium was removed from stellate ganglion explants prepared in 8-well tissue culture dishes and replaced with 700 µL Tyrode solution containing 1 µM desipramine (to inhibit noradrenaline re-uptake after release). The composition of this solution is detailed in Table 10 was bubbled with 95%O_2/5%CO_2 for 10 min, reach a pH after equilibration of 7.40. In a water bath at 37°C, ganglia were then electrically stimulated with 100 mV, 10 ms pulses at 5 Hz, for 5 min. After this the supernatant was extracted and the noradrenaline stabilised by addition of 1 mM EDTA and 4 mM sodium metabisulfite, while the ganglia were put into a metal bead lysing tube (Bertin technologies, France) containing another 700 µL Tyrode solution with 1 µM desipramine, 1 mM EDTA and 4 mM sodium metabisulfite. The ganglia were then mechanically lysed using a Precellys 24 machine and the tubes centrifuged at 16,000 ×g for 15 min, before the resulting supernatant was collected. All samples were stored on ice throughout and protected from light in order to reduce catecholamine oxidation, and then

stored at -80°C. The concentration of noradrenaline in 500 µL of each sample was later determined using a specific ELISA kit (LDN, Nordhorn, Germany), according to the manufacturer's instructions. This kit uses an optical density measurement as an index of [Noradrenaline], and uses a number of standard samples to construct a curve comparing [Noradrenaline] to optical density, from which experimental sample [Noradrenaline] can then be interpreted.

Table 10| Composition of Tyrode's solution used for stellate stimulation experiments.

Stellate Stimulation Tyrode's Solution	**Concentration (mM)**
NaCl	120
KCl	4
$NaHCO_3$ (Merck, US)	25
Glucose	1
$CaCl_2$	2
$MgCl_2$	1

II.10 Chemotaxis assay

A number of assays now exist to quantify the extent of cellular chemotaxis, but one of the earliest and most elegant is the Boyden chamber (Boyden, 1962) (Figure 11). In brief, this comprises two compartments separated by a barrier, containing microscopic pores through which cells can migrate. Different pore diameters are chosen depending on the cell type being assayed, 5 µm being appropriate for monocytes and macrophages according to the manufacturer (Merck, US). Cells are seeded into the upper chamber in culture media, and culture media containing a chemoattractant is loaded into the lower one. After a specified period of time, the number of cells appearing in the lower chamber

is taken as an index of chemotaxis. A number of different methods may be used to count this.

This thesis used the Boyden chamber-based 5 µm colorimetric QCM Chemotaxis Cell Migration Assay (Merck, US), which was performed according to the manufacturer's instructions. In this assay a nucleic dye is used to stain for cells reaching the lower chamber, the intensity of which was quantified on a spectrophotometric plate reader.

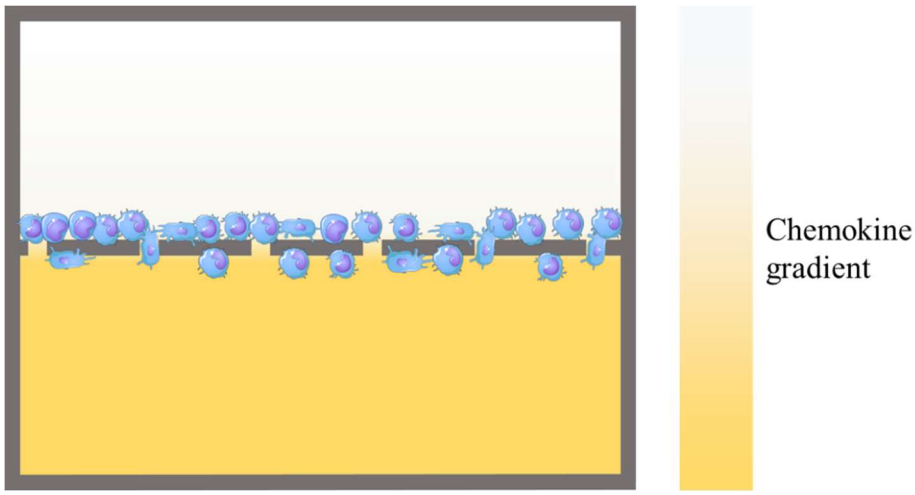

Figure 11| The Boyden Chamber chemotaxis assay. Chemotactic cells are placed into the upper chamber and a chemokine loaded into the bottom. The extent of cell migration through pores in the membrane separating the two compartments provides an index of chemotaxis. (Boyden, 1962). Cell images are from Servier Medical Art (smart.servier.com) by Servier, and licensed under a Creative Commons Attribution 3.0 Unported License (https://creativecommons.org/licenses/by/3.0/).

II.11 Statistical Analysis

Graphpad Prism 8 software was used to compute all statistical analyses. All data collected for this thesis were continuous, which was reflected in the choice of statistical tests employed. Data were first assessed for normality by a combination of Anderson-Darling, D'Agostino & Pearson, Shapiro-Wilk and Kolmogorov-Smirnov tests, and those which passed were analysed using parametric models, while the rest used non-parametric statistical tests. In cases where two groups were being compared, Welch's t-tests (parametric) or Mann-Witney (non-parametric) tests were used. To account for multiple

comparisons, the false discovery rate (FDR) approach was used, with adjusted *p*-values, known as *q*-values, (calculated using the two-step set-up method of Benjamini, Krieger and Yekutieli, with the desired FDR set to 5%) being reported where appropriate. For comparison of three or more groups simultaneously, Brown-Forsythe and Welch's ANOVAs (parametric) or Kruskall-Wallis (non-parametric) tests, with appropriate *post-hoc* tests, were instead employed. Results were considered statistically significant in all cases where $p<0.05$.

CHAPTER III

The immune cell populations of sympathetic ganglia from pre-hypertensive animals

III.1 Introduction

III.1.1 Central neuroinflammation as a driver of hypertension

Neuroinflammation at certain nodes of the central nervous system can produce sympathetic hyperactivity, which in turn raises arterial blood pressure (MAP). Pro-inflammatory cytokines, namely tumour necrosis factor alpha (TNF-α) and interleukin 1 beta (IL-1β) (Shi et al., 2011; Wu et al., 2012), have been shown to heighten sympathetic outflow and raise MAP in particular through actions on two central nervous system nuclei. These are: the hypothalamic paraventricular nucleus (PVN) (Shi et al., 2011), a key centre of autonomic control, and rostral ventrolateral medulla (RVLM) (Wu et al., 2012), the major final sympathetic outflow nucleus. Moreover, markers of inflammation including these have been found in the spontaneously hypertensive rat (SHR) in both these nuclei (Shi et al., 2014; Tan et al., 2017), along with the nucleus tractus solitarii (NTS) (Waki et al., 2010), to which the baroreceptors input.

Activation of the pro-resolution CB_2 receptor in the RVLM of the SHR reduces inflammatory marker expression and simultaneously lowers renal sympathetic nerve activity. It simultaneously produces a fall in MAP, all these effects being dependent upon RVLM CB_2 receptor expression (Shi et al., 2020), suggesting reversing this inflammation may be beneficial in hypertension. Reports have shown minocycline, which has the effect of inhibiting microglial activation, can lower blood pressure in the SHR (Santisteban et al., 2015; Galla et al., 2018). One report in the stroke-prone SHR though suggests that while oral minocycline reduces PVN microglial activation, it does not change blood pressure (Takesue et al., 2017). This disparity may result from the use of the stroke-prone SHR (an inbred line arising from the SHR with higher blood pressure and greater stroke susceptibility (Okamoto et al., 1974)), or the dosing regimen, which in the study of

Takesue et al. (2017), was half that of the others (Santisteban et al., 2015; Galla et al., 2018). Importantly, preliminary data seems to suggest human hypertensive patients are responsive to treatment with minocycline (Qi et al., 2016).

III.1.2 The case for peripheral sympathetic intervention

Sympathetic hyperactivity is not likely to occur exclusively centrally in essential hypertension; in the SHR it is well-established that sympathetic ganglia themselves exhibit dysregulation (Shanks et al., 2013a; Shanks et al., 2013b; Bardsley et al., 2018b), something that persists even in single cell culture (Davis et al., 2020). Although development of a means to tone down increased central sympathetic outflow is promising as a new means of antihypertensive therapy, there is also merit to investigating this phenomenon at the lower nodes of the SNS. Being downstream of the central sympathetic nuclei, if the ganglia are dysregulated, disease-reducing effects of therapies targeting central mechanisms may be blunted due to continued sympatho-excitation at the levels below. Inhibiting the peripheral sympathetic nervous system might therefore serve as a useful adjunct to central therapies. Furthermore, these peripheral nodes are would be much logistically simple to target, given easier access to the target ganglia, than attempting to reach deep brain nuclei, for example.

III.1.3 Role of inflammation in producing local neuronal hyperactivity

Peripheral neuroinflammation has not substantially been studied in the context of essential hypertension. However, evidence from other diseases suggests that an inflammatory reaction is capable of increasing peripheral neuronal activity. This is the case for sensory fibres in neuropathic pain syndromes, on which there has been much work carried out; reviewed by Scholz & Woolf (2007). Following nerve injury, macrophages and other immune cells enter the site and release a range of inflammatory

mediators, and through a nexus of cell-to-cell interactions within this environment, involving the neurons themselves, Schwann cells and glia, neuronal growth and sensitisation is promoted. In this context, IL-6 even promotes sympathetic neuron sprouting into dorsal root ganglia above the site of injury (Ramer et al., 1998), suggesting that the SNS is similarly responsive to such signals. Likewise, post-MI, inflammation as the site of the infarct participates in the remodelling of local sympathetic neurons, increasing sprouting, and predisposing to future arrhythmia (Hasan et al., 2006; Wernli et al., 2009).

To date, three studies have examined the immune cell environment of the stellate ganglion, doing so in those surgically removed from ventricular arrhythmia patients. These revealed immune cell infiltration, chiefly of T cells, in the diseased samples, which was absent from controls (Rizzo et al., 2014; Ajijola et al., 2017; Duffy et al., 2021). While certainly informative, this approach could be improved by employing flow cytometry, to provide a more quantitative and detailed examination of the leukocytes present in the tissue. Whole rat stellate RNA sequencing data from our lab also show expression of markers for leukocytes, T cells, NK cells, macrophages and neutrophils (Davis et al., 2018). This is also supported by recent single-cell RNA sequencing of 4-week old Wistar and SHR stellate ganglia, which showed the presence of a *ptprc* (CD45)-positive cluster of leukocytes, expressing markers for the same subsets. However, only *cd4* (a marker for T helper cells) was differentially expressed between the strains, being more highly expressed by the immune cells of the SHR (Davis et al., 2020; Harvey Davis, personal communication). Of course these studies are limited however, the bulk stellate RNA sequencing examines all RNA in the tissue, meaning the RNA expressed by the small leukocyte population may be dilute, while the single cell sequencing used only

10,000 cells per sample, again equating to a very small number of leukocytes. This means sensitivity for measuring inter-strain differences may be low.

III.1.4 Hypothesis and aim of the chapter

Hypothesis:

- There is an immunological difference in the sympathetic ganglia of pre-hypertensives versus healthy controls.

Aim:

- To quantify the proportions of the major leukocyte populations within the pre-hypertensive SHR stellate ganglion compared to its Wistar control.

III.2 Methods & Materials

III.2.1 Tissue Collection

Rat tissue for flow cytometry was prepared as described in Chapter II.4.4. Wistar and SHR rats were culled by cardiac perfusion and exsanguination under terminal pentobarbital anaesthesia, under protocol 19 (b) ii of the project licence P707EB251. This enabled blood cells to be flushed out of the vasculature of the tissues under question, such that only the tissue-resident leukocytes could be examined, rather than those which happened to be passing through the local capillaries. Sufficient perfusion was visible by the paling of the intercostal vessels, and organs such as the liver and kidneys. Stellate, SC and the combined coeliac/superior mesenteric ganglia, were excised, along with the kidneys, and ~1-2 ml of blood was also collected, and these were processed as described in Chapter II.4.4a.

Human blood was kindly donated by volunteers from the Oxford Biobank, as described in Chapter II.2.

III.2.2 Flow cytometry

Single cell suspensions of sympathetic ganglia, kidneys and blood were prepared from the isolated tissues and stained as described in Chapter II.4.4. The antibodies and live/dead stain used are summarised in Tables 1 (rat) and 2 (human). The rat panel was adapted from Barnett-Vanes et al. (2016), and the human based on species equivalent markers to this. Samples were then processed using a BD LSRFortessa™ X-20, with the laser and filter sets listed in Tables 1 and 2, and the data were analysed as described in Chapter II.4.4c. The gating strategy use to quantify the different populations of leukocytes is shown in Figures 1 (rat) and 6 (human).

Table 1| Rat leukocyte flow cytometry panel.

Antibody	Host species	Concentration	Laser & Filter set
anti-CD11b-V450 (BD Biosciences, US)	Mouse	1:200	405 - 450/50
anti-CD161a-BUV395 (BD Biosciences, US)	Mouse	1:200	355 - 379/28
His48-FITC (Thermofisher, US)	Mouse	1:200	488 - 530/30
anti-CD43-PE (Biolegend, US)	Mouse	1:200	561 - 586/15
anti-B220-PECy7 (Thermofisher, US)	Mouse	1:200	561 - 780/60
anti-CD45-A700 (Biolegend, US)	Mouse	1:200	640 - 730/45
anti-CD3-BV605 (BD Biosciences, US)	Mouse	1:25	405 - 610/20
anti-CD68-A647 (Bio-Rad, US)	Mouse	1:10	640 - 670/30
eFluor™ 780 viability dye (Thermofisher, US)	N/A	1:2000	640 - 780/60

Table 2| Human leukocyte flow cytometry panel.

Antibody	Host species	Concentration	Laser & Filter set
anti-CD33-V450 (BD Biosciences, US)	Mouse	1:20	405 - 450/50
anti-CD56-BUV395 (BD Biosciences, US)	Mouse	1:20	355 - 379/28
anti-CD16-FITC (Biolegend, US)	Mouse	1:20	488 - 530/30
anti-CD14-PE (Biolegend, US)	Mouse	1:20	561 - 586/15
anti-CD19-PECy7 (Biolegend, US)	Mouse	1:20	561 - 780/60
anti-CD45-A700 (Biolegend, US)	Mouse	1:50	640 - 730/45
anti-CD3-BV605 (Biolegend, US)	Mouse	1:20	405 - 610/20
anti-CD68-A647 (BD Biosciences, US)	Mouse	1:20	640 - 670/30
eFluor™ 780 viability dye	N/A	1:2000	640 - 780/60

III.2.3 Immunohistochemistry

Whole stellate ganglia were fixed and prepared for cryosectioning as described in Chapter II.5.1. The stains and primary and secondary antibodies used for this are summarised in Table 3. Images were captured as a Z-stack throughout the 20 µm section, and a 2D maximum intensity Z projection was produced using ImageJ software.

Table 3| Rat stellate immunohistochemistry antibodies.

Target	Cell type	Primary antibody/stain	Secondary antibody	Confocal laser wavelength (nm)
Nuclei	All	DAPI	N/A	405
Tyrosine Hydroxylase	Sympathetic neurons	Sheep anti-rat TH (Bio-Rad, US)	Donkey anti-sheep Alexafluor488 (Thermofisher, US)	488
CD68	Macrophages	Mouse anti-rat CD68 (Bio-Rad, US)	Goat anti-mouse Alexafluor568 (Thermofisher, US)	561

III.2.4 Statistical analysis

Statistical analyses were carried out as described in Chapter II.8.

III.3 Results

III.3.1 Proportions of leukocyte subsets in the SHR compared to Wistar stellate ganglia

The question was first asked whether there were any differences in the frequencies of the populations of tissue-resident leukocytes in the stellate ganglia of the pre-hypertensive SHR, compared to those of the Wistar. A flow cytometry panel of antibodies was designed, based on those validated by Barnett-Vanes et al. (2016) for rat leukocytes, in order to detect: T cells, NK cells, B cells, neutrophils (PMNs) and monocyte-

macrophages[8] (Figure 1). The monocyte-macrophage population was then further divided into the classical and non-classical sub-types found in the rat. In order to gate these latter populations more effectively and objectively an attempt was made to use an automated gating algorithm: flowMeans (Aghaeepour et al., 2011), available as a FlowJo plugin. This correctly identified the classical and non-classical populations in many cases, but it was not entirely robust enough to do this in every case, particularly if one population was very small (Figure 2). For this reason, these monocyte-macrophage gates had to be drawn manually instead.

[8] Monocytes are circulating blood cells which enter tissues and differentiate into macrophages. It is difficult to definitively discriminate between these two when found in the tissues, hence the term "monocyte-macrophages" is used within the literature to cover all of these cells.

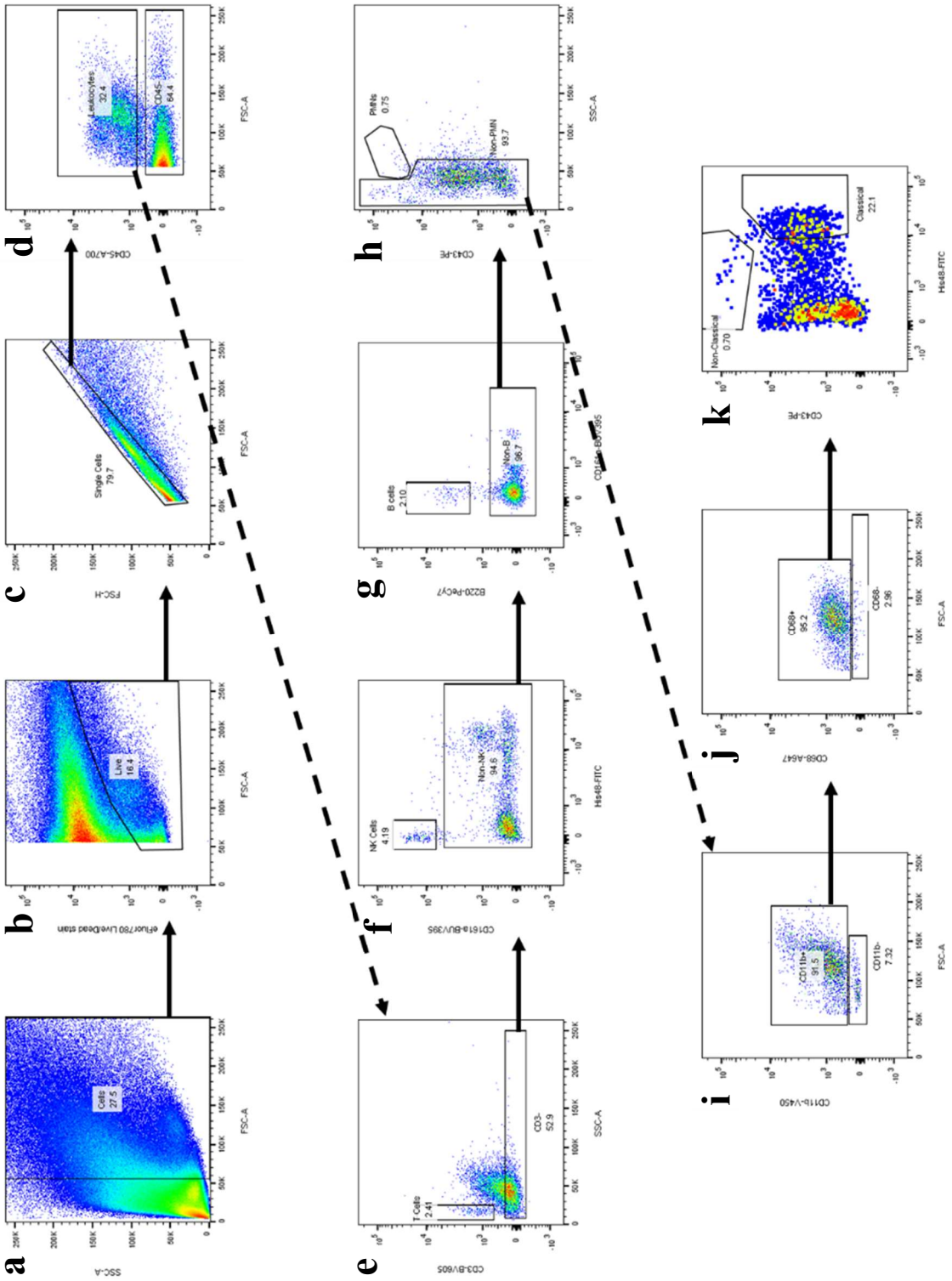

Figure 1| Gating strategy for analysis of rat leukocytes in sympathetic ganglia, running sequentially from a) to j). Each selected gate was carried forward to the next panel (indicated by the arrows) for the next step. In panel a) all recorded events are present, and the true cells are selected with a positive gate based on FSC and carried over to panel b). Here, the live cells are identified by low live/dead stain fluorescence, from which the single cells are selected by comparing the FSC-A and FSC-H values. *(Figure legend continued on next page)*

Figure 1 continued| In panel d) the leukocytes are selected, defined as $CD45^{+}$, and subsequently the following major leukocyte populations are gated off sequentially (with the negative populations being passed to the next step): e) T cells ($CD3^{+}$); f) NK cells ($CD161^{high}/His48^{low}$); g) B cells ($B220^{+}$), h) neutrophils ($SSC^{high}/CD43^{high}$). Next the remaining myeloid population ($CD11b^{+}$) is identified in i), and from these the monocyte-macrophages ($CD68^{+}$) are selected in j). Finally, in k) the classical ($His48^{high}/CD43^{low}$) and non-classical ($CD43^{high}/His48^{low\text{-}intermediate}$) monocytes-macrophages are delineated.

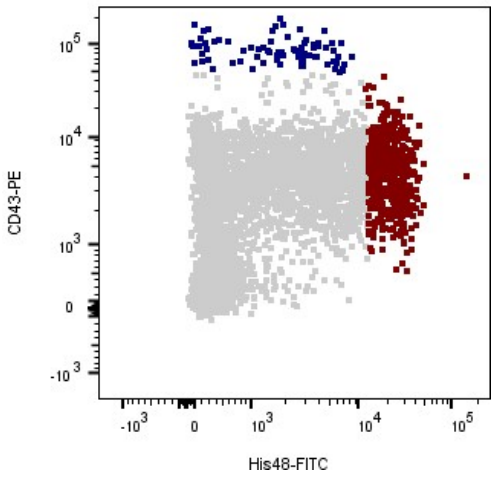

Figure 2| Gating the monocyte-macrophage populations using the flowMeans algorithm (Aghaeepour et al., 2011). As the cells present on the plot should be made up of classical monocyte-macrophages, non-classical monocyte-macrophages, and a negative population, the algorithm was set to define three populations. Those it detected are shown in red (classical monocyte-macrophages), blue (non-classical monocyte-macrophages) and grey (negative). While this worked in many cases (such as that depicted), suggesting that these were the true populations, in many others it did not.

As the ganglia were of different sizes, and those of the SHR tended to be smaller in size than Wistar ganglia, cell counts were normalised to the total number of single cells recorded for each sample, and expressed as the number per 1000 single cells. There were significantly more leukocytes (defined at $CD45^{+}$) in the Wistar compared to SHR stellates (372 ± 16.1 versus 285 ± 25.5 per 1000 single cells; p=0.014; q=0.025; Figure 3a). Part of this increase in leukocytes was accounted for by increased numbers of NK cells (10.3 ± 1.91 versus 3.39 ± 0.329 per 1000 single cells; p=0.0037; q=0.0097; Figure 3b) in the Wistar strain, while the SHR had higher numbers of neutrophils (3.90 ± 0.259 versus 1.73 ± 0.253; p<0.0001; q=0.00033; Figure 3b).

Examining the monocyte-macrophage population further revealed a striking difference in the proportions of the subtypes between these two strains: the ratio of classical ($His48^{high}/CD43^{low}$) to non-classical ($CD43^{high}/His48^{low\text{-}int}$) monocyte-macrophages was

significantly higher in the Wistar (13.8 ± 4.77 versus 0.551 ± 0.148; p=0.0082; Figure 3e). This appeared to made up of both more classical (20.52 ± 7.54 versus 1.81 ± 0.662; p=0.029; q=0.039; Figure 3d), and fewer non-classical (1.60 ± 0.476 versus 3.24 ± 0.556; p=0.047; q=0.0497; Figure 3d), monocyte-macrophages in the Wistar compared to SHR.

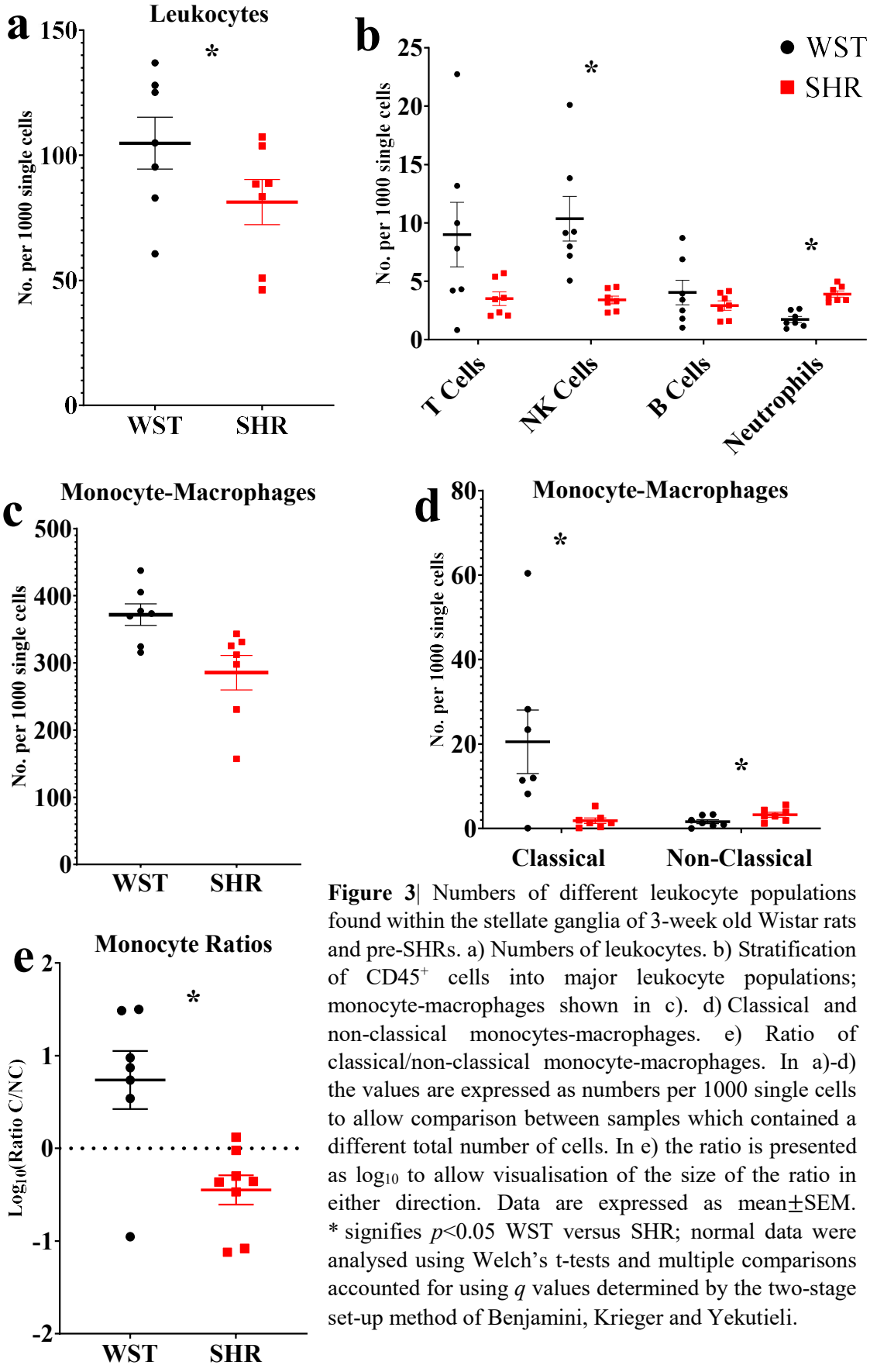

Figure 3| Numbers of different leukocyte populations found within the stellate ganglia of 3-week old Wistar rats and pre-SHRs. a) Numbers of leukocytes. b) Stratification of $CD45^+$ cells into major leukocyte populations; monocyte-macrophages shown in c). d) Classical and non-classical monocytes-macrophages. e) Ratio of classical/non-classical monocyte-macrophages. In a)-d) the values are expressed as numbers per 1000 single cells to allow comparison between samples which contained a different total number of cells. In e) the ratio is presented as $\log_{10}$ to allow visualisation of the size of the ratio in either direction. Data are expressed as mean±SEM. * signifies $p<0.05$ WST versus SHR; normal data were analysed using Welch's t-tests and multiple comparisons accounted for using q values determined by the two-stage set-up method of Benjamini, Krieger and Yekutieli.

III.3.2 The altered monocyte-macrophage subset proportions are sustained in older SHRs

This study subsequently focussed on the altered monocyte-macrophage ratio in SHR stellate ganglia, as these were the largest single population of leukocytes, it was the most striking difference, and macrophages seem to be an important cell type within the SNS (Pirzgalska et al., 2017). The above data collected from the 3-week old pre-hypertensive SHR avoided the confounding effects of actual blood pressure elevation. However, the same trends were also apparent in the stellates of SHRs aged 5-6 weeks (during hypertension development) and at 12-18 weeks of age (at which stage they exhibit severe, established hypertension), compared to age-matched Wistars (Figure 4a), suggesting this observation is sustained during the course of the disease. Combining these two groups of rats, the difference in monocyte-macrophage subset ratio (1.29 ± 0.209 versus 0.48 ± 0.134) reached statistical significance (p=0.021; Figure 4b).

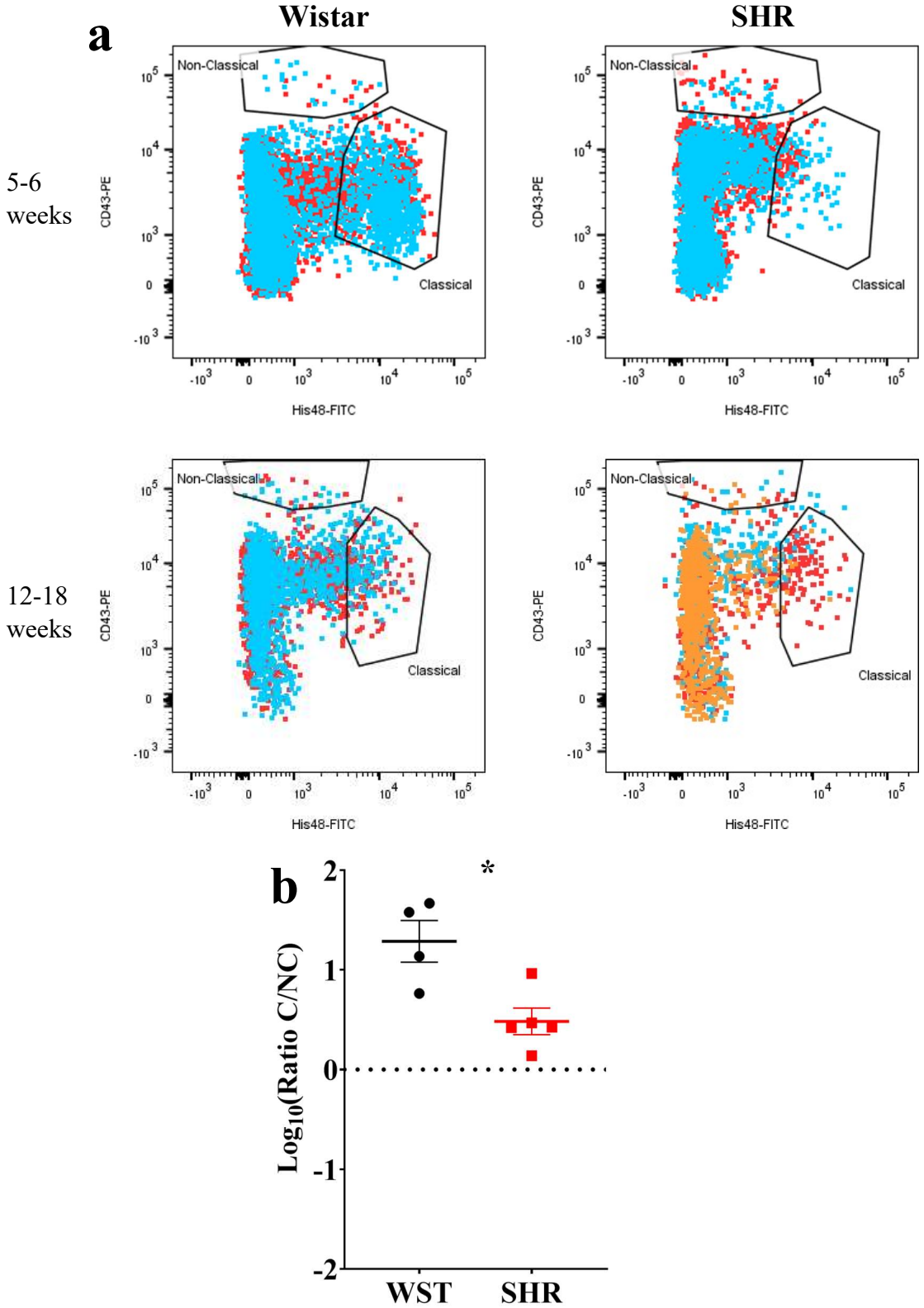

Figure 4| Monocyte-macrophages from the stellate ganglia of SHR and age-matched Wistars at 5-6 weeks (developing hypertension) and 12-18 weeks (established hypertension). a) Flow cytometry plots of all samples; each colour represents a separate sample of ganglia from 2-3 rats. b) Classical/non-classical monocyte-macrophage ratio from all 5-18 week old animals; Data are expressed as mean±SEM. * signifies $p<0.05$ WST versus SHR, Welch's t-test.

III.3.3 The classical/non-classical monocyte-macrophage ratio is also lower in the SHR than Wistar, within the SCG, blood and kidneys

The same flow cytometry panel was then employed on two other SHR sympathetic ganglia to examine whether this was an SNS-wide phenomenon: the coeliac ganglion (which innervates the kidney, so is likely important to hypertensive pathophysiology) and the superior cervical ganglion (innervating the head, so likely has minimal impact on hypertension), except possibly via bone-marrow effects (Scheiermann et al., 2012).

In the SCG, the Wistar ganglia had a significantly higher classical/non-classic monocyte-macrophage ratio (8.99 ± 2.46 versus 0.359 ± 0.148; p=0.0023; q=0.0012), while in the coeliac ganglion there was a clear trend in the same direction (0.391 ± 0.145 versus 0.112 ± 0.021), but this did not reach statistical significance (p=0.12; q=0.032; Figure 5). The SCG also shared the greater numbers of leukocytes (Figure 6a), NK cells and lower numbers of neutrophils in the Wistar, compared to SHR, as well as higher numbers of B cells and T cells (Figure 6b), while the coeliac displayed no such changes (Figure 6c).

A similar monocyte-macrophage subset ratio result was apparent in the whole blood compared between strains (Wistar: 0.123 ± 0.0422 versus SHR: 0.0337 ± 0.00600; p=0.0323, q=0.011; Figure 5), suggesting this phenomenon is not specific to the SNS, but occurs systemically. Finally, this was also the case in the kidneys (Wistar: 0.0742 ± 0.107 versus SHR: 0.0151 ± 0.0853; p=0.0014; p=0.0012; Figure 5), typically referred to as the 'final common node of hypertensive pathophysiology' (Crowley and Coffman, 2014). No differences in any of the other leukocyte populations were detected in either the blood or kidneys however.

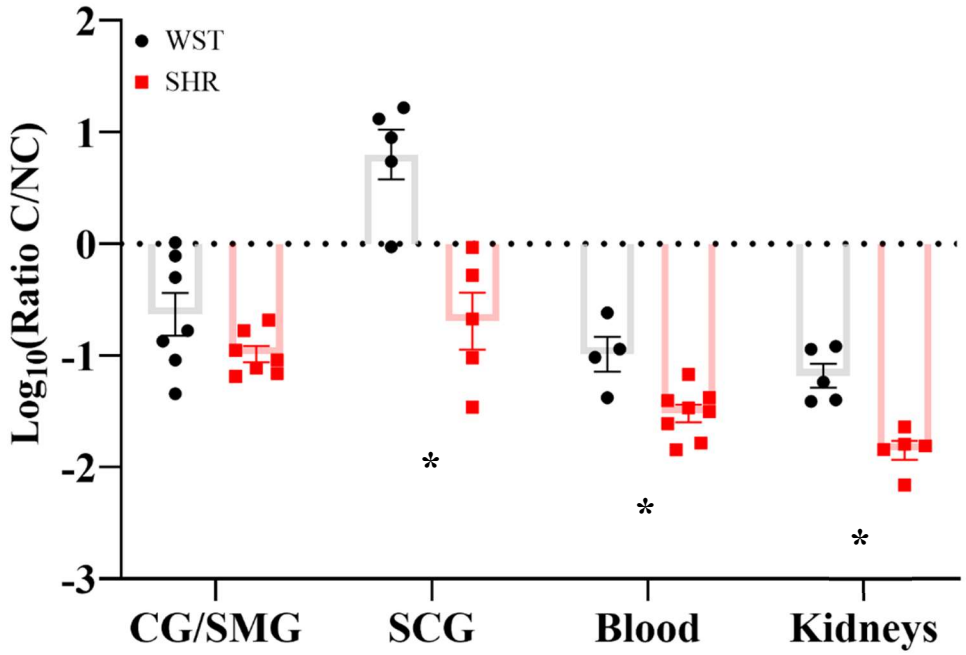

Figure 5| Classical/non-classical monocyte-macrophage ratios in the coeliac/superior mesenteric ganglia (CG/SMG), superior cervical ganglia (SCG), blood and kidneys of 3-week old Wistar rats and pre-SHRs. Data are expressed as mean±SEM. * signifies $p<0.05$ WST versus SHR, Welch's t-tests with q values determined by the two-stage set-up method of Benjamini, Krieger and Yekutieli.

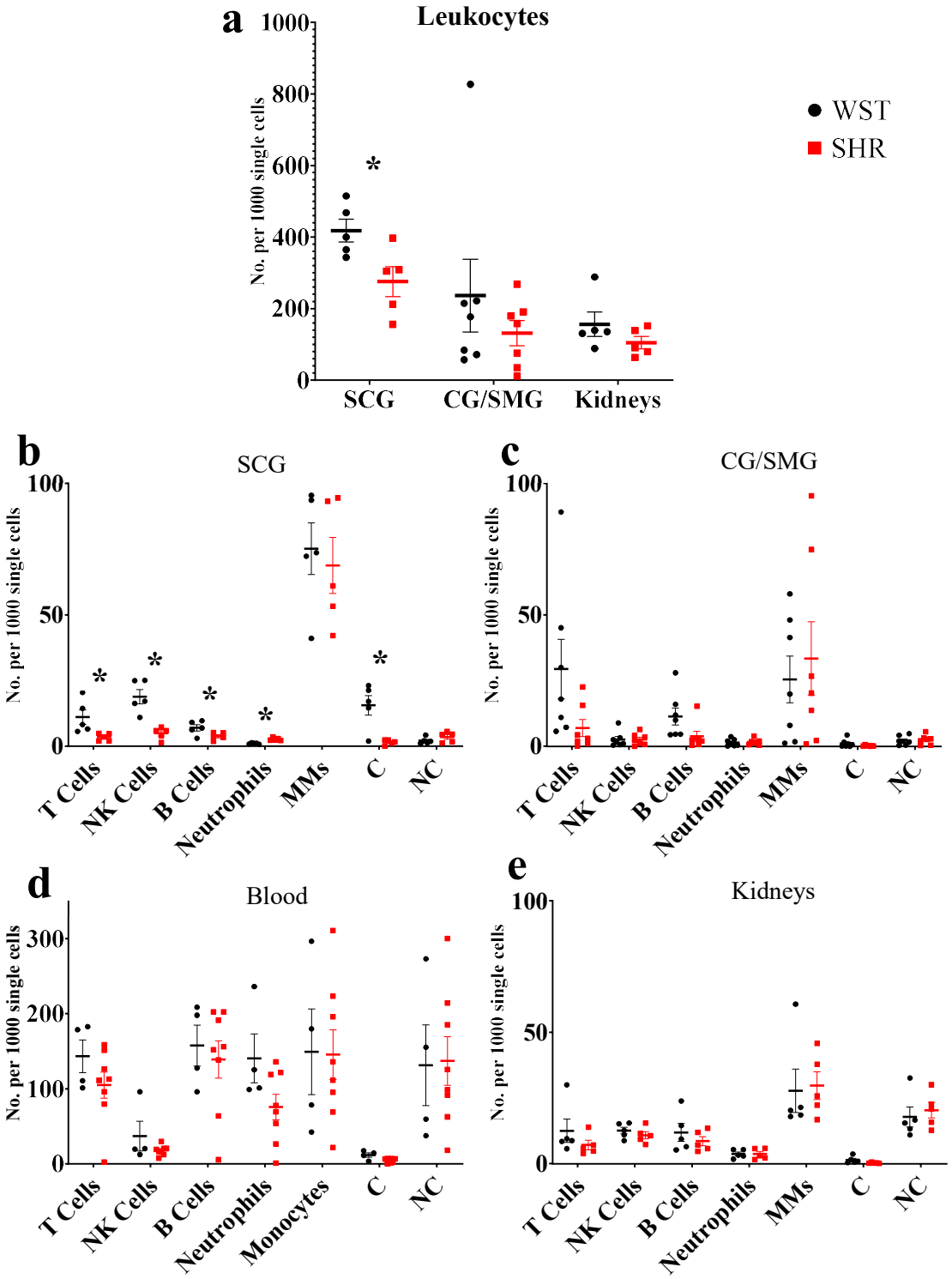

Figure 6| Quantification of leukocyte populations showing total leukocytes (a), and the specific cell types in the: b) SCG, c) CG/SMG, d) blood and e) kidneys of the SHR compared to Wistar rats. Note that in the blood, leukocytes were not quantified as these should be all the cells present. *signifies $p<0.05$ SHR versus Wistar; normal data were analysed using Welch's t-test with q values determined by the two-stage set-up method of Benjamini, Krieger and Yekutieli, while non-normal data were assessed using a Mann-Whitney test.

MM = Monocyte-Macrophages; C = Classical MMs; NC = Non-classical MMs.

III.3.4 Spatial localisation of stellate monocyte-macrophages

The spatial localisation of the stellate ganglion monocyte-macrophages relative to the neurons was examined using immunohistochemistry. This revealed large numbers of spindle-shaped $CD68^+$ cells, scattered amongst the TH^+ sympathetic neurons, of both the Wistar (Figure 7a) and SHR (Figure 7b) stellates, whereas the no-primary antibody control showed no fluorescence in the CD68 568 nm channel, and only some background tissue auto-fluorescence in the TH 488 nm channel (Figure 7c). Additionally, the appearance of large nucleus-free cavities within the tissue suggested that the ganglionic vasculature had been substantially flushed of circulating cells. A splenic sample was used as a positive control for $CD68^+$ macrophages, which also revealed a TH^+ sympathetic nerve fibre (Figure 7d). Unfortunately, all images suffered from the presence of 488 nm fluorescent punctate artefacts, likely caused by aggregates of the Alexafluor 488 antibody. These persisted despite centrifugation of the antibody tube in attempt to draw such aggregates to the bottom, and sampling from the top.

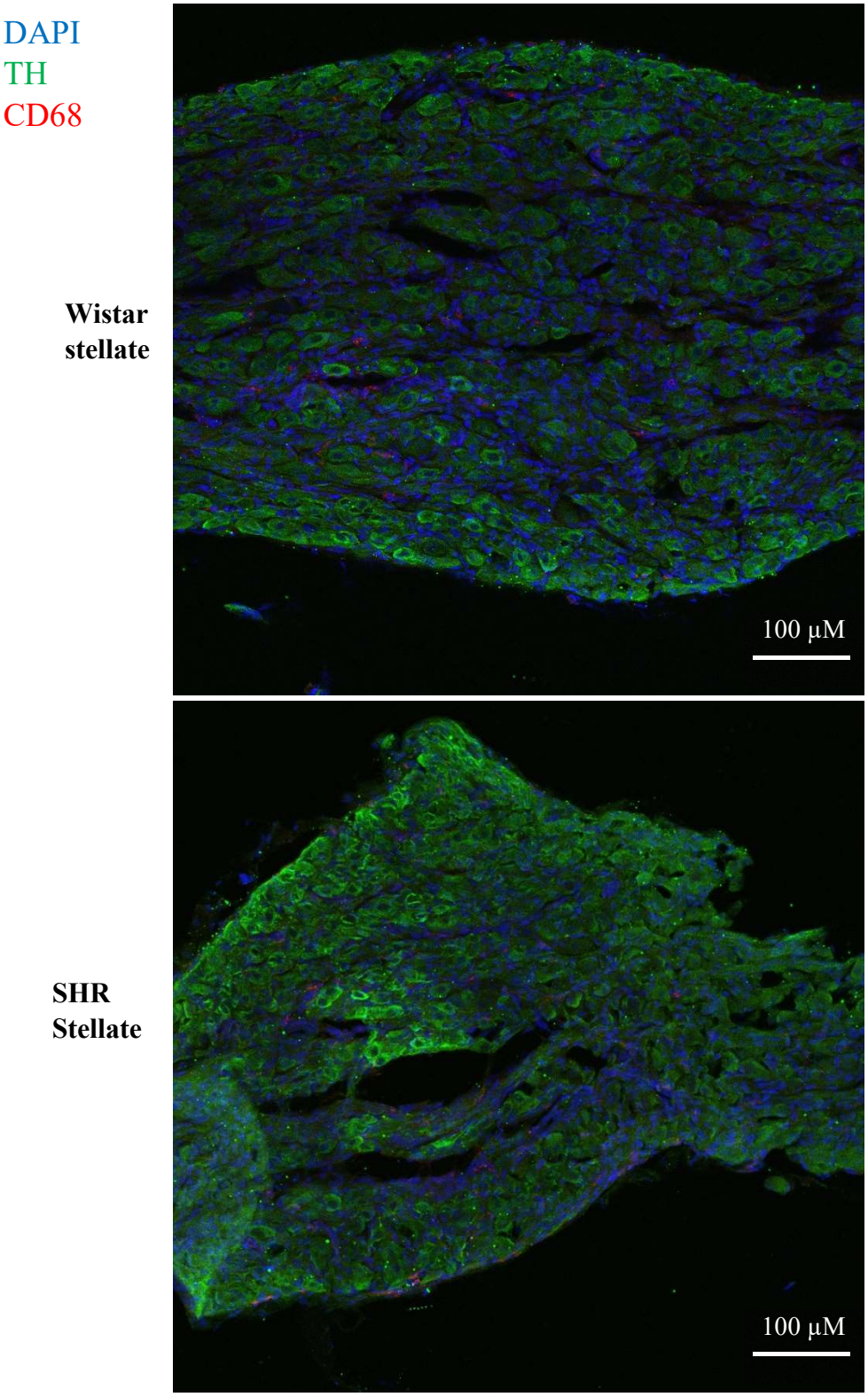

Figure 7| Immunohistochemical images of sympathetic neurons (TH) and macrophages (CD68) in 3-week old Wistar and pre-SHR rat tissue. A nuclear stain, DAPI, was also used. a) Wistar stellate ganglion, b) SHR stellate ganglion. These ganglia comprise a large number of sympathetic neurons (green) with some small macrophages (red) amongst them. The acellular spaces within the tissue likely reflect empty blood vessels following cardiac perfusion. *(Figure legend continued on next page)*

DAPI
TH
CD68

WST stellate no primary antibodies

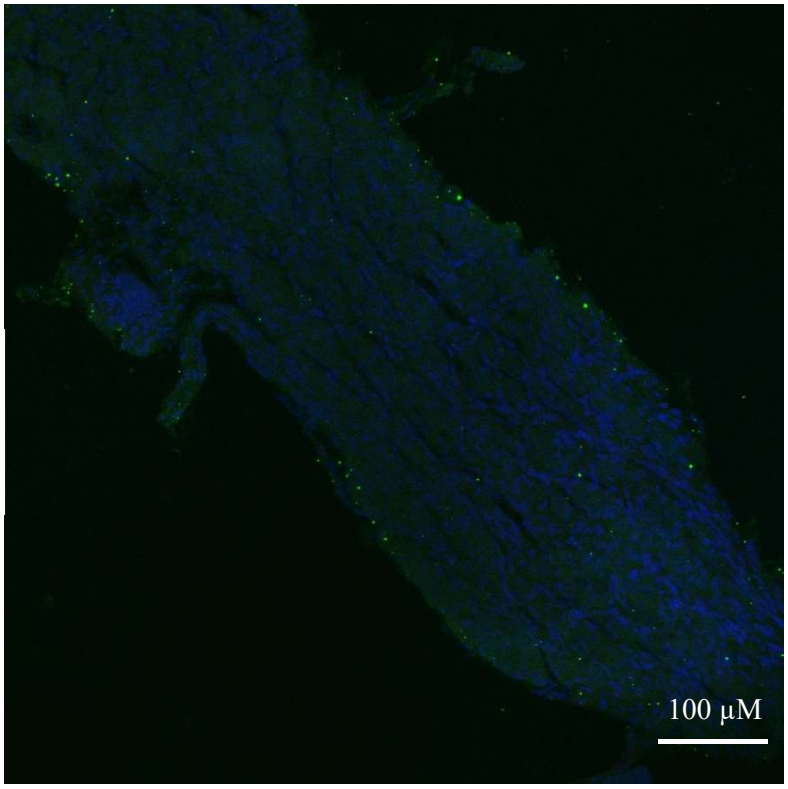

WST spleen

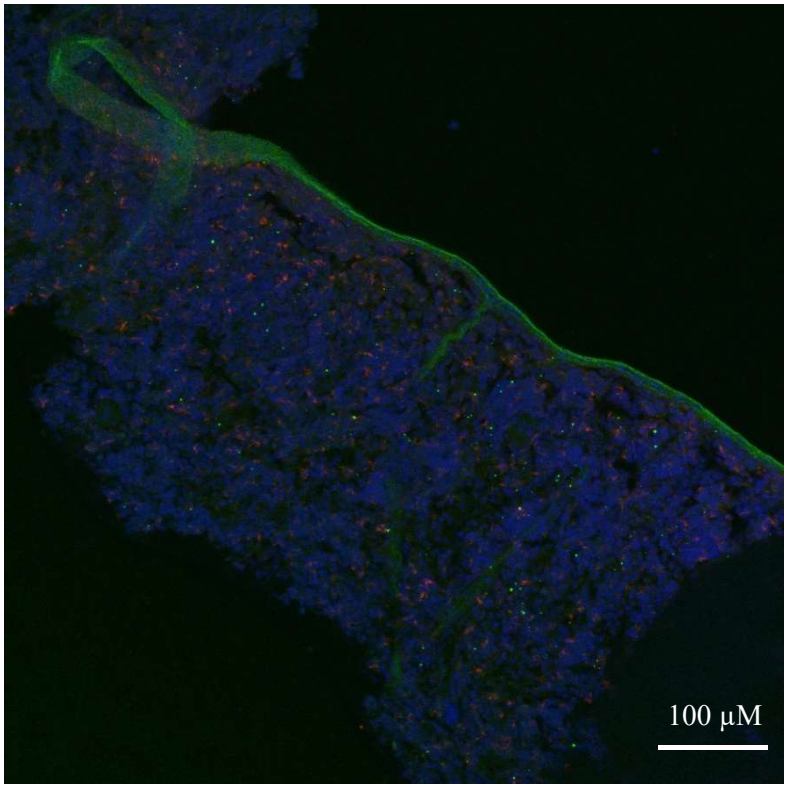

Figure 7 continued| c) Wistar stellate ganglion stained with only DAPI and the secondary antibodies, serving as a negative control. There appears to be some 488 nm auto-fluorescence, but the tissue clearly lacks the cellular pattern of a). d) Wistar spleen stained as a positive control for $CD68^{+}$ macrophages; many punctate cells appear similarly to those of a) and b). A large TH^{+} ribbon which penetrates the rest of the tissue is interestingly also present, likely representing a sympathetic nerve fibre.

III.3.5 The altered monocyte-macrophage subset ratio is not conserved in the blood of human essential hypertensive patients

To examine the relevance of the findings from the SHR, blood samples from humans with diagnosed essential hypertension were analysed using an equivalent flow cytometry panel, and compared to sex-, age-, and BMI-matched controls. Ideally stellate ganglia monocyte-macrophages would have been examined in these participants, but this tissue is not readily available, and can only be obtained from those undergoing stellectomy or deceased organ donors. For this reason, blood had to suffice as the only available sample for comparison, blood having been tested in the rat models as well.

The selection criteria for each group are described in Chapter II.3. These were chosen to provide a confirmed hypertensive group (A), and a control group (B) which were normotensive (BP ≤120/80 mmHg). This meant any patients not formally diagnosed with hypertension, with a clinic-measured blood pressure in the range of 120/80-139/89 mmHg (the prehypertensive range) were excluded. This was done to provide two distinct populations, with minimal overlap, allowing a more powerful assessment of whether there exists *any* difference in the blood monocyte populations associated with hypertension. This was important given the high degree of heterogeneity of human participants, and the relatively low n numbers in each group of the study. "Prehypertension" is also rarely confirmed with ambulatory or home blood pressure monitoring, as is full hypertension, so it would have been difficult to assess if those with blood pressures in the range of 120/80-139/90 mmHg measured on the one occasion of their presentation to the clinic reflected *true* prehypertension. For these reasons, this ambiguous range of blood pressures was not tested. Although the focus of the rat data was on prehypertensive animals, these are a significantly more homogeneous population

where the subtler effects can be more easily examined, whereas the focus of the human study was to test for *any* evidence of an effect. Furthermore, the stellate ganglion observations of these animals were still conserved in older ones.

Volunteer details are given in Table 4; there were no significant differences between the groups in terms of the matched factors, but the essential hypertensive group, despite the use of a number of anti-hypertensive medications, had higher systolic and diastolic blood pressure readings. Upon diagnosis of hypertension, all patients will be offered treatment, which is another variable added to those studied. However, as these target pathways supposedly downstream of the immune system changes hypothesised to be part of hypertensive pathology, these were not likely to affect any monocyte-macrophage phenotype present in human hypertension.

Humans have three monocyte subsets: in addition to the classical ($CD14^{++}/CD16^{-}$) and non-classical ($CD14^{+}/CD16^{+}$) types, an intermediate subset ($CD14^{++}/CD16^{+}$) is also observable. Nine of the hypertensive and six of the normotensive samples produced viable flow cytometry data, which were gated according to the scheme in Figure 8. There were, however, no significant differences in the relative proportions of any of these three subsets between the essential hypertensive and control groups (Figure 9). There were also no significant differences between the proportions of any other leukocyte types between the two groups.

Table 4| Characteristics of the human blood donor participants in this study, from the Oxford Biobank. *=p<0.05 group A versus group B; Welch's t-test (normal data), Mann-Whitney test (non-normal data) or Fisher's exact test (sex).

Patient	Sex	Age	BMI	Mean SBP	Mean DBP	Hypertension Medication
A1	M	56	27.8	147	90	None (taken off by GP)
A2	F	69	25.0	176	88	Atenolol (no meds that morning)
A3	M	59	23.5	129	77	Amlodipine (10 mg OD), ramipril (2.5 mg OD)
A4	F	55	26.2	147	96	Losartan (100 mg OD)
A5	F	61	25.9	127	74	Ramipril (10 mg OD), amlodipine (5 mg OD)
A6	M	55	26.8	132	86	Amlodipine (10 mg OD)
A7	F	59	25.8	147	82	Felodipine (5 mg), perindopril (2 mg)
A8	F	59	25.1	129	86	Lisinopril (5 mg)
A9	M	54	26.8	157	86	Amlodipine, Enalapril
A10	F	55	23.9	124	84	Ramipril
Mean	4M/6F	58.2	25.68	141	85	N/A
B1	F	61	25.8	115	76	-
B2	F	61	29.4	121	78	-
B3	F	55	24	128	81	-
B4	F	62	26.6	120	80	-
B5	F	59	24.8	119	78	-
B6	M	54	23.9	105	75	-
B7	M	33	23.9	115	70	-
B8	M	40	26.6	126	80	-
B9	F	57	27.2	110	76	-
B10	M	57	27.3	121	74	-
Mean	4M/6F	53.9	25.95	118	77	N/A
p value: A vs B	>0.99	0.75	0.71	0.0013*	0.0034*	

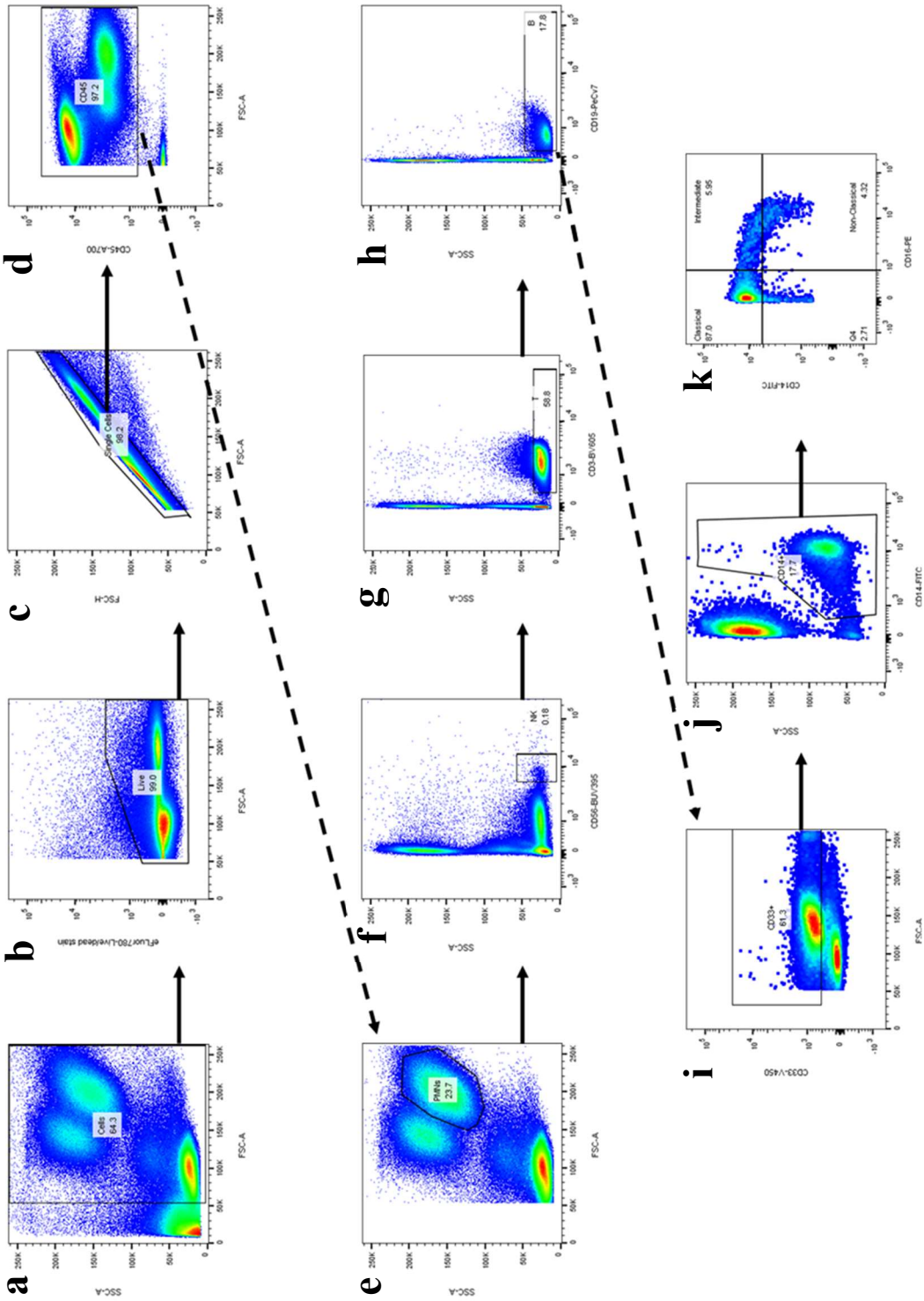

Figure 8| Gating strategy for analysis of leukocytes in human blood, running sequentially from a) to h). Each selected gate was carried forward to the next panel (indicated by the arrows) for the next step. The following populations were selected in each panel: a) real cells; b) live cells; c) single cells; d) leukocytes ($CD45^{+}$); e) non-neutrophil (FSC/SSC location, negative gate); f) non-NK cells ($CD56^{-}$), g) non-T cells ($CD3^{-}$); h) non-B cells ($CD19^{-}$); i) myeloid ($CD33^{+}$); j) 'true' monocytes ($CD14^{+}$); k) classical ($CD14^{++}/CD16^{-}$), intermediate ($CD14^{++}/CD16^{+}$) non-classical ($CD16^{+}/CD14^{+}$) monocytes-macrophages.

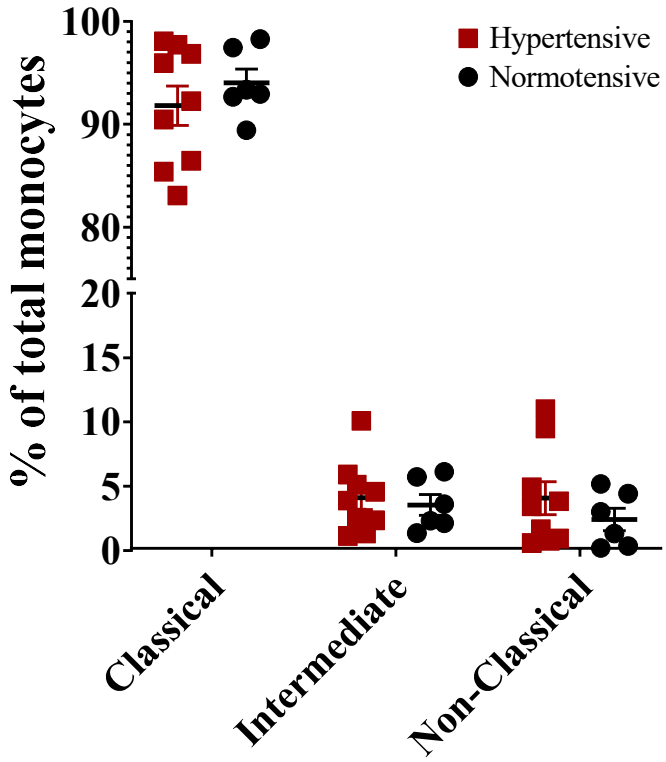

Figure 9| Proportions of human monocyte subsets in the blood of normotensive and hypertensive volunteers. Data are expressed as mean±SEM. * signifies $p<0.05$ WST versus SHR; Welch's t-test with q-values determined by the two-stage set-up method of Benjamini, Krieger and Yekutieli.

III.4 Discussion

The main findings of this chapter are:

1. The SHR stellate ganglia and SCG contained fewer total leukocytes, fewer NK cells, and more neutrophils, than those of the Wistar rat.
2. The SHR sympathetic ganglia generally displayed a lower classical-to-non-classical monocyte-macrophage ratio than those of Wistar rats.
3. This monocyte-macrophage ratio shift was also present in the blood and kidneys of the SHR.

4. There was no difference in the relative proportions of monocyte subsets in the blood of human essential hypertensive patients compared to normotensive controls.

III.4.1 Wistar and SHR SNS leukocytes

There reside fewer leukocytes in the sympathetic ganglia of the SHR compared to Wistar rat. This reaches statistical significance in the stellate and SCG, while not in the CG/SMG, despite a similar, albeit weaker, trend being apparent. Similarly, the stellate and SCG of the SHR show fewer NK cells and more neutrophils than their Wistar counterparts, and the ratio of classical/non-classical monocyte-macrophages is much lower.

With regard to the lack of these differences in the CG/SMG, this is a substantially more technically difficult tissue to isolate, and the flow cytometry samples obtained all produced many fewer leukocytes of all types than the previous two tissues. For this reason, it is possible that there is not sufficient statistical power to detect a difference here, despite the similar trends as for the stellate and SCG being apparent.

The only differences found between the Wistar and SHR blood and renal leukocytes were the lowered classical/non-classical monocyte-macrophage ratios, although in the case of the blood data, a high degree of data variation could potentially mask any underlying differences. Schmidschonbein et al. (1991) found higher counts of leukocytes, combined monocytes and lymphocytes and neutrophils in SHRs compared to age-matched Wistar rats, although these were recorded as cells per mm^3 blood, different to the per 1000 single cells measurements made using the flow cytometric methods of this chapter, making comparisons difficult. It is important to note however, that their neutrophil count

difference did not reach significance for the younger 4-8 week old SHRs, as all the other comparisons did.

III.4.2 Neutrophils and NK cells

Neutrophils are generally the first cell type recruited to a site of inflammation, and enter the tissue in attempt to kill pathogens, particularly extracellular bacteria or fungi. More recently, they are increasingly emerging as important contributors to chronic inflammation (Soehnlein et al., 2017), and the greater number of neutrophils in the SHR SNS ganglia may hint at some form of inflammation within this tissue. It also appears that the neutrophils of the SHR have greater oxidative activity than do those of the Wistar rat (Schmidschonbein et al., 1991; Ohmori et al., 2000; Chatterjee et al., 2009), potentially contributing to inflammation, oxidative stress and tissue damage in this hypertensive model. Again though, there has been no study of these phenomena in the pre-hypertensive SHR.

Neutrophils release chemoattractant signals which induce monocyte recruitment to sites of inflammation, as well as alarmins which polarise monocyte-macrophages towards a pro-inflammatory phenotype. Macrophages in turn can release mediators which promote neutrophil survival, thereby delaying resolution. Interestingly it has been suggested that neutrophil ROS production may inhibit macrophage efferocytosis of apoptotic neutrophils, prolonging inflammation (Soehnlein et al., 2017). However, a number of other sources show that inhibition of phagocyte ROS production prevents efferocytosis, for example in chronic granulomatous disease, and therefore contradict this (reviewed by Lin et al. (2021)). It is therefore unclear how ROS affect efferocytosis, although it could be the case that a basal level of ROS is required for efferocytosis (perhaps particularly from macrophages), above which it is inhibitory. Further study of this phenomenon is

clearly required, however if true, taken together with the apparent enhanced ROS production by SHR neutrophils (Schmidschonbein et al., 1991, Ohmori et al., 2000, Chatterjee et al., 2009), this suggests they could drive chronic inflammation in these animals. It is possible the shift in monocyte-macrophage subsets seen within the SHR ganglia could be related to this, although this shift was also found in the blood and kidneys (to a lesser extent), so would appear to be systemic.

NK cells are important cytotoxic effectors, which kill infected, senescent and tumour cells, and are usually involved in type 1 inflammatory responses, being closely related ILC-1s (Spits et al., 2013). Their higher numbers in the Wistar ganglia, in addition to higher numbers of T and B lymphocytes in the Wistar SCG could be interpreted such that it is this strain which exhibits a more inflammatory SNS phenotype. Similarly, within the SCG there were also significantly higher numbers of T cells and B cells in Wistar rats, and this was reflected in a non-significant trend in this same direction in the stellate. However, it seems unlikely that healthy, wild-type animals would have exhibit such an inflammatory reaction under baseline conditions, and this finding is not likely biologically significant as the Wistar stellate ganglion transmission is seemingly normal.

III.4.3 Classical and non-classical monocytes

Monocytes are derived from the myeloid haematopoietic lineage, and circulate in the blood until chemoattractant signals cause their extravasation into the tissues, where they may differentiate into macrophages or myeloid dendritic cells (Jakubzick et al., 2017). Many tissue-resident populations of macrophages are not derived from circulating monocytes, although sympathetic associated macrophages (SAMs) are highly positive for CD45, and when depleted are repopulated from the bone marrow (Pirzgalska et al., 2017). While these findings were demonstrated for sympathetic *fibres*, the high CD45 positivity

of our "monocyte-macrophages" suggests this may be tentatively inferred to the ganglia, which are continuous with sympathetic fibres.

It appears that classical monocytes, while having their own functionality, also serve as a parent population, giving rise to the other subtypes (Yrlid et al., 2006; Tak et al., 2017; Patel et al., 2017; Wolf et al., 2019). Many attempts have been made to attribute specific functionalities to each subset of monocytes. A review in 2005 of Gordon & Taylor ascribed, based on mouse data, the terms "inflammatory" to the classical monocytes, and "resident" to non-classical cells; the former were suggested to promote inflammation and move to inflamed tissues to clear pathogens (principally due to its high CCR2 expression (Geissmann et al., 2003)), while the latter formed homeostatic, tissue-resident macrophages. The intermediate subset was claimed to express certain features of both. Despite its persistent usage in the literature, as might be expected, this categorisation is a substantial oversimplification. Perhaps the main line of evidence underlying this paradigm comes from the observation that, resulting from their higher CCR2 expression, classical monocytes were more readily recruited to sites of inflammation than non-classical cells in murine inflammation models (Geissmann et al., 2003). However, it was later shown that the non-classical "resident" monocytes are rapidly recruited to sites of tissue infection in a manner dependent on their major chemokine receptor CX_3CR_1 (which has low expression in classical monocytes) and contribute to early inflammation by release of cytokines such as TNF-α (Auffray et al., 2007).

Furthermore, in a number of systemic inflammatory diseases, numbers of non-classical monocytes are increased, and in some cases specific disease-promoting pro-inflammatory roles demonstrated, notably: systemic lupus erythomatosis (SLE) (Mukherjee et al., 2015; Zhu et al., 2016), sepsis (Mukherjee et al., 2015) and obesity and metabolic syndrome

(Poitou et al., 2011) (although this latter study didn't distinguish between non-classical and intermediate monocytes). In rheumatoid arthritis the role of non-classical monocytes is more complex: some reports claim their blood numbers are increased (Lacerte et al., 2016), others that they are reduced (Cairns et al., 2002; Smiljanovic et al., 2018), or unchanged (Rossol et al., 2012; Yoon et al., 2014). As suggested by Smiljanovic et al. (2018), a confounding factor in all such studies is the use of glucocorticoids as a rheumatoid arthritis therapy, which has been shown (albeit in the context of uveitis) to increase the proportion of human intermediate blood monocytes (Liu et al., 2015), and interestingly many of these studies showed such an increase in the rheumatoid arthritis patients (Rossol et al., 2012; Yoon et al., 2014; Lacerte et al., 2016). For this reason, Smiljanovic et al. (2018) compared rheumatoid arthritis patients to those with osteoid arthritis (which lacks the same immunopathology, but for which a common treatment is also glucocorticoids), and found a lower proportion of blood non-classical monocytes in the rheumatoid patients, with no change in intermediate monocytes. Compared to healthy controls they also found a lower proportion of non-classical, as well as a higher proportion of classical monocytes in the blood of rheumatoid arthritis patients. It remains unclear therefore which monocytes, if any, are actually enriched in human rheumatoid arthritis. Similarly, in the rodent serum-transfer inflammatory arthritis model, non-classical monocytes seem to be the primary mediators of disease (Misharin et al., 2014; Puchner et al., 2018; Montgomery et al., 2019), in which there are no confounding effects of glucocorticoids, but pro-resolution roles of these cells have also been described (Brunet et al., 2016).

In other diseases such as atherosclerosis, or post-MI, non-classical monocytes seem to be protective (see review of Narasimhan et al. (2019)), but it is true that at least in certain

disease states, non-classical monocytes appear to have a pro-inflammatory phenotype. Additionally, non-classical monocytes seem to increase in number during ageing, and a corresponding shift towards inflammatory activity may contribute to the phenomenon termed “inflamm-ageing” (Ong et al., 2018).

Some reports have suggested that classical and intermediate monocytes release greater levels of pro-inflammatory cytokines in response to toll-like receptor stimulation (Cros et al., 2010; Thiesen et al., 2014; Boyette et al., 2017), but others have shown that in many cases, it is the non-classical monocytes which are the major secretors of certain key inflammatory mediators (Wong et al., 2011; Mukherjee et al., 2015; Ong et al., 2018). Wong et al. (2011) suggest that such discrepancies could be due to a difference in the purification CD14 antibody used. The above studies which showed non-classical monocytes not to be the major producers of inflammatory cytokines either used the M2E5 anti-CD14 clone to isolate the monocytes (Cros et al., 2010; Thiesen et al., 2014), which is known to inhibit responsiveness to LPS stimulation (Power et al., 2004), or didn’t list the clone used (Boyette et al., 2017). Those which reported higher inflammatory cytokine release from these non-classical monocytes used the 61D3 anti-CD14 antibody for monocyte isolation (Wong et al., 2011; Ong et al., 2018), or performed the stimulation in whole-blood and only separated the monocytes after this (Mukherjee et al., 2015). Additionally, non-classical monocytes seem to be the most potent in inducing naïve $CD4^+$ T cell activation (Liu et al., 2015). In any case, this evidence suggests that at least in a number of cases, non-classical monocytes are pro-inflammatory cells.

Mukherjee et al. (2015) also found that classical monocytes express higher levels of phagocytic receptors, CD36 and CD163, while having little inflammatory function, potentially suggested a more homeostatic, phagocytic role for these cells. For example,

CD36 plays a role in clearing apoptotic cells (Ferracini et al., 2013) while CD163 is involved in the clearance of hapto-haemoglobin complexes (Kristiansen et al., 2001). Phagocytosis assays performed by Cros et al. (2010) also support this phagocytic phenotype.

III.4.4 Potential functional effects of monocyte-macrophage subset shift on sympathetic ganglia

The experiments carried out in this chapter suggest that the pre-SHR has a shift in its monocyte-macrophage subset proportions, having relatively more non-classical, and fewer classical monocytes, in their sympathetic ganglia, blood and kidneys. According to the aforementioned evidence it would thus seem that this strain may have an enriched population of inflammatory cells, while losing a useful homeostatic phagocytic cell type. As described in Chapter 1, a range inflammatory reactions can increase neuronal activity in a number of contexts, such as neuropathic pain (Scholz and Woolf, 2007), post-MI (Zhou et al., 2004; Hasan et al., 2006; Wernli et al., 2009), and even central sympathetic outflow in hypertension (Wu et al., 2012; Santisteban et al., 2015). For this reason, it will be interesting to address what impact, if at all, the altered monocyte-macrophage ratio has on the physiology of the SHR stellate neurons.

No significant differences in monocyte subset proportions were found in the human volunteers. This may suggest that SHR hypertension is mechanistically different to the human form, with regard to monocyte-macrophages, which is a caveat to the translatability of this thesis. Furthermore, humans have an extra monocyte subset compared to the rat, and while there is no clear functional significance of this difference, it adds complexity in comparing rat and human data. At the least this negative human result could result from inflammatory driven neurogenic hypertension representing only

a proportion of the human disease. Nevertheless, the human subjects examined reflect a substantially more heterogeneous pool than the genetically identical rats used here, both within the hypertensive and normotensive groups. It may be the case that if a difference does exist between these two human populations, this small study (with viable sample n numbers of 9 hypertensive and 6 normotensive subjects), may be underpowered to detect subtle changes in monocyte-macrophage subset proportions. This is especially true given the lack of control for the potential differing aetiologies of hypertension in the subjects (for example only >50% of cases are thought to have a neurogenic origin; DiBona & Esler, 2010), and medications the hypertension patients were taking. Other studies cited here have detected such differences between patients with inflammatory diseases and healthy controls. However, these either examined severe inflammatory conditions: SLE (Mukherjee et al., 2015; Zhu et al., 2016), sepsis (Mukherjee et al., 2015) and rheumatoid arthritis (Smiljanovic et al., 2018), which are more markedly associated with systemic inflammation than essential hypertension (and therefore monocyte subset shifts are likely to be more apparent), or used substantially higher n numbers than the study performed in this chapter (Poitou et al., 2011). Additionally, the SHR versus monocyte ratio difference in the blood was substantially smaller than in the stellate ganglia or SCG. If this were comparable in humans, as only the blood of human subjects was tested, it is much less likely that such a small difference in the blood would be found. In the future, a larger-scale examination of human monocyte subsets in essential hypertension would be useful to clarify this, in addition to a study restricted to only patients with a dysautonomic phenotype. Additionally, studying a defined prehypertensive group would be useful as a comparison to the results of the SHR experiments, and to examine the human monocyte populations throughout disease progression. This would potentially enable a continuous

co-variate relationship between monocyte ratios and blood pressure to be explored, where this study was unfortunately limited to a binary categorisation of blood pressure, due to sample sizes. Studying human stellate ganglion monocyte-macrophages would also be more powerful. Unfortunately, for the purposes of this thesis, it was not possible to examine sympathetic drive in the volunteers, nor collect ganglionic tissue.

III.4.5 A difference in monocyte recruitment, or production?

There are two main possibilities for which the lowered classical-to-non-classical monocyte ratio may be present in the pre-SHR sympathetic ganglia. First, it may be the case that the SHR inherently produces a greater proportion of non-classical monocytes than the Wistar; as non-classical monocytes arise from classical ones (Yrlid et al., 2006; Tak et al., 2017; Patel et al., 2017). This would mean an inherent increase in the extent of differentiation from the classical to non-classical monocytes. This idea is supported by the observation here reported that the monocyte ratio is altered in the circulating pool within the blood, and also within the kidneys. Second, there may be a greater extent of non-classical monocyte recruitment to the sympathetic ganglia, or a higher degree of classical-to-non classical transitioning within these loci. Future work should aim to probe the reason for this altered ratio within sympathetic ganglia and the blood, so that a means of reversing it could be identified, if it is revealed to contribute to sympathetic hyperactivity.

III.4.6 Limitations

The experimental approach in this chapter was not without limitations, many of which were unavoidable for various reasons. First, a better technique for assessment of the stellate ganglia leukocytes would have been single cell sequencing, rather than flow cytometry. This approach provides an insight into the mRNA signature of individual cells

of a sample, and therefore would have been more informative in not only more thoroughly categorising the different leukocyte populations, but also comparing the transcriptomic signature of the same populations between rat strains. While our laboratory has published a single-cell sequencing dataset from the stellate ganglion (Davis et al., 2020), this was able to be performed only on 10,000 cells from each sample, meaning only a small number of leukocytes were recorded, which was insufficient for specific immune cell analysis. Ideally, one would have fluorescently-sorted the leukocytes, or even monocytes, from the tissue, before using these for single-cell sequencing. However, single-cell sequencing is very expensive as a technique, such that it was not available for use in this thesis. Second, the datasets from older SHRs suffer from low n numbers. Unfortunately, rats at this age have a high financial cost and therefore analysis of more of these was not affordable, particularly as the focus of this study was on the pre-hypertensive SHR. Thirdly, the human study reported here did not examine large numbers of participants, as may be required for detection of subtle immunological changes in such a heterogeneous population.

III.4.7 Conclusions

1. The SHR appears to systemically show a lower ratio of classical/non-classical monocyte-macrophages, including sympathetic ganglia, the blood and kidneys.
2. This monocyte subset difference was not apparent in the blood of a small study of human essential hypertension patients compared to controls, which may reflect a type II error.

CHAPTER IV

Comparing the inflammatory and chemotactic phenotype of SHR and Wistar classical and non-classical monocytes

IV.1 Introduction

IV.1.1 Inflammatory mediators in the SHR sympathetic ganglia?

In Chapter III, a shift in the monocyte-macrophage subset proportions within the SHR sympathetic ganglia was described: the SHR has relatively more non-classical, and fewer classical monocyte-macrophages than its Wistar control. The literature suggests that an enrichment of non-classical monocytes is related to a number of systemic inflammatory diseases (Poitou et al., 2011; Misharin et al., 2014; Mukherjee et al., 2015; Zhu et al., 2016; Smiljanovic et al., 2018; Puchner et al., 2018) This monocyte-macrophage shift was accompanied by an increase in ganglionic neutrophil content, and these cells are known to contribute to monocyte-macrophage driven inflammation, particularly through release of ROS, of which SHR neutrophils tend to produce more (Schmidschonbein et al., 1991; Ohmori et al., 2000; Chatterjee et al., 2009). Monocyte-macrophages are seemingly the most abundant sympathetic ganglion leukocyte (Chapter III) and may have important functional roles in the SNS (Pirzgalska et al., 2017). Given the subset ratio shift was the most striking and conserved finding of Chapter III, and they are often dominant in chronic inflammatory disorders (even if neutrophils are involved) these cells were the focus of study henceforth.

Having assessed the cellular component of the SHR sympathetic ganglia, it was next necessary to determine whether these ganglia contain an inflammatory milieu, and if so how the macrophages relate to this. As described in Chapter I, rostral ventrolateral medullary inflammation involving the cytokines TNF-α, IL-1β and IL-6, and PGE_2 can promote heightened sympathetic outflow and hypertension (Wu et al., 2012). In neuropathic pain, macrophage release of TNF-α, IL-1, IL-6, IL-18, and LIF contributes to an inflammatory reaction, the ultimate result of which is heightened pain fibre activity

and neuropathic pain. These macrophages are recruited to the tissue by the CCL2 and CCL3 chemokines (Scholz & Woolf, 2007). It is possible similar mechanisms may be able to produce sympathetic neuron hyperactivity. In relation to this, in the same pain syndrome, IL-6 even promotes sympathetic neuron sprouting into the dorsal root ganglia (Ramer et al., 1998). Of the above-mentioned mediators, non-classical monocytes have been shown to produce more: TNF-α (Wong et al., 2011; Mukherjee et al., 2015; Ong et al., 2018), IL-1β (Wong et al., 2011; Mukherjee et al., 2015), IL-6 (Wong et al., 2011; Ong et al., 2018) and CCL3 (Ong et al., 2018). It is therefore conceivable that a type 1 inflammation may underlie sympatho-excitation in essential hypertension.

IV.1.2 Other potential mediators of sympathetic hyperactivity

Also involved in the inflammatory reactions producing sympathetic hyperactivity in nerve injury-induced neuropathic pain, and post-MI, are classic neurotrophic signals such as NGF. This is released by Schwann cells and macrophages respectively, and increases neuronal sprouting and activity. Moreover, NGF may also promote further macrophage activation (Barouch et al., 2001).

Oxidative stress may also contribute to sympathetic hyperactivity. In the LPS-induced RVLM inflammation model of Wu et al. (2012), increased superoxide production occurs, and localised anti-oxidant treatment is able to antagonise the hypertensive effect. ROS-induced mitochondrial dysfunction also occurs in the RVLM of the SHR, where it has been shown to similarly contribute to sympathetic hyperactivity (Chan et al., 2009).

IV.1.3 Monocyte chemotaxis

Monocytes continually circulate in the blood and are recruited to the tissues by chemokine signals, including: CCL2 and CCL7 (via CCR2), CX_3CL1 (CX_3CR1) and CCL3 and

CCL5 (CCR1 and CCR5) (Shi & Pamer, 2011). Of these, CCL2 is one of the most important classical monocyte attractants (these expressing CCR2), while non-classical monocytes respond preferentially to CX_3CL1 (Geissmann et al., 2003).

In Chapter III it was shown that the relative enrichment of non-classical monocytes in the SHR stellate ganglia is also present in the blood. However, it is also possible that an altered inflammatory environment within this tissue could involve altered chemokine expression, and therefore the difference in monocyte subset ratio could in part arise from a difference in recruitment.

IV.1.4 Hypotheses and aims of the chapter

Hypothesis:

- There exists a type 1 inflammatory mediator profile within the SHR sympathetic ganglia and specifically the monocyte-macrophages.
- A difference in sympathetic ganglion chemokine release mediates the altered classical-to-non classical ratio found within these tissues.

Aim:

- To characterise the type 1 inflammatory gene expression signature of the SHR stellate ganglion.
- To examine the chemokine expression of the SHR stellate ganglion.

IV.2 Methods & Materials

IV.2.1 Quantitative PCR

The qPCR experiments were performed as described in Chapter II.4. Isolated stellate ganglia, FAC-sorted monocytes and BMDMs were snap frozen in liquid N_2 before the

contained RNA was extracted using an RNeasy mini-kit (QIAGEN, Germany), according to the manufacturer's instructions. In the case of monocyte-macrophages isolated from stellate ganglia, the extracted RNA was then amplified using a MessageBOOSTER™ cDNA Synthesis Kit (Lucigen, US), which subsequently converts this to cDNA. Otherwise, extracted RNA was stored at -80°C until conversion to cDNA using a commercially available kit. Briefly, the samples were incubated with DNase at 37°C for 2 min, in order to lyse contaminating DNA, before the reverse transcription reaction was performed using Superscript IV Vilo with UNG (Thermofisher, US). cDNA was stored at -20°C for up to a week before use in the qPCR reaction.

Sample gene expression was then determined using specific Taqman gene expression assays (all components supplied by ThermoFisher, US). 20 µL reactions, each comprising the template cDNA, Taqman Universal MasterMix II with UNG, and a specific primer (all of which are listed in Table 1), were performed on, and analysed by an ABI Prism 7000 PCR machine. Experiments for each gene of interest in each sample were performed in triplicate on the same 96-well plate.

Table 1| Taqman primers used in the qPCR analysis experiments of this chapter.

Gene	**Primer**	**Role**
actb	Rn00667869_m1	Housekeeping gene
b2m	Rn00560865_m1	
gapdh	Rn01462661_g1	
il1b	Rn00580432_m1	Pro-inflammatory type 1 cytokine
tnf	Rn99999017_m1	
il6	Rn01410330_m1	
nos2	Rn00561646_m1	M1 macrophage marker

cd80	Rn00709368_m1	
il10	Rn01483988_g1	Anti-inflammatory cytokine
arg1	Rn00691090_m1	M2 macrophage marker
cd163	Rn0149519_m1	
ccl2	Rn00580555_m1	Classical monocyte chemoattractant
cx3cl1	Rn00593186_m1	Non-classical monocyte chemoattractant
ngf	Rn01533872_m1	Growth factor for neurons
sod1	Rn00566938_m1	Oxidative stress marker
cat	Rn00560930_m1	
ccr2	Rn00573193_s1	Classical monocyte chemokine receptor
cx3cr1	Rn00591798_m1	Non-classical monocyte chemokine receptor
cd43	Rn02749526_s1	Rat non-classical monocyte marker
cd68	Rn01495634_g1	Monocyte/macrophage marker

Data were analysed using the delta-Ct method. Any of the triplicate Ct values for a given gene measurement in a sample which differed by more than two from the mean of the three were excluded from analysis, and the means of all remaining values were taken forward. The mean Ct values were then normalised by subtraction of the mean Ct for the *b2m* housekeeping gene, analysed on the same plate. Gene expression was then compared between SHR and Wistar samples, statistical analyses being performed on raw delta-Ct

values, while fold changes between the strains were calculated, for graphical presentation, via the following equation:

$$Fold\ change\ of\ SHR\ compared\ to\ WST = 2^{-(SHR\ Ct\ value - WST\ mean\ CT)}$$

IV.2.2 FACS & Flow Cytometry

Cell and tissue samples were prepared and stained as described in Chapter II.4. Rat stellate and blood samples were stained using the panel shown in Table 2 and run on a BD FACSAria™ III Cell Sorter. BMDMs were stained with the panel of Table 3 and analysed using a BD LSRFortessa™ X-20. Data were then processed with FlowJo 10 software.

Table 2| Rat leukocyte FACS panel.

Antibody	Host species	Concentration	Laser & Filter set
anti-CD11b-V450	Mouse	1:200	405 - 450/50
anti-CD161a-BV711 (BD Biosciences, US)	Mouse	1:200	405 - 710/50
His48-FITC	Mouse	1:200	488 - 530/30
anti-CD43-PE	Mouse	1:200	561 - 586/15
anti-B220-PECy7	Mouse	1:200	561 - 780/60
anti-CD45-A700	Mouse	1:200	640 - 730/45
anti-CD3-BV605	Mouse	1:25	405 - 610/20
anti-CD68-A647	Mouse	1:10	640 - 670/30
eFluor™ 780 viability dye	N/A	1:2000	640 - 780/60

Table 3| Rat leukocyte flow cytometry panel.

Antibody	Host species	Concentration	Laser & Filter set
anti-CD11b-V450	Mouse	1:200	405 - 450/50
anti-CD161a-BUV395	Mouse	1:200	355 - 379/28
His48-FITC	Mouse	1:200	488 - 530/30
anti-CD43-PE	Mouse	1:200	561 - 586/15
anti-B220-PECy7	Mouse	1:200	561 - 780/60
anti-CD45-A700	Mouse	1:200	640 - 730/45
anti-CD3-BV605	Mouse	1:25	405 - 610/20
anti-CD68-A647	Mouse	1:10	640 - 670/30
eFluor™ 780 viability dye	N/A	1:2000	640 - 780/60

IV.2.3 Chemotaxis assay

A QCM 5 µm 24-well colorimetric chemotaxis assay (Merck, US) was used to measure monocyte chemotaxis towards CCL2 and CX_3CL1, according to the manufacturer's instructions. Briefly, ~1,500 monocytes were loaded into the upper chamber of each well in 250 µl of serum-free media, containing 0.5% BSA. The assay recommends using a range of 0.2-2 × 10^6 cells in each well; however as the monocytes had to be isolated from blood by FACS, this minimum figure was unachievable. In the lower chamber, 500 µl of same media containing 90 ng/ml CCL2, or 50 ng/ml CX_3CL1 (concentrations within the EC_{50} on their respective datasheets) was loaded and the assay left for 24 h at 37°C, under 5% CO_2. After this period, a nuclear stain was used to quantify the number of cells reaching the lower chamber, the intensity of this being measured by a spectrophotometer.

IV.2.4 BMDM culture

BMDMs were cultured as described in Chapter II.3.4. These cells were detached from their plates on day 6 using TrypLE, except where they were being prepared for flow cytometry, in which case 2 mM EDTA in PBS was used to prevent receptor cleavage.

IV.2.5 Statistical analysis

Statistical analyses were performed as described in Chapter II.8.

IV.3 Results

IV.3.1 Inflammatory status of the SHR stellate ganglion

In order to test for evidence of an inflammatory reaction within the pre-SHR stellate ganglia, qPCR was used to examine the mRNA expression of a panel of cytokines, and these compared to Wistar stellates. *il1b*, *tnfa* and *il6* were selected as classic (type 1) pro-inflammatory cytokines (for which much evidence suggests a role in hypertension, as described above), *nos2* and *cd80* as M1 macrophage markers (which align with this type of inflammation), *il10* as an anti-inflammatory pro-resolution mediator, and *arg1* and *cd163*. There were surprisingly no significant differences in these mediators observed between the strains (Figure 1), suggesting inflammatory signals are not involved in the early development of pre-hypertensive sympathetic dysfunction.

Likewise, examining the expression levels of the neurotrophic signal *ngf*, involved in many inflammatory-induced neuronal excitation phenomena (described above), or oxidative stress markers *sod1* and *cat*, also revealed no differences between SHR and Wistar stellate ganglia (Figure 1).

Finally, *ccl2* and *cx3cl1* mRNA expression was tested, these being the main chemoattractants of classical and non-classical monocytes, respectively. Interestingly this

revealed an approximately 4-fold increase in *ccl2* expression in the SHR stellates (p=0.0241), despite no difference in *cx3cl1*. However, the q-value for this *ccl2* result was 0.253 (Figure 1).

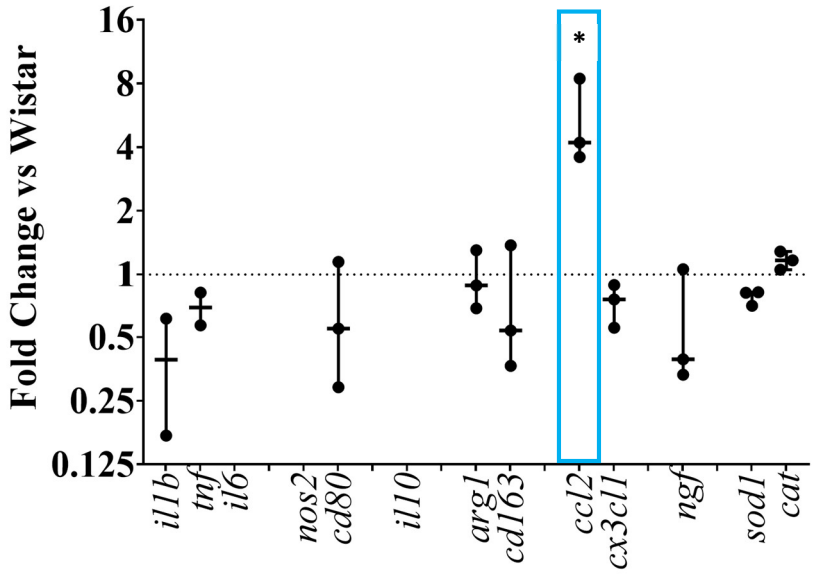

Figure 1| RNA expression of key inflammatory-related genes in the 3-week old SHR stellate ganglia presented as fold expression compared to Wistar. Data are presented as median and range. In cases where no copies of a gene were detected, that data point is not present. * signifies $p<0.05$ SHR versus Wistar. For all normal data, Welch's t-tests were employed, with q values determined by the two-stage set-up method of Benjamini, Krieger and Yekutieli; for non-normal data, Mann-Whitney tests were instead used.

IV.3.2 Mediator profile of SHR monocyte-macrophages

As there were no mediator differences between the SHR and Wistar stellate ganglia (save for *ccl2*), it was next asked whether the monocyte-macrophages themselves show any difference in their expression of the same mediators, with the replacement of the chemokine genes *ccl2* and *cx3cl1* with their respective receptors *ccr2* and *cx3cr1*. A FACS antibody panel was designed (Table 2), based off that used to analyse the immune cells of the stellate in Chapter III, but with the CD161a antibody switched to a different fluorophore in order to accommodate the four, rather than three, lasers on the available cell sorter.

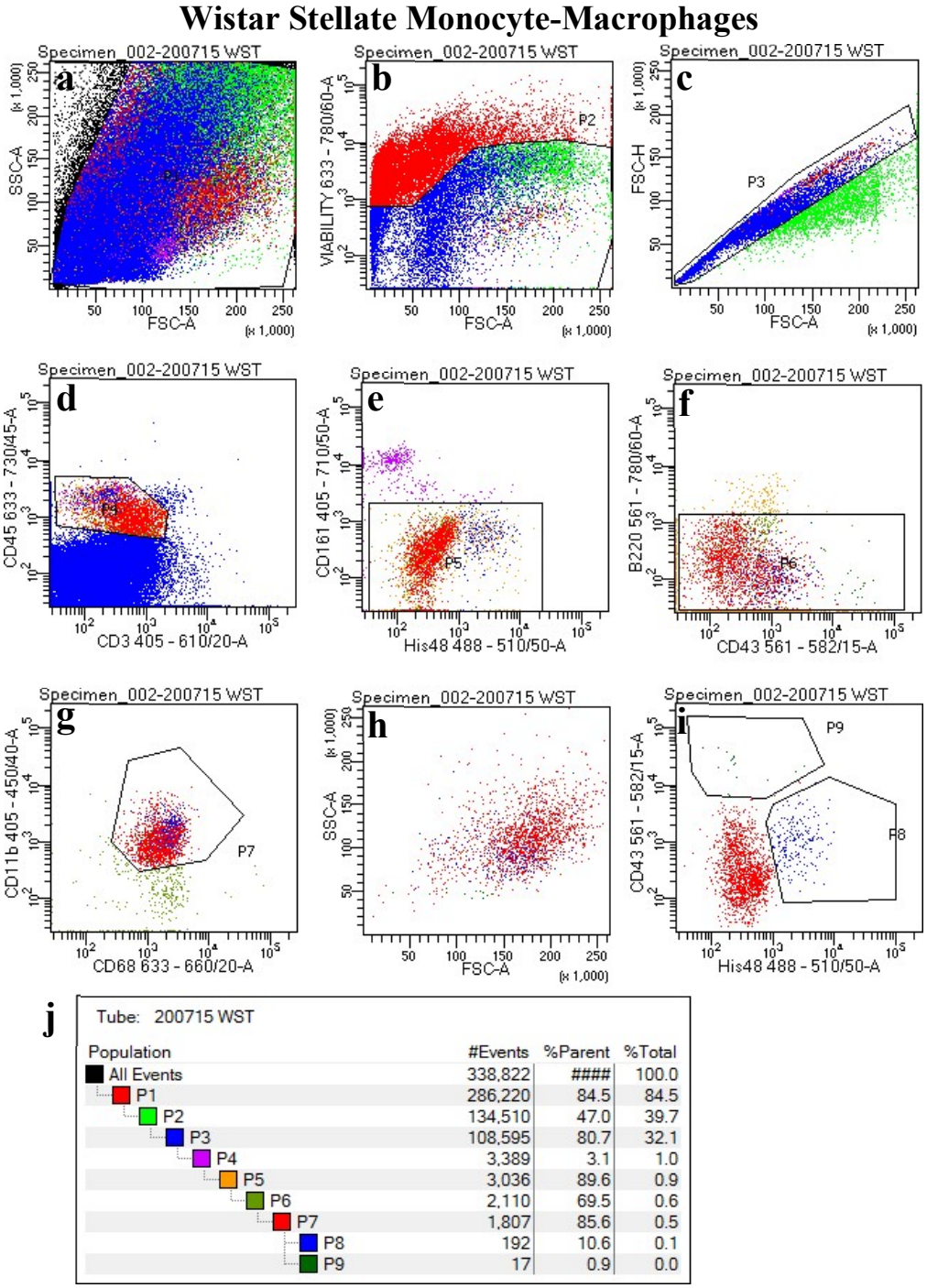

Figure 2| Gating strategy and representative plot from FAC-sorting of Wistar stellate monocyte-macrophages; each major leukocyte population was sequentially gated off, eventually leaving the classical and non-classical monocytes to be sorted and collected. Gates are sequential from a) to i), with the overall tree shown in j). Gates are as follows: P1 = cells; P2 = live; P3 = single cells; P4 = leukocyte and non-T cells; P5 = non-NK cells; P6 = non-B cells; P7= $CD11b^{+}/CD68^{+}$ monocytes; P8 = classical monocytes; P9 = non-classical monocytes. Note, the software reached its maximum number of gates, so a non-neutrophil gate could not be drawn in panel h). Instead, the monocytes were gated off based on CD43 and His48 in panel i), and the remaining population confirmed to be neutrophils by their higher SSC when back-gated in panel h) where they are the red population.

Using this panel, classical and non-classical monocyte-macrophages were isolated from rat stellate ganglia. However, even after amplifying the RNA extracted from these cells, there was not sufficient expression to detect the majority of genes of interest by qPCR; even the housekeeping genes *actb*, *b2m* and *gapdh* examined all had Ct values >25 in the Wistar, and >30 in the SHR (Figure 3). For this reason, comparisons of stellate monocyte-macrophage gene expression were not possible.

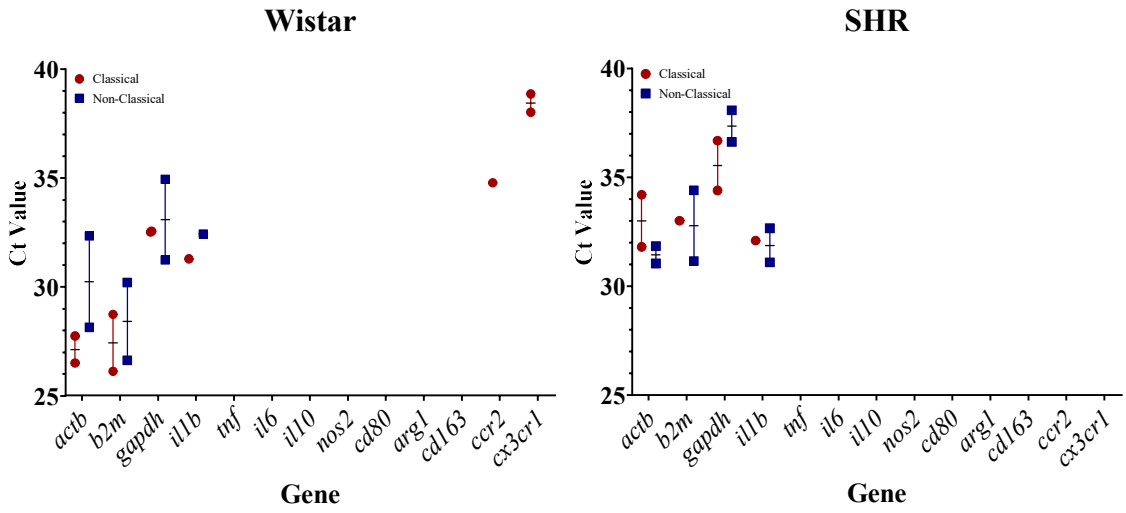

Figure 3| qPCR data obtained from FAC-sorted Wistar stellate monocyte-macrophages. Data are presented as median with range. In cases where no copies of a gene were detected, no data point is shown.

The stellate ganglia appear to contain too few monocyte-macrophages for effective mRNA analysis. As the shift in monocyte subset proportions originally determined in the stellate in Chapter II was also reflected in the blood, this much larger pool of monocytes was then used to attempt the same FACS (Figure 4) and subsequent qPCR analysis. Neither the classical, nor non-classical monocytes displayed any inter-strain differences with this qPCR panel. To compare between these monocyte subsets, the Wistar and SHR groups were therefore combined in order to provide more statistical power. The altered subset ratio would mean a potential difference between strains if there were any differences between the classical and non-classical monocytes themselves. The only

mediator difference to reach statistical significance was the higher *il10* expression by the non-classical monocytes, while no classical monocyte samples expressed this (p=0.048).

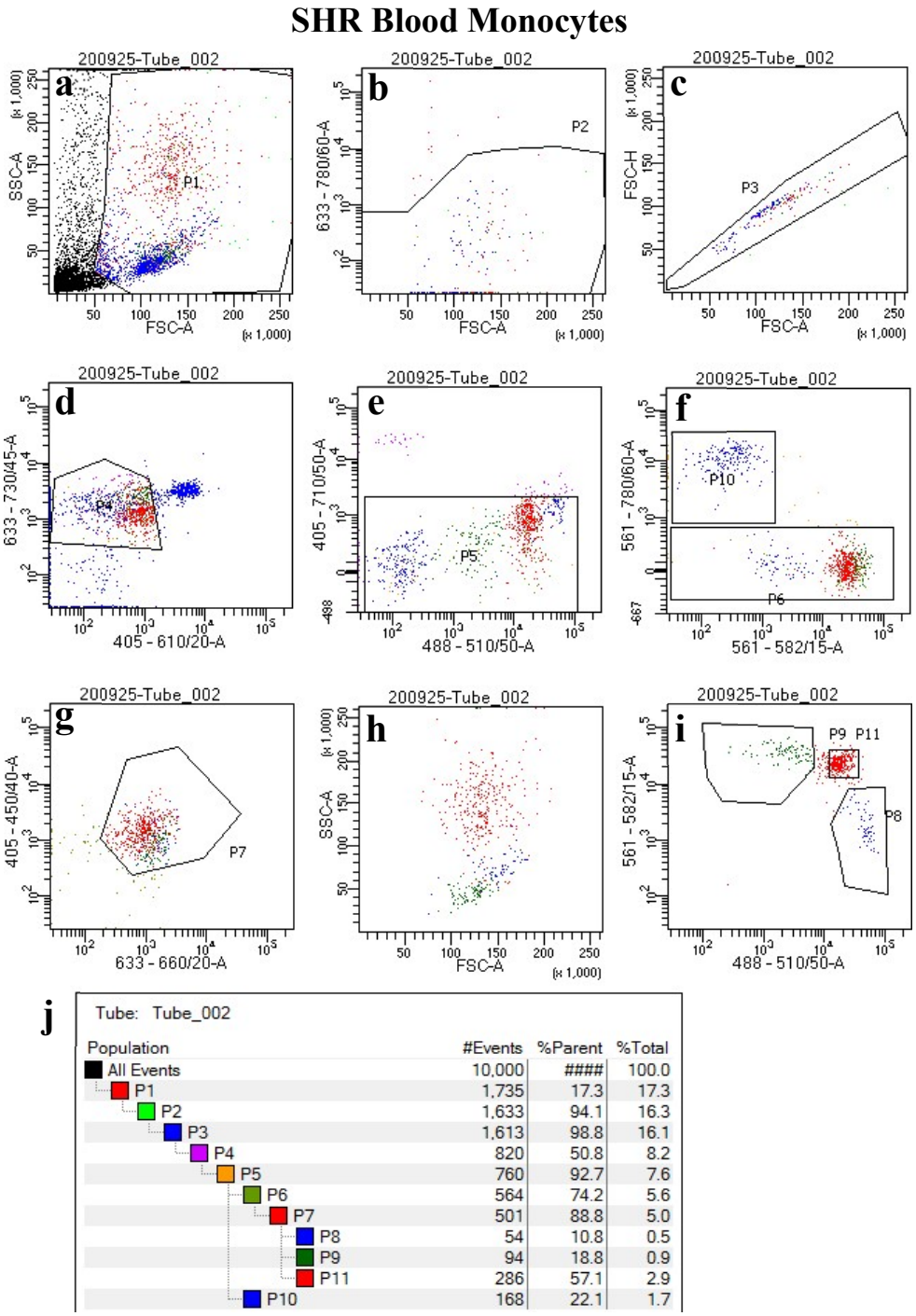

Figure 4| Gating strategy and representative plot showing 10,000 events from FAC-sorting of blood monocytes; each major leukocyte population was sequentially gated off, eventually leaving the classical and non-classical monocytes to be sorted and collected. Gates are sequential from a) to i), with the overall tree shown in j). Gates are as follows: P1 = cells; P2 = live; P3 = single cells; P4 = leukocyte and non-T cells; P5 = non-NK cells; P6 = non-B cells; P7= $CD11b^{+}/CD68^{+}$ monocytes; P8 = classical monocytes; P9 = non-classical monocytes; P11 = neutrophils. Note, the software reached its maximum number of sequential gates, so a non-neutrophil gate could not be drawn in panel h). Instead, the monocytes were gated off based on CD43 and His48 in panel i), and the remaining population confirmed to be neutrophils by their high SSC when back-gated in panel h) where they are the red population.

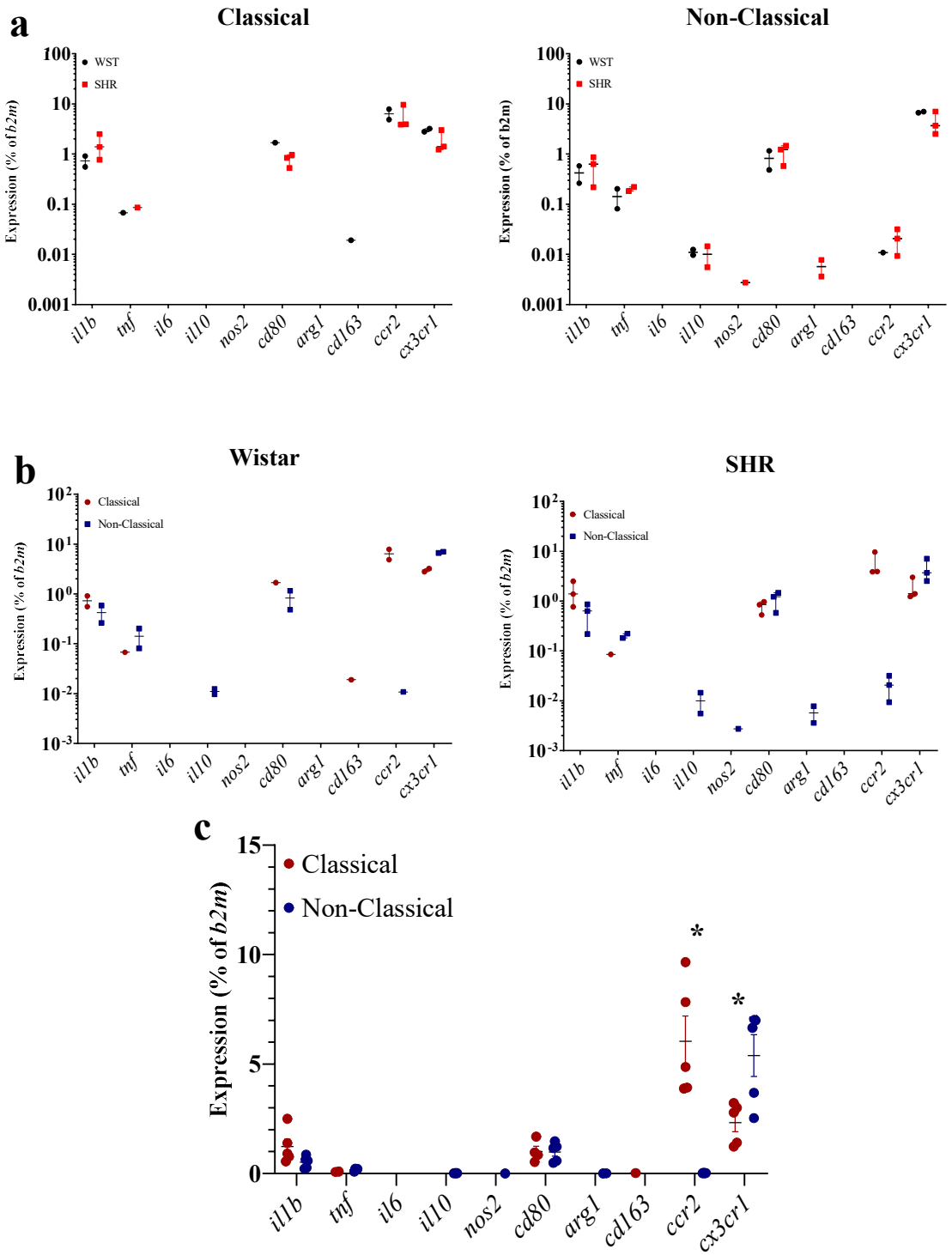

Figure 5| RNA expression of inflammatory-related genes in FAC-sorted Wistar and SHR blood monocytes, shown as a) comparison between Wistar and SHR cells, and b) comparison between classical and non-classical monocytes. c) shows the same data as b), but pools Wistar and SHR cells. Data are presented as median with range. In cases where no copies of a gene were detected, no data point is shown. * signifies $p<0.05$ Wistar versus SHR (a) or classical versus non-classical monocytes (b and c). For all normal data, Welch's t-tests were employed, with q values determined by the two-stage set-up method of Benjamini, Krieger and Yekutieli; for non-normal data, Mann-Whitney tests were instead used.

IV.3.3 Chemotaxis potential of classical versus non-classical monocytes

The higher expression of *ccl2* by SHR stellate ganglia is seemingly paradoxical as they are also lacking in the classical subset of monocytes, for which this is the major chemoattractant, while being if anything enriched in the *cx3cr1*-expressing non-classical monocytes. For this reason, the possibility was explored that there is a switching in the chemotaxis of SHR monocytes to these mediators. However, the SHR cells showed identical expression patterns to those of the Wistar. When the two strains were pooled to provide sufficient numbers for statistical analysis, consistent with normal monocyte subset receptor expression, the classical monocytes expressed higher levels of *ccr2* (p=0.0008; q=0.0069), and lower *cx3cr1* (p=0.0186; q=0.0522) than did the non-classical monocytes (Figure 5). However, the *cx3cr1* result did exceed a 5% false discovery rate.

These data are not challenged by a chemotaxis assay performed on FAC-sorted classical and non-classical monocytes. In general, there was a trend towards the classical monocytes responding more to CCL2 than non-classical monocytes, the converse for CX_3CL1, although no inter-group differences reached statistical significance, likely due to the low n numbers (Figure 6). These experiments were conducted to explore the possibility of a switching of these preferences in the SHR, but owing to the high financial cost of performing them, as the data were trending towards the expected classical and non-classical monocyte chemotaxis preferences, they were not continued.

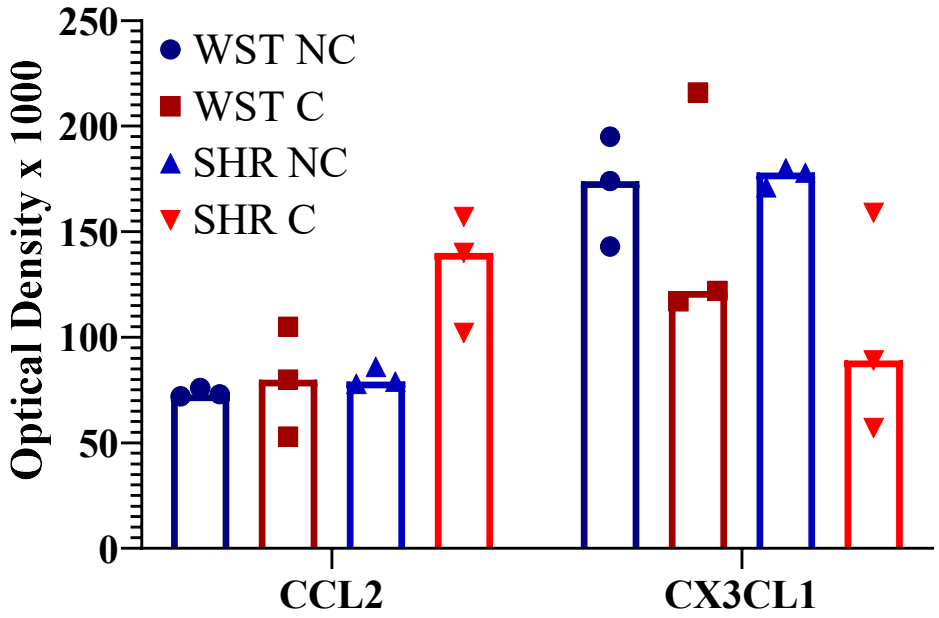

Figure 6| Chemotaxis of FAC-sorted Wistar and SHR blood monocytes towards CCL2 and CX_3CL1. Data are presented as median with all data points. Data were analysed using a Kruskall-Wallis test (p=0.02) followed by Dunn's multiple comparisons *post-hoc* test.

IV.3.4 Bone marrow-derived macrophage gene signature

A similar qPCR panel was also used to compare the gene signatures of Wistar and SHR BMDMs. First, in order to validate that the cultured cells could be considered macrophages, flow cytometry was used to assess expression of macrophages markers CD11b and CD68. Of the live, single cells, there was an 85.2% double-positivity for CD11b and CD68 (Figure 7a), and of these 98.3% were $CD45^+$ (Figure 7b). However, employing the same markers as used to delineate blood leukocyte populations from Chapter 3, these BMDMs also highly expressed T cell marker CD3 (Figure 7c), and B cell marker B220 (Figure 7e). Only a very small proportion of these cells fitted the specific T (Figure 7f) or B (Figure 7g) cell gates delineated by other markers, from Chapter 3.

The SHR and Wistar BMDMs had a very similar inflammatory and anti-inflammatory mediator signature (Figure 8). As the His48 antibody used along with anti-CD43 to

categorise the monocyte-macrophage subsets does not target the product of a specific known gene, *ccr2* and *cx3cr1* were used instead in this qPCR assay to test for any differences in inherent production of classical versus non-classical monocytes in the SHR bone marrow compared to Wistar. These were similarly expressed however, suggesting against this idea (Figure 8). Interestingly, no *cd43* expression was detected (Figure 8), which suggests these BMDMs are not entirely the same as the monocyte-macrophages isolated from the rat sympathetic ganglia and blood. This reflects a potential limitation with their use as a model for these monocyte-macrophages.

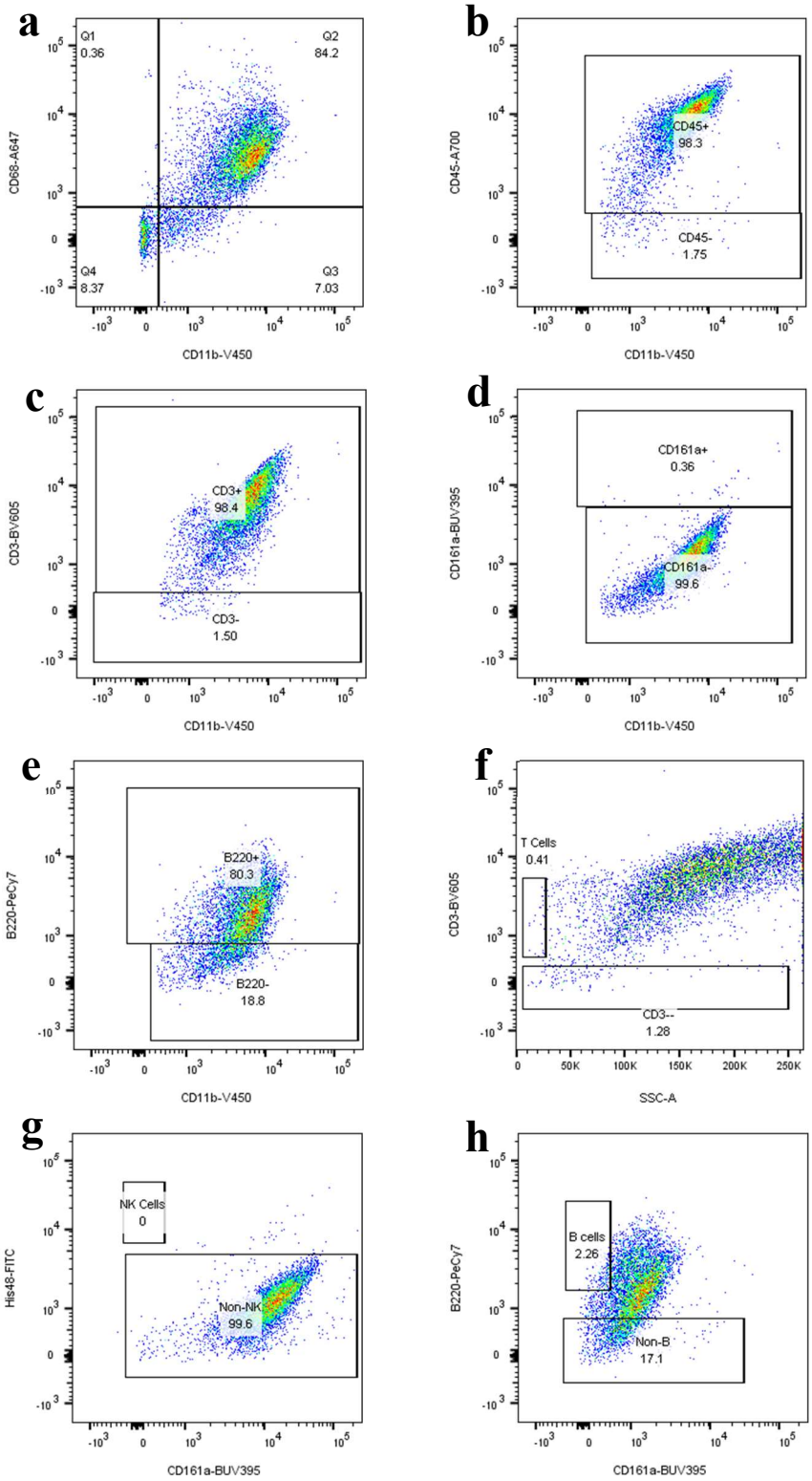

Figure 7| Flow cytometric analysis of expression of various leukocyte markers by Wistar rat bone marrow-derived macrophages. Top five panels show percentage positivity of live single cells for a) macrophage markers Cd11b and CD68; b) leukocyte marker CD45; c) T cell marker CD3; d) NK cell marker Cd161a and e) B cell marker B220. Lower three panels show percentages of live single cells fitting the f) T cell, g) NK cell or h) B cell gates from the gating strategy of Chapter 3.

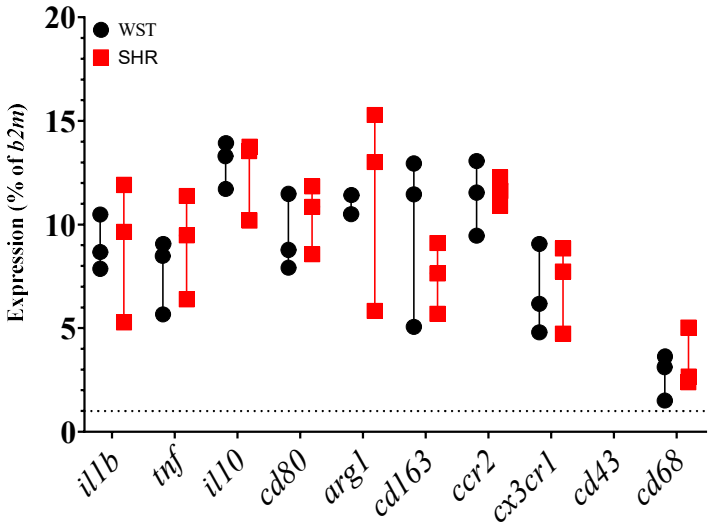

Figure 8| RNA expression of marker and mediator panel of genes by Wistar and SHR BMDMs. Normal data were analysed using Welch's t-tests, while non-normal data were analysed using Mann-Whitney tests.

IV.4 Discussion

The main findings of this chapter are:

1. There are no differences in the expression of common pro- or anti-inflammatory cytokines, *ngf*, or oxidative stress markers between the pre-SHR and Wistar stellate ganglia.
2. There appears to be an increase in *ccl2* expression in the pre-SHR stellate ganglion.
3. Pre-SHR and Wistar blood monocytes display no differences in expression of classic pro- or anti-inflammatory mediators.
4. Classical monocytes from both Wistar and pre-SHR blood are *ccr2*^{high}/*cx3cr1*^{low}, while the non-classical monocytes are *ccr2*^{low}/*cx3cr1*^{high}.
5. There is no evidence to suggest pre-SHR classical or non-classical monocyte chemotaxis towards CCL2 or CX_3CL1 are abnormal.

6. Wistar and pre-SHR BMDMs do not show any differences expression of common inflammatory and anti-inflammatory mediators, nor do they appear to give rise to different numbers of classical or non-classical cells.

IV.4.1 Inflammatory environment of the pre-SHR stellate ganglia

Despite some cellular differences as determined in Chapter III, the experiments of this Chapter found no alteration in expression of a panel of classic type 1 inflammatory or pro-resolution mediators or macrophage markers, nor was there any evidence of increased oxidative stress. This is evidence against the hypothesis of an inflammatory reaction occurring in the pre-SHR stellate ganglia. Although one could suggest that even though there are immune cell changes in this tissue, it may take longer for full inflammation to be detectable by this qPCR method, one would still expect to see some changes, particularly if these were, as hypothesised in Chapter I, responsible for dysautonomia, which is already present at this age. These experiments did suffer from a low n number (3), but even so the trend was even towards lower expression of *tnf* or *il1b* in the SHR samples.

It was possible that as the immune cells (which would be expected to be the major producer of inflammatory cytokines) make up such a small proportion of the ganglionic cells (Chapter III; Davis et al., 2020), these could be diluted by the other cell types in analysis using whole stellates. Unfortunately, FAC-sorting the small numbers of monocyte-macrophages, the population experiencing perhaps the most drastic shift in the pre-SHR compared to Wistar, did not allow for useful qPCR analysis, even when the mRNA was amplified. Examining instead the blood monocyte pools of these animals again showed no real differences in levels of cytokines tested, providing no evidence of any inflammatory alterations in the pre-SHR. The BMDMs also showed no inter-strain

differences in the same panel of mediators. This is surprising given that studies have found increased expression of a number of inflammatory markers in a variety of SHR tissues (Sun et al., 2006; Shi et al., 2014; Tan et al., 2017), so the present findings are to an extent surprising.

This does not rule out the possibility that it is only when the monocytes enter the tissue and differentiate into macrophages that they start producing increased levels of cytokines. This argument is weakened by the presence of the same monocyte-macrophage subset shift in the blood as in the sympathetic ganglia, although it is unclear as to their degree of activation within each locus. The pre-SHR stellate and SCG both also have increased numbers of neutrophils, meaning the monocytes might be exposed to more inflammatory stimuli only once in the ganglionic tissue. Monocytes can be expected to produce cytokines while still circulating in the blood, but perhaps an SHR versus Wistar difference might only be apparent in the site of inflamed tissue.

IV.4.2 SHR stellate ganglion *ccl2*

While the pre-SHR stellate showed no changes in classic pro-inflammatory cytokines, it did express ~4-fold higher levels of *ccl2*, a chemokine, which is expressed by a large range of cell types (so was more likely to be detected by qPCR of whole stellate samples) and mediates mainly the trafficking of monocytes. However, paradoxically this chemokine, by binding to CCR2, mediates mainly the recruitment of classical monocytes ($CCR2^{high}$), which are the population which is smaller in the pre-SHR ganglia compared to Wistar. By contrast, non-classical monocytes, which are greater in proportion in the SHR ganglia, respond principally to CX3CL1. Additionally, CCL2 mediates the recruitment of many other leukocytes, including NK cells, of which there were fewer in the SHR stellate.

If *ccl2* is expressed more highly in the SHR stellate ganglia, why is there a reduced classical/non-classical ratio in this tissue? First, this chapter explored the possibility that the SHR may have altered monocyte chemotaxis; potentially that their non-classical monocytes exhibited strong chemotaxis towards CCL2. However, the above findings demonstrated that SHR monocytes expressed the correct proportions of *ccr2* and *cx3cr1*, and the chemotaxis assay performed showed a trend towards the corresponding correct responses. The chemotaxis assay only used an n number of 3 per group, but due to the high cost of FAC-sorting the monocytes and performing the assay, no more repeats were economically possible. The trend was towards the null hypothesis regardless.

Second, there may be a higher extent of classical to non-classical monocyte differentiation in the SHR stellate. It has long been thought this occurs in the blood, but a modelling study of Tak et al. (2017) suggests that human classical monocytes differentiate into intermediate ones in the blood, but that these next leave the circulation, differentiate into non-classical monocytes, then return. Of course it is unclear how this relates to the single differentiation step from classical to non-classical monocytes in the rat (or mouse), or whether non-classical monocytes could remain outside the circulation (such as in the stellate) once they are formed. It is conceivable that higher SHR stellate CCL2 could lead to greater classical monocyte recruitment, but then that these differentiate to a greater extent into non-classical monocytes within the tissue, causing the shift in ratio. The lower classical/non-classical monocyte ratio already exists in the blood, but to a lesser extent than in the stellate or SCG (Chapter III).

It would seem therefore that the SHR monocytes have a tendency *in vivo* to give rise to non-classical cells. The full mechanisms underlying control of monocyte differentiation from classical to non-classical are currently unclear. However, much evidence suggests

M-CSF is a potent stimulus of this process; injection of this factor causing an increase in intermediate and non-classical monocytes in humans (Weiner et al., 1994), while its inhibition has the opposite effect (Korkosz et al., 2012). Interestingly no differences in *ccr2* or *cx3cr1* expression were observed in BMDMs produced from Wistar or SHR bone marrow, but as these were grown in the presence of a high concentration (20 ng/ml) of M-CSF, perhaps this could have masked any differences. A study of human hypertensives revealed an increase in plasma M-CSF levels (Radaeva et al., 2019), although one cannot say for sure whether this is a result of hypertension, or related to the cause, particularly as those patients which were treated showed a more typical M-CSF circadian rhythm while this was often disturbed in disease. In any case though, such M-CSF changes could potentially serve to exacerbate disease. If M-CSF levels are similarly elevated in the pre-SHR, this could possibly be responsible for increased classical to non-classical monocyte differentiation. It is possible that the SHR also displays an altered M-CSF circadian rhythm like the human patients, and most of the flow cytometry experiments of Chapter III were performed during daylight hours. It seems unlikely though that this would lead to significant alterations in the proportions of classical and non-classical monocytes in the blood and tissues sampled because this mediator acts over a long time period. For example, in the BMDM culture protocol, bone marrow progenitors are exposed to M-CSF for 7 days before use.

This leaves it unclear what, if at all, is the effect of such an increase in *ccl2* in the SHR stellate ganglia. It is possible it mediates increased classical monocyte recruitment, which then transdifferentiate into non-classical monocytes. Although, given overall monocyte-macrophage numbers tend to be lower in the SHR ganglia, and there isn't generally a significant absolute increase in the numbers of non-classical monocytes, this would be

unlikely unless there is extremely high turnover of these cells dying or egressing from the tissue. It would be interesting to examine the dynamics of these cells' migration *in vivo*. Nevertheless, higher *ccl2* may be a marker of localised inflammation, although if this is true, strangely it is not backed up by changes in the levels of any other inflammatory mediators. It may simply be the case that, while higher in expression, SHR stellate *ccl2* is of little functional significance.

IV.4.3 Limitations

The main issue with the experimental work of this chapter is the isolation of sufficient numbers of monocyte-macrophages for analysis. After amplification there was still insufficient mRNA to detect almost all genes in question from FAC-sorted stellate monocyte-macrophages, and even when taken from blood, there were sub-optimal numbers of cells (on the order of 10^4-10^5) for qPCR analysis. Additionally, this process is highly expensive so only a small number of technical repeats were economically possible. Similarly, for this reason the chemotaxis assay suffered from a number of cells per repeat that was an order of magnitude lower than the recommended minimum, and only three repeats per condition. As suggested in Chapter III, single-cell sequencing may have been a more effective method to analyse sympathetic ganglion monocyte-macrophages, although the financial cost of this is greater still.

IV.4.4 Conclusions

1. Pre-hypertensive SHR stellate ganglia express higher levels of chemokine gene *ccl2*, than do Wistar ganglia.
2. Pre-hypertensive SHR stellate ganglia display no elevation in molecular markers of type 1 inflammation or oxidative stress.

3. FAC-sorting stellate monocyte-macrophages is too low yield to allow qPCR analysis of these cells.
4. SHR blood monocyte *ccr2* and *cx3cr1* expression appears to be in the correct proportions within the classical and non-classical subsets.
5. SHR blood monocytes show no differences in inflammatory profile compared to those of Wistar.
6. SHR bone marrow macrophage precursors do not seem to have an inherent bias towards production of non-classical monocytes *in vitro*.

CHAPTER V

Functional effects of monocyte-macrophages on stellate neuron activity *in vitro*

V.1 Introduction

V.1.1 Inflammatory mediators in hypertension

Essential hypertension is typically characterised by a systemic inflammatory syndrome; levels of inflammatory markers such as: C-reactive protein (CRP) (Smith et al., 2005), interleukin-6 (IL-6) (Bautista et al., 2005; Yu et al., 2010), interleukin-1β (IL-1β) (Dalekos et al., 1997) and tumour necrosis factor α (TNF-α) (Bautista et al., 2005; Yu et al., 2010) have all been reported to be raised in patients with essential hypertension. Furthermore, CRP and IL-6 have been shown to be predictors of hypertension development (Jayedi et al., 2019), implying an inflammatory pre-hypertensive state, from which one could hypothesise that inflammation may play a causative role in the aetiology of essential hypertension. Deeper statistical analysis and Mendelian randomisation in the study of Smith et al. (2005) suggested that CRP itself is not causative of essential hypertension, while Jayedi et al. (2019) showed that IL-1β is not a predictor of hypertensive risk. The predictive relationship of TNF-α and future essential hypertension remains to be investigated. Overall therefore, it seems there is evidence for a (type 1) inflammatory reaction in human hypertension, which seems to develop even before blood pressure elevation.

As described in Chapter I, antibody blockade of some inflammatory cytokines and mediators is used in, or has been investigated for, treatment of a number of human diseases, and in many cases blood pressure was recorded in clinical trials for these. While a trial each for anti- IL-1β (Rothman et al., 2020) and IL-6 (van Rhee et al., 2015) therapy did not report any reduction in blood pressure (and in fact 3/19 patients developed hypertension in the anti-IL-6 study), some studies of anti-TNF-α treatment have shown anti-hypertensive effects (Klarenbeek et al., 2010; Sandoo et al., 2011; Yoshida et al.,

2014). Of course a caveat to these studies, is that the reduction in disease severity and pain within the rheumatoid arthritis patients tested caused by the anti-TNF-α treatment, could have contributed to a blood pressure decrease. However, from this one could hypothesise that TNF-α may contribute to sympathetic impairment in hypertensive disease.

In the SHR, raised expression compared to WKY rats, of IL-1β and TNF-α has been reported in a variety of tissues (Sun et al., 2006), in addition to central nuclei involved in sympathetic outflow (Shi et al., 2014; Tan et al., 2017). Interestingly though, while a study of plasma levels of SHR versus WKY cytokines in response to LPS stimulation showed increased TNF-α in the diseased animal, IL-1β did not differ, and IL-6 was in fact lower in the SHR (Andrzejczak et al., 2006). However, measurement only of the response to LPS makes it difficult to translate to each strain's baseline physiology.

In Chapter IV of this thesis, no differences in IL-1β, TNF-α, IL-6 nor several other inflammatory markers were found in the pre-hypertensive SHR stellate, blood monocytes or BMDMs, compared to equivalent samples from the Wistar rat. However, due to the difficulties in isolating sufficient numbers of monocytes for qPCR analysis, the inability to directly examine the stellate-specific monocyte-macrophages, and the fact that both TNF-α and IL-1β were still expressed in these tissues of both strains, suggests that they may still merit investigation in a functional context.

IV.1.2 Influence of cytokines on neuronal activity

Many lines of evidence support the idea that inflammatory cytokines can increase local neuronal activity, but to date this has not been studied in sympathetic ganglia in the context of hypertension, so one must infer hypotheses from other neuronal loci or

pathologies. In nerve-injury, macrophages infiltrate the site of lesion and release, among other factors TNF-α, IL-1β and IL-6, all of which act directly on nociceptor neurons to increase excitability (Scholz & Woolf, 2007). Schwann cells also release similar cytokines, along with neuronal growth factors, producing a similar effect. It is therefore worth examining if these mechanisms could function similarly in sympathetic ganglia. Sympathetic neurons are involved in nerve injury though; the IL-6 released in this reaction contributes to sympathetic neurons sprouting into the dorsal root ganglia (Ramer et al., 1998). Additionally, in the heart post-MI, an inflammatory reaction of which macrophages are an integral component, leads to increased NGF release and sympathetic neuronal sprouting (Hasan et al., 2006; Wernli et al., 2009).

IL-6 may act as a survival factor for sympathetic neurons, as its presence allows for these cells to be grown in culture without requiring NGF, which is normally essential (Marz et al., 1998), and it has been reported that IL-1β increases the responsiveness of SCG neurons to acetylcholine (Cuddy et al., 2020). Furthermore, centrally it seems that IL-1β and TNF-α can increase sympathetic outflow via actions at the hypothalamic paraventricular nucleus (Shi et al., 2011) or rostral ventrolateral medulla (Wu et al., 2012). Contrastingly, in the enteric nervous system, IL-1β (Xia et al., 1999), IL-6 (Xia et al., 1999) and TNF-α (Straub et al., 2005) all seem to be sympatho-inhibitory, suggesting there may be locus-specific effects.

IV.1.3 Influence of monocyte-macrophages on sympathetic neurons?

Macrophages are major producers of inflammatory cytokines, and there is a shift towards a higher proportion of non-classical monocytes in the pre-SHR, these cells having been shown to be pathologically inflammatory in a number of diseases (Poitou et al., 2011; Misharin et al., 2014; Mukherjee et al., 2015; Zhu et al., 2016; Puchner et al., 2018;

Montgomery et al., 2019). Owing to this, combined with the evidence about that inflammatory type 1 cytokines may increase neuronal excitability, it is possible that these monocyte-macrophages are in part responsible. Akin to this hypothesised effect of macrophages, seems to be the role of microglia in hypertensive central nervous system inflammation; inhibiting microglial activation in either Sprague-Dawley rats with central nervous system inflammation-induced hypertension (Wu et al., 2012), or SHRs (Santisteban et al., 2015), reduces sympathetic tone and blood pressure.

IV.1.4 Hypotheses and aims of the chapter

The hypotheses underlying this chapter were:

1. SHR monocyte-macrophages drive heighten post-ganglionic sympathetic neuron activity.
2. Type 1 inflammatory cytokines contribute to this effect and can increase sympathetic stellate neuron excitability in culture.

The aims were therefore to:

1. To test the effects of co-culture and SHR/Wistar cross-culture of monocyte-macrophages with sympathetic stellate neurons.
2. To examine the effects of cytokines TNF-α, IL-1β and IL-6 on sympathetic stellate neuron activity in culture.

V.2 Methods & Materials

V.2.1 Cell and tissue culture

All cells and tissues used in this Chapter were cultured as described in the relevant sections of Chapter II. Cytokines and anti-cytokine antibodies were added at

concentrations based off EC_{50} or ND_{50} values respectively, reported on the manufacturer's datasheet.

V.2.2 Noradrenaline release experiments

Stellate ganglion noradrenaline release experiments were performed as described in Chapter II. The ELISA was also performed on noradrenaline standard concentrations of: 0.2, 0.6, 2, 8 and 32 in triplicate, and their mean spectrophotometric values used to interpolate a standard sigmoidal 4PL curve with GraphPad Prism 8 software. This was then used to infer [NA] values for all experimental samples and two control samples.

V.2.3 Calcium imaging

Fura-2 Ca^{2+} imaging was carried out as described in Chapter II. Neurons were selected for analysis based on a healthy appearance under the microscope, which typically includes a polygonal shape and well-defined borders, in addition to adequate dye loading. Recorded neurons were excluded from analysis if they did not demonstrate a clear $[Ca^{2+}]_i$ transient response to stimulation with 100 mM $[K^+]_o$. Peak data-points were taken as the maximal $[Ca^{2+}]_i$ transient value reached immediately following stimulation with either nicotine or K^+.

V.2.4 Flow cytometry

After incubation in Neurobasal Plus + 10% FBS media containing 100 µL Clodrosomes or Encapsosomes (as described in Chapter II), blood leukocytes were separated from the liposomes and stained with the live-dead stain and antibody panel of Chapter III. Flow cytometry was performed also as described in the same chapter.

V.2.5 Statistical analysis

Statistical analyses were performed as described in Chapter II.8.

V.3 Results

V.3.1 Whole stellate ganglion stimulation-evoked noradrenaline release

In order to examine the effect of SHR leukocytes on sympathetic neuronal function, whole stellate ganglion explants from both Wistar rats and SHRs were prepared and cultured either alone, or with whole blood leukocytes from either strain. These results showed large intra-group variability (Figure 1), making results difficult to interpret. This set of experiments produced 10-fold higher [NA] values than previously reported for similar experiments in our lab, and showed a trend against our group's previous finding that SHR ganglia release more noradrenaline than Wistar when stimulated in this way (Bardsley et al., 2018b). This previously published study used high-performance liquid chromatography to measure noradrenaline, which is widely accepted as a more reliable method for detection. Furthermore, looking at the [NA] values obtained from the control samples supplied with the ELISA kit, 4 out of 6 of the values fell outside the ±40% range given by the supplier. For this reason, no conclusions were drawn from the limited amount of data obtained using this technique, and its experimental use was discontinued in this thesis.

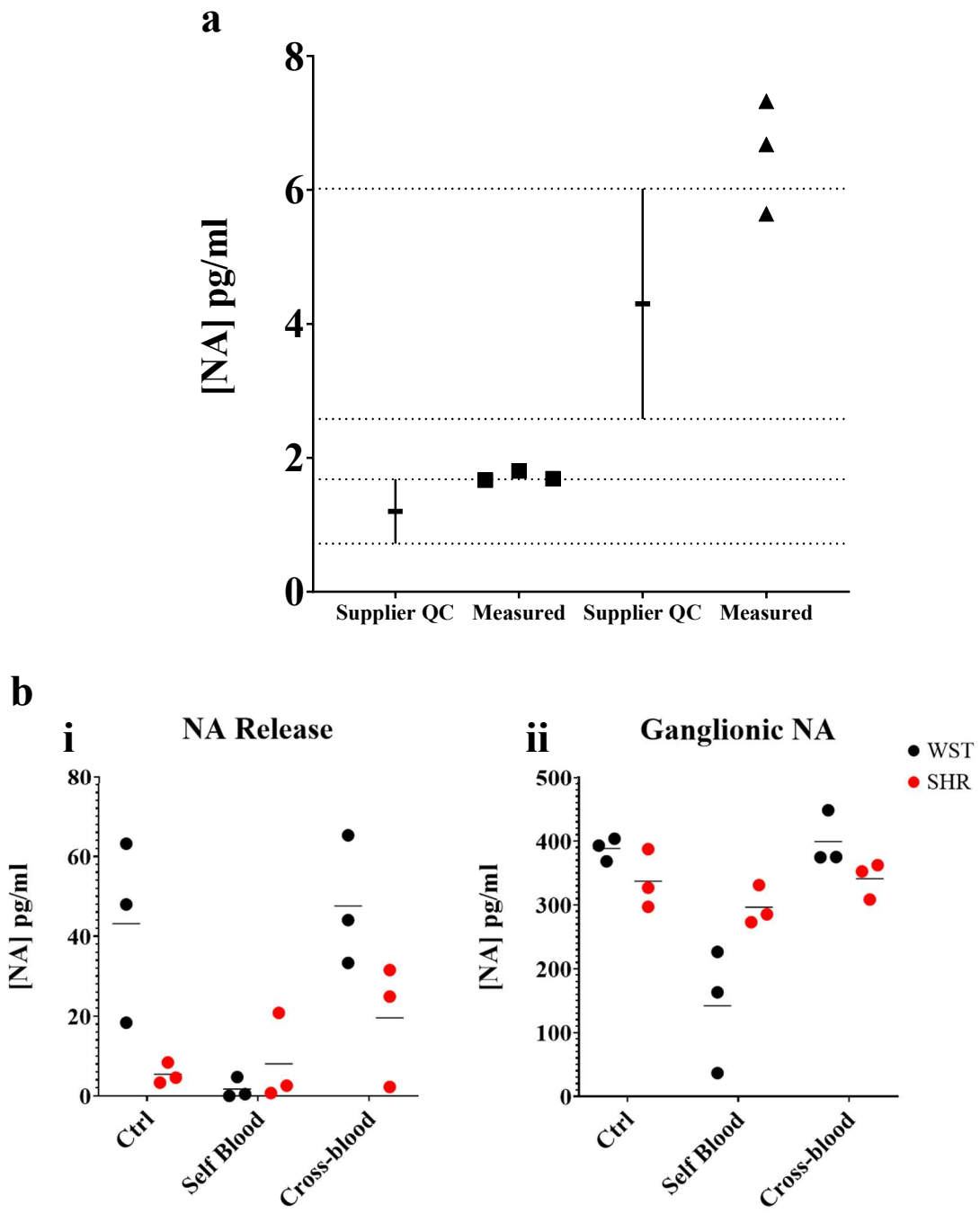

Figure 1| Results of the noradrenaline release experiments, quantified by ELISA. Five manufacturer-supplied standard samples were analysed in parallel and 4-parameter analysis used to interpolate [NA] values from recorded 450 nm optical density readings for the experimental samples. a) Recorded [NA] values for the manufacturer-supplied control samples compared to their reported quality control value ranges. b) [NA] values measured from ganglion culture supernatant (i) and tissue homogenate (ii).

V.3.2 Response of cultured single Wistar and SHR stellate neurons to nicotine and high $[K^+]_o$

As the noradrenaline release assay seemed unreliable, the Ca^{2+} transient responses of cultured single stellate neurons to nicotine and high $[K^+]$ were instead as an assay of neuronal activity. The peak $[Ca^{2+}]_i$ transient magnitude of SHR sympathetic stellate neurons in response to both cholinergic stimulation with 100 µM nicotine, and depolarisation with 100 mM $[K^+]_o$, were used as an index of neuronal activity. Both were significantly higher than those taken from Wistar rats; nicotine (expressed as % ratio change from baseline): 194.5 ± 23.4 versus 119.5 ± 11.87, p=0.022; K^+: 369.7 ± 20.74 versus 246.1 ± 22.51, p=0.00020 (Figure 2), which is consistent with previous reports (Li et al., 2012).

Particularly within the SHR population of neurons, there were a number of cells which showed an essentially absent nicotinic response (<10%) and therefore large outliers. These all had a positive high K^+ stimulation response though and therefore were included in the same analysis. As far as the field is aware, post-ganglionic sympathetic neurons should all express nicotinic receptors, so this unresponsiveness of a small group of neurons is likely a culture artefact potentially due to stripping of the receptors during enzymatic digestion of the tissue.

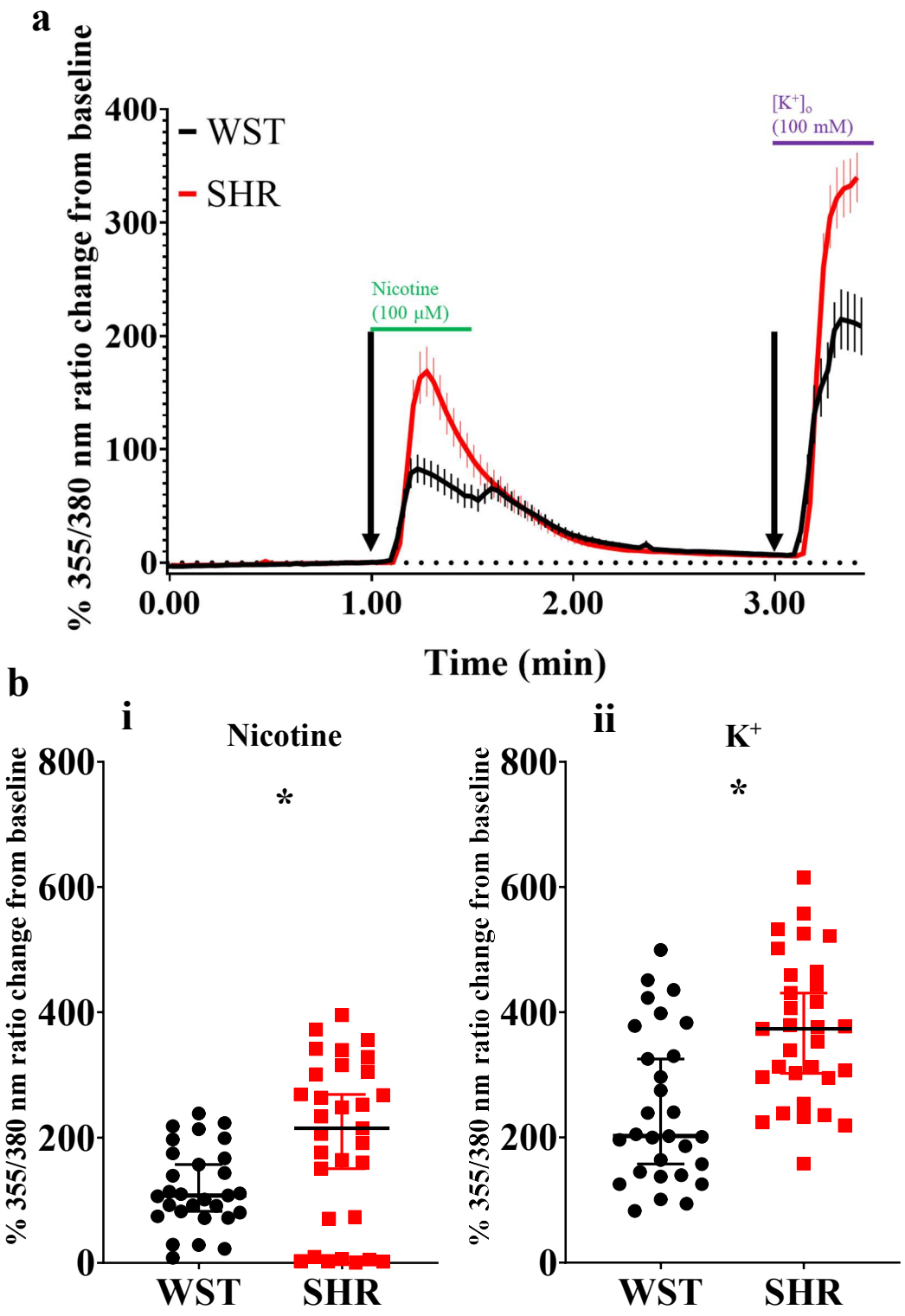

Figure 2| Wistar and SHR stellate neuron Ca^{2+} transients in response to pharmacological stimulation. a) Mean trace (with SEM) of stellate neuron $[Ca^{2+}]_i$ during the experimental protocol involving exposure to 100 µM nicotine, followed by 100 mM K^+. b) Peak stellate neuron $[Ca^{2+}]_i$ transient in response to nicotine (i) and K^+ (ii). Peak response data are presented as median with IQR; * signifies $p<0.05$ for Wistar versus SHR, Mann-Whitney test.

V.3.3 Effect of leukocyte co-culture with stellate neurons

In Chapter III, it was established that the SHR sympathetic ganglia displayed an altered monocyte-macrophage subset ratio. In order to see if this has an effect on neuronal activity, ideally one could co-culture Wistar and SHR stellate neurons with stellate monocyte-macrophages of either strain and record the nicotine and high [K^+] responsiveness. However, as described in Chapter IV, it is almost impossible to obtain substantial numbers of stellate macrophages. As the SHR's lower classical/non-classical monocyte ration was also present in the blood, the pool from which the sympathetic-associated macrophages appear to arise (Pirzgalska et al., 2017), these could be used as a surrogate. FAC-sorting even this larger pool of monocytes also has very low-efficiency (Chapter IV), and therefore a different approach was attempted. Stellate neurons were co-cultured with whole blood leukocytes and this was to be compared to blood leukocytes treated with clodronate liposomes, in order to deplete monocytes. The protocol of Claassen et al. (1990) was tested for its monocyte-depletion efficiency; blood leukocytes were incubated with either 100 µL/mL Clodrosomes, or the same concentration of PBS-filled "Encapsosomes". Using flow cytometry, and employing the same leukocyte gating strategy used in Chapter III, this method only reduced the percentage of leukocytes which were not NK cells, T cells, B cells or PMNs, that were CD11b/CD68 double-positive from 87.8% to 54.0% (Figure 3). From this, it could not be concluded that this method sufficiently depletes monocytes, and therefore a different approach was taken; whole blood leukocyte co-cultures were examined, as well as later BMDM-neuron co-cultures (Figure 4).

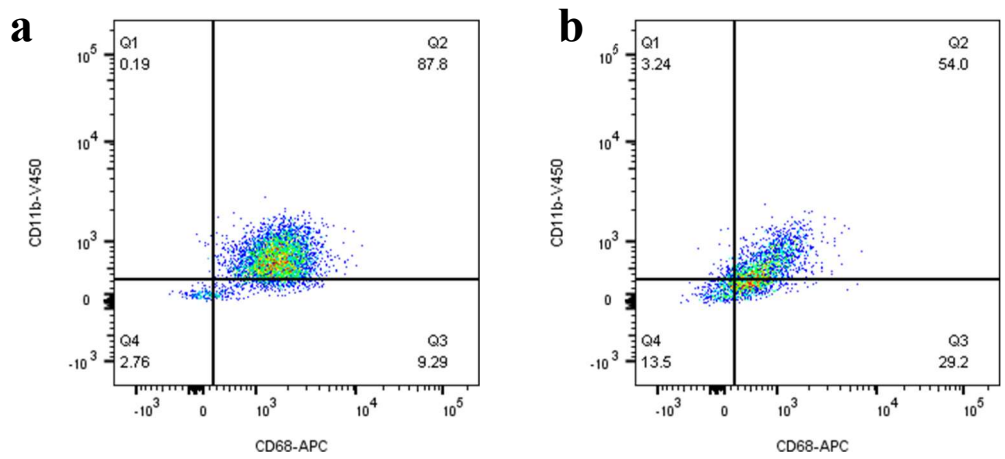

Figure 3| CD11b/CD68 double-positive monocytes in Wistar whole blood treated with a) Encapsosomes or b) Clodrosomes.

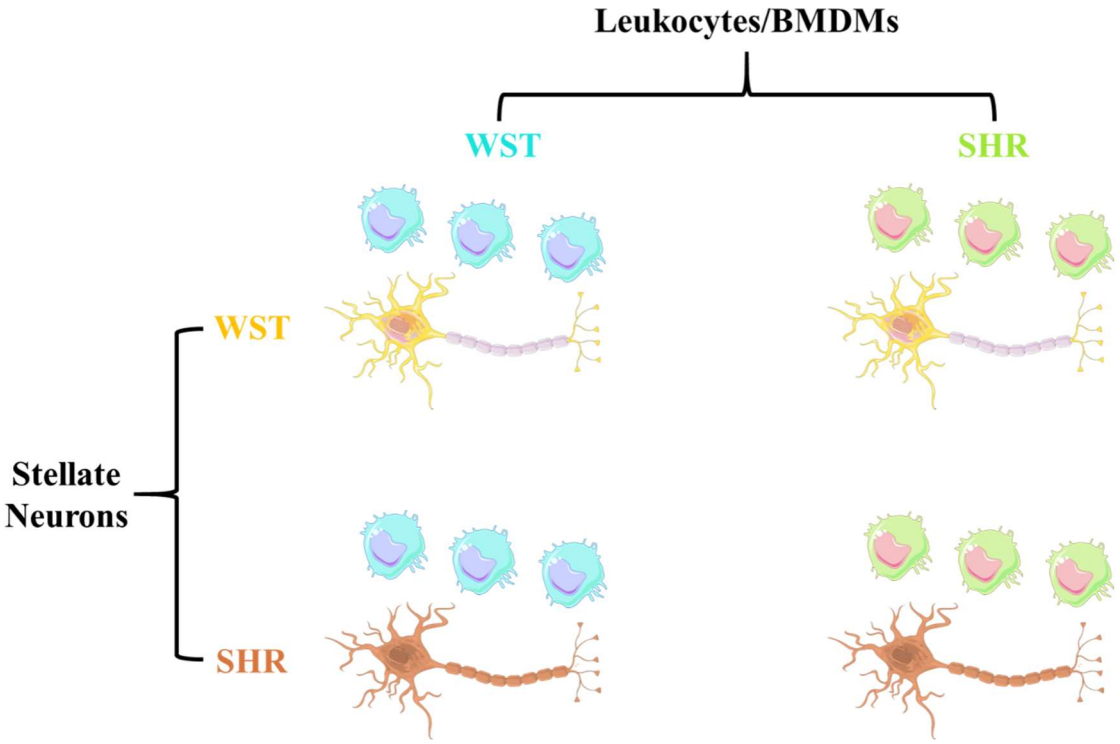

Figure 4| Co-culture permutations; Wistar and SHR neurons were each cultured with their own blood leukocytes or macrophages, and with those of the other strain. The evoked neuronal $[Ca^{2+}]_i$ transients in response to nicotinic or high $[K^+]_o$ stimulation were recorded. Cell images are from Servier Medical Art (smart.servier.com) by Servier, and licensed under a Creative Commons Attribution 3.0 Unported License (https://creativecommons.org/licenses/by/3.0/). "Neuron" image recoloured.

Co-culturing Wistar stellate neurons with their own blood leukocytes significantly increased their responsiveness to both nicotine and high $[K^+]_o$. With SHR leukocytes, while this increased the response to high $[K^+]_o$, for nicotine there was a clear trend to this effect, but which did not quite reach statistical significance (p=0.080). However, this nicotinic response with SHR leukocytes did not differ significantly from that with the Wistar leukocytes either, and these responses were much closer in magnitude than the baseline and SHR leukocyte co-culture. For these reasons it seems more likely a type II error. By contrast, SHR neurons showed no differences when co-cultured with these leukocytes, except a weakened high K^+ response when co-cultured with self-leukocytes (Figure 5).

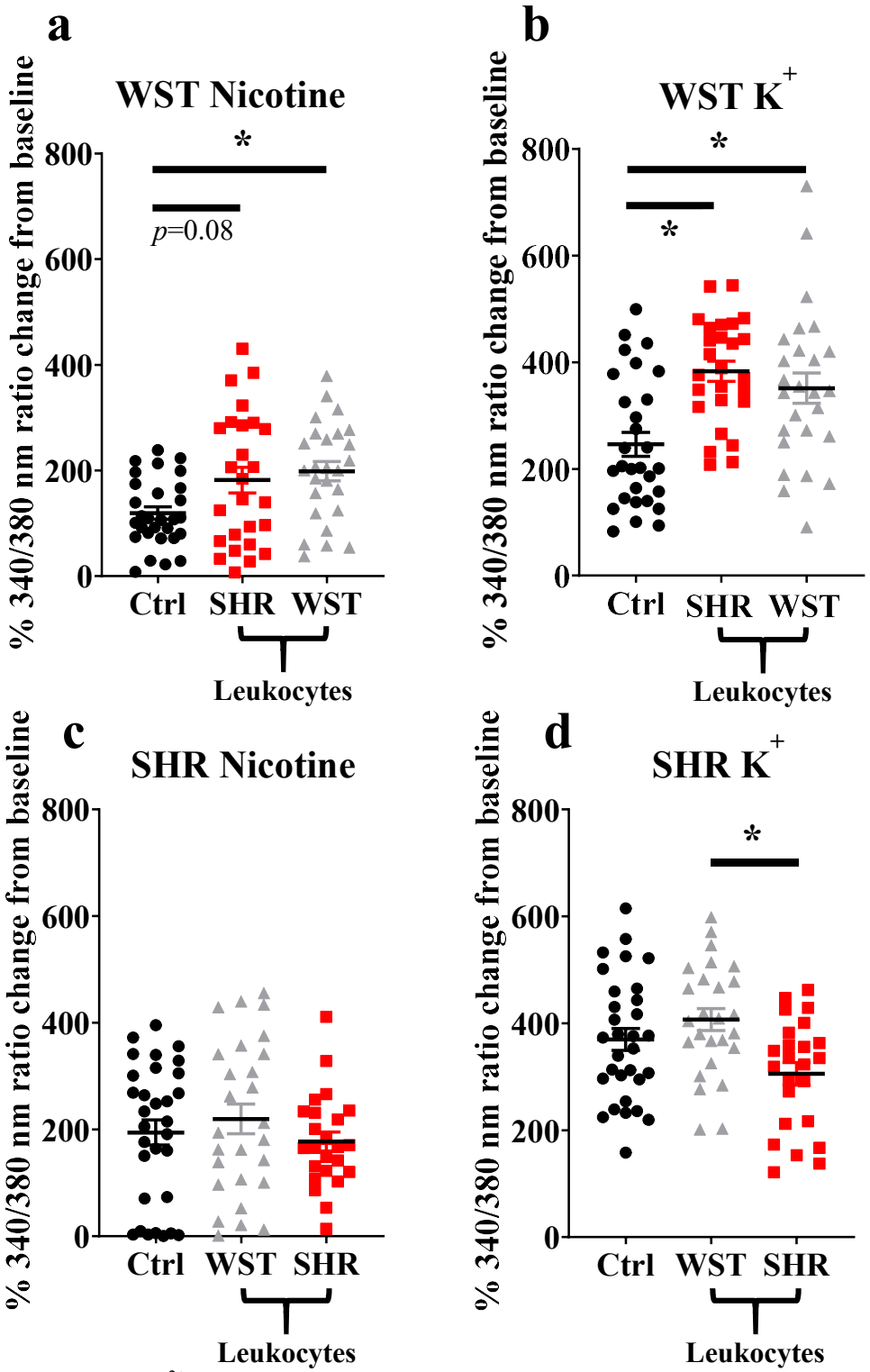

Figure 5| Peak $[Ca^{2+}]_i$ transient responses of stellate neurons co-cultured with blood leukocytes in response to 100 µM nicotine or 100 Mm $[K^+]_o$. Panels show responses of: a) Wistar neurons to nicotine; b) Wistar neurons to high $[K^+]_o$; c) SHR neurons to nicotine; d) SHR neurons to high $[K^+]_o$. Data are presented as mean ± SEM; * signifies $p<0.05$ between the indicated groups; normal data were analysed using Brown-Forsythe and Welch's ANOVAs with Dunnett's T3 multiple comparisons test, while non-normal data were analyses with a Kruskall-Wallis test followed by Dunn's multiple comparisons test.

V.3.4 Response of stellate neurons to co-culture with BMDMs

Immunocytochemistry was used to verify successful co-culture of sympathetic stellate neurons (TH^+) with BMDMs ($CD68^+$), which revealed the presence of both cell types in close proximity (Figure 6).

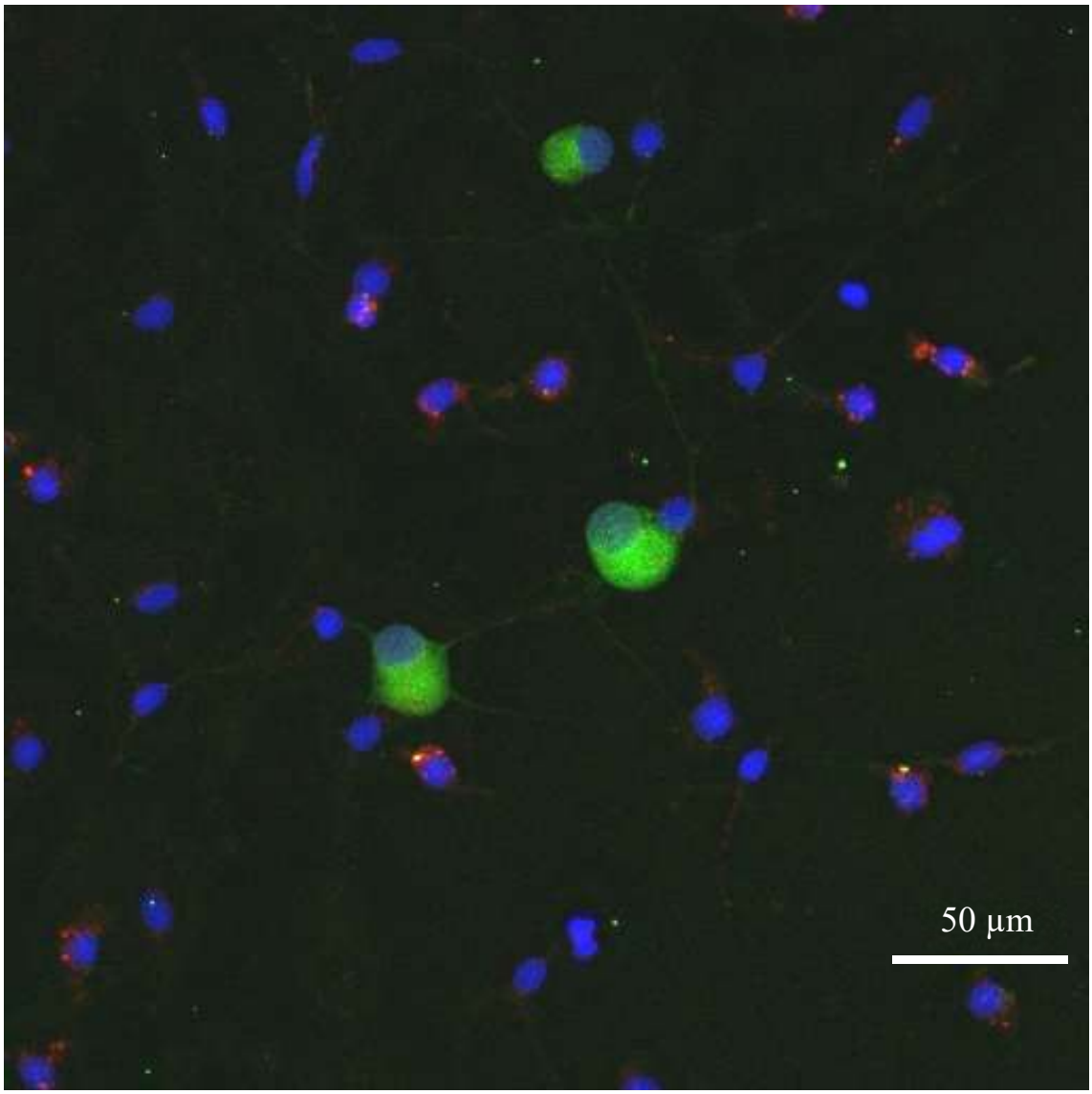

Figure 6| Immunocytochemical image of Wistar stellate neurons (TH^+, green), with BMDMs ($CD68^+$, red).

Upon BMDM co-culture, as with the blood leukocytes, the Wistar stellate neurons showed increased nicotine responsiveness in the presence of BMDMs from either strain, while the SHR neurons only showed an increased response when cultured with their own

BMDMs, not those of Wistar rats (Figure 7a & c). Interestingly these results did not translate to the K^+ responses, although similar trends were apparent (Figure 7b & d). As the BMDM co-culture required addition of M-CSF to keep the BMDMs alive, control experiments were performed in which Wistar neurons alone were cultured with the same concentration of this factor. While these neurons did not display a nicotinic response differing significantly from baseline, there was a trend towards an increase, and there was no significant difference between this response and those from the BMDM co-cultures (Figure 6a). Additionally, for the K^+ responses, it was only the M-CSF control response which differed significantly from the baseline (Figure 7b).

As the presence of BMDMs seemed to increase Wistar stellate neuron responsiveness to nicotine, an attempt was made to identify potential mediating factors in this observation. It seemed unlikely, supported by co-culture images, that a physical interaction could underlie this mechanism, and therefore the focus was on chemical mediators. In other contexts, as detailed above, macrophages contribute to neuronal hyperactivity through release of pro-inflammatory cytokines. TNF-α and IL-1β were shown to be expressed in the Wistar and SHR stellate ganglia and blood monocytes in Chapter IV, although no inter-strain differences were observed. This however does not exclude the possibility of differential expression in the stellate monocyte-macrophages, from which sufficient mRNA samples could not be obtained. These cytokines, along with IL-6, if BMDMs do truly increase stellate neuron nicotinic responsiveness, would be prime candidates to mediate this. Although IL-6 was not detected in any of the stellate, or monocyte samples of Chapter IV, it can be readily expressed by this cell-type (Bauer et al., 1989), and is raised in pre-hypertensive humans (Lakoski et al., 2011; Jayedi et al., 2019). In order to more efficiently examine whether any of these mediators could play a role in BMDM-

induced neuronal hyper-responsiveness, combined blockade of TNF-α, IL-1β and IL-6, covering this 'classical triad' of inflammatory cytokines was tested. The nicotinic responsiveness of Wistar stellate neurons co-cultured with Wistar BMDMs appeared still to be enhanced in the presence of antibodies targeted against TNF-α (100 ng/mL), IL-1β (140 ng/mL) and IL-6 (833 ng/mL) however (Figure 7a). These concentrations were based off the manufacturer-reported EC_{50} values.

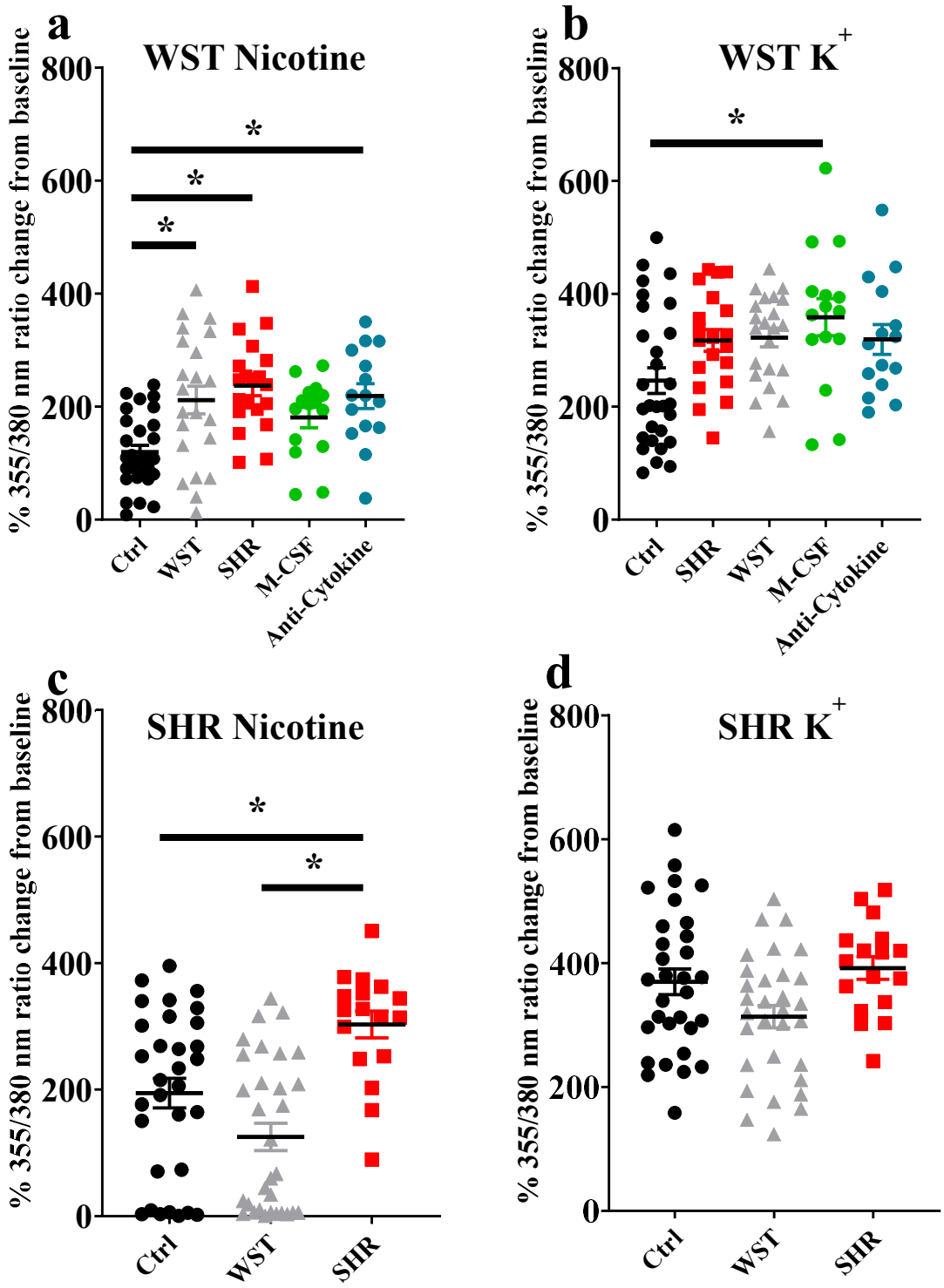

Figure 7| Peak $[Ca^{2+}]_i$ transient responses of stellate neurons co-cultured with BMDMs in response to 100 µM nicotine or 100 Mm $[K^+]$. a) Wistar response to nicotine; b) Wistar response to high $[K^+]_o$; c) SHR response to nicotine; d) SHR response to high $[K^+]_o$. Data are presented as mean ± SEM; * signifies $p<0.05$ between the indicated groups; normal data were analysed using Brown-Forsythe and Welch's ANOVAs with Dunnett's T3 multiple comparisons test, while non-normal data were analyses with a Kruskall-Wallis test followed by Dunn's multiple comparisons test.

V.3.5 Response of stellate neurons to culture with inflammatory cytokines

Finally, TNF-α and IL-1β were tested for their ability to alter neuronal activity themselves; Wistar and SHR stellate neurons were cultured alone, but in the presence of one of these cytokines: 10 pg/mL TNF-α, or 1 ng/mL IL-1β. Wistar neurons did not differ in their response to nicotine after culture with either cytokine (Figure 8a), although the K^+ response was significantly increased (Figure 8b). By contrast, SHR neurons also showed no alteration of responsiveness to nicotine (Figure 8c), and the response to K^+ tended to decrease (Figure 8d).

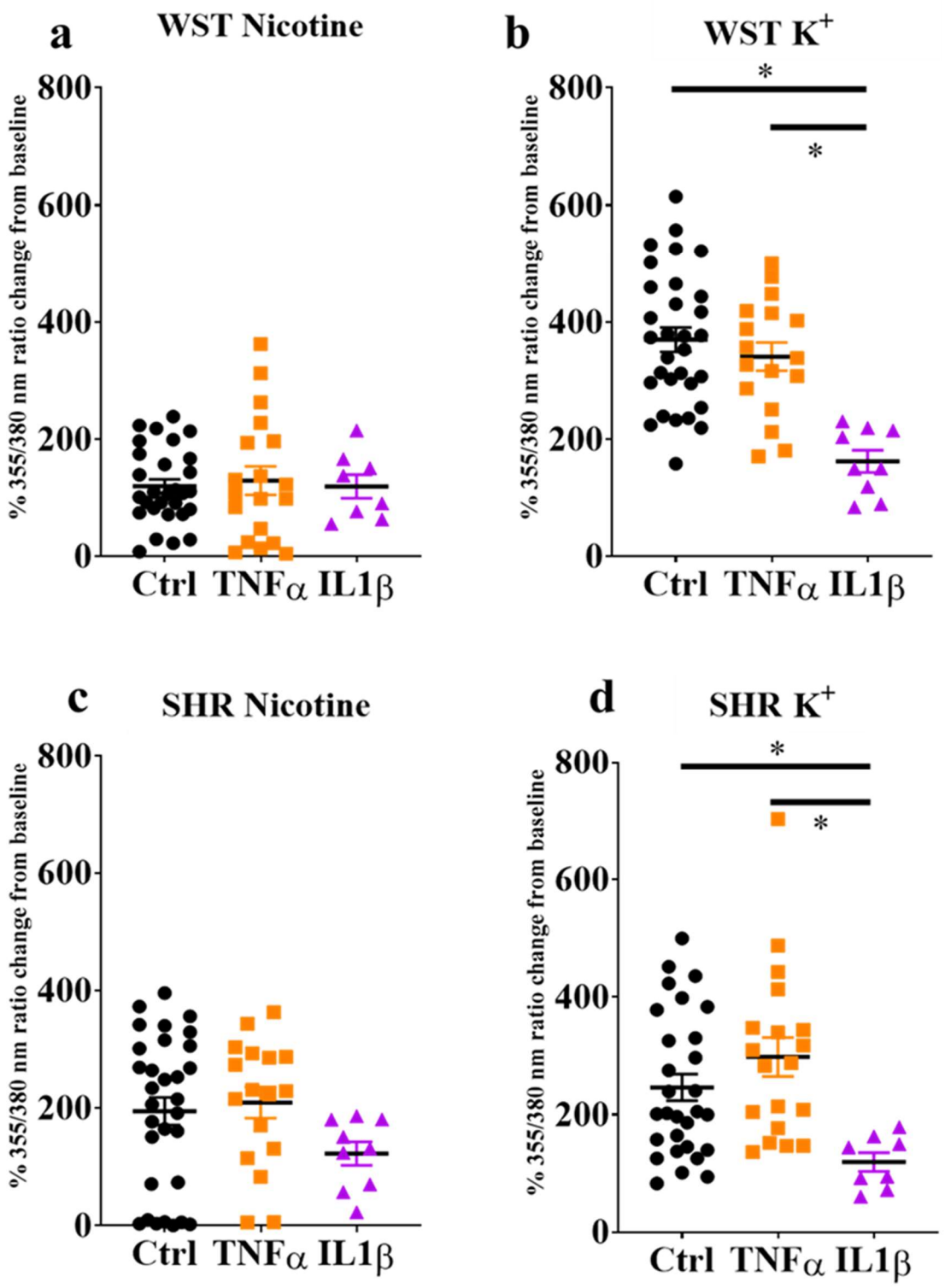

Figure 8| Wistar and SHR stellate neuron Ca^{2+} transients in response to pharmacological stimulation after culture with TNF-α or IL-1β, as compared to those cultured in plain media. a) Wistar nicotine; b) Wistar K^+; c) SHR nicotine; d) SHR K^+. Data are presented as mean ± SEM; * signifies $p<0.05$ between the groups indicated; normal data were analysed using Brown-Forsythe and Welch's ANOVAs with Dunnett's T3 multiple comparisons test, while non-normal data were analyses with a Kruskall-Wallis test followed by Dunn's multiple comparisons test.

V.4 Discussion

The main findings of this chapter are:

1. Co-culture with whole blood leukocytes from either strain increases the excitability of Wistar, but not SHR stellate neurons.
2. Co-culture with BMDMs from either strain increases the excitability of Wistar, but not SHR stellate neurons.
3. The effect of BMDM co-culture on Wistar stellate neuron activity is not mediated by TNF-α, IL-1β or IL-6.
4. Neither TNF-α, nor IL-1β increase the excitability of Wistar or SHR stellate neurons in response to nicotinic or high K^+ stimulation.

IV.4.1 SHR sympathetic neuron hyperactivity in culture

The baseline SHR and Wistar Ca^{2+} transient data in response to nicotine and high K^+ depolarisation support previous published findings (Li et al., 2012), and other unpublished observations from our lab. Consistent with a wealth of literature, the SHR displays sympathetic hyperactivity at the level of the post-ganglionic sympathetic stellate neurons (Li et al., 2012; Shanks et al., 2013a; Shanks et al., 2013b; Larsen et al., 2016; Shanks et al., 2017; Davis et al., 2020). The intra-neuronal molecular mechanisms underpinning this are thought to include dysregulation of the membrane potential-stabilising M-current, leading to a state of hyper-excitability (Davis et al., 2020), along with dysfunctional Ca^{2+} handling (Li et al., 2012; Lu et al., 2015; Larsen et al., 2016; Shanks et al., 2017). The Ca^{2+} dyshomeostasis may in turn arise from altered cyclic nucleotide signalling; specifically, there seems to be impairment of the neuro-inhibitory cGMP pathway, in part brought about by heightened phosphodiesterase 2 (PDE2) activity (well-reviewed by Li and Paterson, 2019).

IV.4.2 Monocyte-macrophage influence on sympathetic neuron activity

The only previous example of macrophage-sympathetic neuron co-culture of which the author is aware is that of Arantes et al. (2000), who cultured murine SCG neurons with peritoneal macrophages. This led to neuronal death and a substantial reduction in cell density within 24 h of culture, an effect which was able to be reduced by dexamethasone. In the experiments of this chapter, during which stellate neurons were co-cultured with leukocytes or BMDMs for >48 h, an increase in Wistar neuronal activity was instead observed. This does not discount a reduction in neuronal cell survival, and the culture protocol used for this thesis produces such a range of stellate neuron densities, depending on the number of ganglia used and number of coverslips plated, that this was not able to be assessed. One cannot completely exclude the possibility that macrophage co-culture removes the least healthy cells, leaving only the most responsive to the stimuli, although the observation that co-cultured neuron responses showed similarly wide ranges of value to those from mono-cultures suggests against this.

Do monocyte-macrophages increase sympathetic neuron excitability? For Wistar stellate neurons it seems the case that blood leukocytes in general, or just BMDMs, of either Wistar or SHR origin, increase their $[Ca^{2+}]_i$ transient responsiveness to nicotinic stimulation, with similar, trends for responsiveness to high K^+ depolarisation. It seems likely that the blood monocyte-macrophages would therefore contribute to the whole blood leukocyte effect (not discounting potential effects of other cells), which was of a similar magnitude to that of the BMDMs alone. A small caveat to this though is the observation that simple inclusion of M-CSF in the culture media of Wistar stellate neurons, appeared to itself increase $[Ca^{2+}]_i$ transient responsiveness to a limited extent; while the M-CSF response did not differ significantly from baseline, it also did not

significantly differ from the response with BMDMs present. This is a surprising finding given that stellate neurons are not known to express M-CSF receptor CSF1R (especially as no physiological purpose could be easily ascribed to this if they did), which is thought to be limited in expression to myeloid cells (Rojo et al., 2017). One study detected the presence of *csf1r* mRNA in a small population of hippocampal and cortical mouse neurons (Luo et al., 2013), but there is still no reason to suggest stellate neurons broadly express this receptor. It is important to consider that the stellate cultures of this chapter do include other cells; potentially as many different cell types as are present in the ganglion, provided these can survive. It is therefore possible, and perhaps the most likely explanation, that the inclusion of M-CSF may promote survival of intrinsic macrophages, already present in the ganglion at the time of culture, which then have an effect on neuronal Ca^{2+} handling.

Interestingly in the SHR, whole blood leukocyte co-culture interventions did not affect stellate neuron responsiveness, while BMDMs only increased activity if they came from the SHR, and not Wistar rats. From this one can make two inferences: first, Wistar neurons are more sensitive to the responsiveness enhancing effect of leukocytes or BMDMs, and second, SHR BMDMs are more potent in this effect. From this one could speculate that some form of immunological macrophage-related difference to which the SHR neurons are exposed *in vivo*, is at least partly responsible for the stellate neuron hyper-responsivity phenotype. When the Wistar neurons are exposed to these SHR macrophages, their nicotinic responsiveness reaches similar levels to those of mono-cultured SHR neurons, suggesting their presence is sufficient for the phenotype. It is difficult to determine whether this is necessary to produce the phenotype *in vivo*. However, the observation that Wistar BMDMs do not raise SHR neuronal activity

suggests that this stimulus may be below the level of that received in vivo. Adding to this the fact that SHR BMDMs do enhance SHR neuronal Ca^{2+} activity, as the SHR stellate neurons will likely be exposed to these *in vivo*, one could therefore suggest they may contribute to their heightened activity, which appears to be sustained even when removed from the organism.

As BMDMs seemingly therefore do possess the ability to increase sympathetic neuron responsiveness to stimulation, what is the mechanism by which this occurs? As mentioned above, physical interaction seems rather unlikely, especially given the lack of substantial direct apposition in the co-culture images. The most probably mechanism would therefore involve release of cytokines and other mediators by the macrophages which may act directly on the neurons, or via effects on local glia (likely present in the stellate cultures), to raise activity. This chapter tested the effects of what seemed the most likely candidates, the pro-inflammatory cytokine triad of: TNF-α, IL-1β and IL-6, and found these not to be necessary. Additionally, neither TNF-α, nor IL-1β were sufficient to mimic the BMDM effect when added to stellate neuron cultures. Further examination of the co-culture medium, for example by mass spectrometry, could therefore perhaps be useful as a future experiment in attempt to determine the macrophage-to-neuron signal.

An increasingly recognised source of macrophage signalling are extracellular vesicles. These are released from the cell membrane and can contain a variety of bioactive mediators, such as miRNAs, which are then taken up by other cells, altering their behaviour (reviewed by Wang et al., 2020). It is possible that these vesicles may be responsible for mediation of the BMDM effects on stellate neurons, and future work could aim to isolate these particles, and if present examine the nature of their components.

In the SHR, stellate neuron hyperactivity is thought to be due to a loss of the electrophysiologically-stabilising M-current (Davis et al., 2020), and to dysregulated cyclic nucleotide signalling which leads to aberrant Ca^{2+} handling (Li and Paterson, 2019). It could be the case that macrophage signalling produces these effects on stellate neurons in the SHR, which then persist after *ex vivo* culture. It would be interesting to assess these features in the Wistar neurons induced by immunological intervention to phenocopy SHR neuron $[Ca^{2+}]_i$ transients, to see if similar mechanisms underlie this. While these specific molecular mechanisms have not yet been documented in other forms of immune cell-induced neuronal sensitisation, in other contexts in which leukocytes or cytokines enhance neuronal activity, this is often due to electrophysiological changes. For example, TNF-α increases TTX-sensitive channel expression in nociceptor neurons (Jin and Gereau, 2006) and central nervous system inflammation reduces expression of the Kv4.3 channel (which tends to oppose neuronal firing) in the RVLM (Wu et al., 2012). Additionally, cytokines and growth factors can enhance neuronal growth and sprouting, notably IL-6 in the case of sympathetic neurons (Ramer et al., 1998), and naturally NGF. It seems likely that the macrophages in this study may also affect the electrophysiology and growth of neurons, through release of an as yet undetermined factor.

Finally, another strict control experiment involving co-culture of neurons with relatively inert, non-macrophage cells (such as HEK 293 cells) will need to be performed in future to completely exclude the possibility that the mere culture of another cell type with the neurons increases their activity non-specifically. In the case of SHR neurons though, co-culture with whole blood leukocytes, or Wistar BMDMs did not increase their activity, which suggests against the co-culture process itself being able to non-specifically increase activity, albeit only shown in the diseased strain.

IV.4.3 Limitations

There always exist translatability issues when modelling physiological processes in cultured cells. In this chapter an attempt was made to minimise this by culturing whole stellate ganglia to preserve the cellular composition and architecture of this tissue, although reliable data were not able to be obtained from this system. For this reason, a switch to cultured single cells had to be made, but of course this potentially alters the influence of glial cells (although many non-neuronal stellate cells were present on the coverslips) over the various manipulations that were made to each preparation. For example, in response to neuronal injury and local inflammation, Schwann cells are a key source of cytokines which affect neuronal activity (Scholz & Woolf, 2007).

IV.4.4 Conclusions

1. Pre-hypertensive SHR stellate neurons display an enhanced $[Ca^{2+}]_i$ responsiveness to nicotinic or high $[K^+]_o$ stimulation, consistent with previous reports.
2. Whole blood leukocytes can make Wistar stellate neurons phenocopy those the pre-hypertensive SHR.
3. BMDMs can make Wistar stellate neurons phenocopy those of the pre-hypertensive SHR.
4. Pre-hypertensive SHR BMDMs, but not those from Wistar rats, can enhance pre-hypertensive SHR neuron responsiveness to nicotinic stimulation.
5. These leukocyte-induced enhancements of neuronal responsiveness seem not to involve the classic triad of type 1 inflammation: TNF-α, IL-1β or IL-6.

CHAPTER VI

Discussion & Conclusions

VI.1 Novel findings of the thesis

This thesis examined the immune system influence over peripheral sympathetic ganglia in essential hypertension, using the SHR as the primary model.

The main novel findings of this thesis are:

1. The SHR sympathetic ganglia, blood and kidneys display a reduced classical/non-classical monocyte ratio, when compared to sympathetic ganglia from age matched Wistar rats.
2. A small group of human patients with essential hypertension do not to show any differences in the relative proportions of blood monocyte subsets.
3. SHR stellate ganglia express higher levels of chemokine gene *ccl2*, than do Wistar ganglia.
4. SHR stellate neurons express stronger $[Ca^{2+}]_i$ transients in response to nicotine or high $[K^+]_o$ depolarisation than do Wistar neurons.
5. Co-culturing blood leukocytes with Wistar stellate neurons increases their $[Ca^{2+}]_i$ transient responsiveness to nicotinic stimulation, making them phenocopy those of the SHR, but does not affect pre-hypertensive SHR neurons.
6. Co-culturing either Wistar or SHR bone marrow-derived macrophages (BMDMs) with Wistar stellate neurons increases their $[Ca^{2+}]_i$ transient responsiveness to nicotinic stimulation, but only SHR (and not Wistar) BMDMs can further enhance the responsiveness of SHR neurons to the same stimulus.

VI.2 Monocyte-macrophage subset shift: a feature of hypertension?

In Chapter III, data are presented suggesting that the pre-SHR displays a lack of classical monocyte-macrophages in its sympathetic ganglia, and a potential relative enrichment of non-classical monocyte-macrophages. This lower classical/non-classical monocyte ratio is also

lowered in the blood and kidneys of the pre-SHR. This was the most striking and consistently observed difference between the SHR and Wistar strains.

What is the significance of this finding? Many other inflammatory-related diseases feature a relative enrichment of non-classical blood monocytes, including: systemic lupus erythematosus (Mukherjee et al., 2015; Zhu et al., 2016), sepsis (Mukherjee et al., 2015), obesity and metabolic syndrome (Poitou et al., 2011), and according to some sources, rheumatoid arthritis (Lacerte et al., 2016). Furthermore, these cells seem to exhibit a pro-inflammatory phenotype (Wong et al., 2011; Liu et al., 2015; Mukherjee et al., 2015; Ong et al., 2018), and may contribute to many of these disease states. Is this altered monocyte-macrophage ratio therefore an immunological feature of essential hypertension in the same way as for these other diseases?

The human data reported in Chapter III showed no differences in the proportions of any of the three human monocyte subsets in patients with hypertension compared to healthy controls. This could suggest that the SHR's immunological phenotype is specific to its genetic form of hypertension, but that this is not conserved in the human disease. However, it should be noted that this human study may be underpowered, with group sizes of 10 hypertensive patients and 10 healthy controls, and only 9 and 6 such flow cytometry samples respectively were viable for monocyte proportion analysis. In all of the above diseases where non-classical monocyte enrichment was observed, the diseases were either severe inflammatory conditions in which a more robust immune phenotype could be expected to be detected, or the numbers of patients used were substantially larger. Moreover, in the case of rheumatoid arthritis, there have been a wide range of mixed results when attempting to determine the relative proportions of monocytes (Cairns et al., 2002; Rossol et al., 2012; Yoon et al., 2014; Lacerte et al., 2016; Smiljanovic et al., 2018). This may highlight the heterogeneity of the human population, which in addition to the potential presence of varied essential hypertension aetiologies, could be responsible for the lack of a difference found here. Additionally, as the difference between

even the SHR and Wistar blood classical-to-non classical monocyte ratio was subtle, this suggests one would be much less likely to find such a difference in the human blood samples than if human stellate tissue was examined. For this reason, it may be worth repeating this analysis in a larger study of hypertensive patients, with measurement of sympathetic tone to confirm neurogenic origin, and possibly examination of human stellate tissue, both of which unfortunately were unachievable in the experimental timeline of this thesis.

VI.3 Role of macrophages in sympathetic neuron hyperactivity?

Does the altered monocyte macrophage subset ratio within the SHR sympathetic ganglia have a functional effect on local neuronal activity? As referenced above, non-classical monocytes have been shown in many contexts to possess pro-inflammatory properties. These cells have been demonstrated to be major producers of inflammatory cytokines (Wong et al., 2011; Mukherjee et al., 2015; Ong et al., 2018) and possess a strong ability to activate naïve T cells (Liu et al., 2015). In each of these cases the non-classical monocytes were observed to be the most potent monocyte subset in each of these assays. Zhu et al. (2016) also showed $CD16^+$ monocytes were strongly able to activate B cells, although they grouped non-classical and intermediate monocytes together in this way, so a specific non-classical effect cannot be determined. As non-classical monocyte numbers are elevated in these diseases, and seem to be potent inflammatory cells, a role in disease pathology is implied. Furthermore, looking at more specific disease contexts, $CD16^+$ from SLE patients seem to display enhanced inflammatory attributes (again, this includes non-classical and intermediate monocytes), and in the murine serum-transfer rheumatoid arthritis model, clodronate-depletion of monocytes and replacement with non-classical monocytes enhances disease, while replacement with classical ones delays it (Misharin et al., 2014). By contrast, pro-phagocytic, homeostatic roles for classical monocytes have been observed (Cros et al., 2010; Mukherjee et al., 2015).

If the SHR stellate has lost a homeostatic cell type, and gained a pathological one, this may interfere with local neuronal functioning. Local inflammation promotes states of local neuronal hyper-excitability in a number of contexts, many involving the sympathetic nervous system (Zhou et al., 2004; Hasan et al., 2006; Scholz and Woolf, 2007; Wernli et al., 2009; Wu et al., 2012; Santisteban et al., 2015). Moreover, anti-TNFα treatment infliximab causes an increase in circulating non-classical monocytes in Crohn's disease patients (Nazareth et al., 2014), along with an increase in all $CD16^+$ monocytes (not stratified into non-classical and intermediate) in rheumatoid arthritis patients (Aeberli et al., 2016). The latter study showed a concomitant reduction in circulating CCL2 (incidentally the mediator whose expression was found in Chapter IV to be increased in the SHR stellate ganglion) causing them to hypothesise that this increase in blood non-classical monocytes was due to reduced recruitment to inflamed tissues. However, CCL2 is mainly a chemoattractant for *classical* monocytes. The mechanism would thus have to involve reduced classical monocyte recruitment to the tissues and therefore reduced subsequent differentiation into non-classical monocytes, but as blood classical monocyte numbers increased, this seems unlikely. Expression of CX_3CL1, the non-classical chemokine, was not examined however, and it would be interesting to measure this and further assess non-classical monocyte trafficking, to test the above hypothesis. Interestingly though, in a study of patients with spondyloarthropathy, infliximab also produced a reduction in the numbers of $CD163^+$ macrophages within the synovial tissue (Baeten et al., 2002). Although classical monocytes can express this marker, the synovial $CD163^+$ cells were major producers of TNF-α and did not release IL-10 (Baeten et al., 2002), which suggests they are more likely to be $CD16^+$ monocytes (Wong et al., 2011; Mukherjee et al., 2015; Ong et al., 2018), potentially of the non-classical subset. Of course the rat has no intermediate monocyte subset, so it is unclear how the functional roles of the $CD16^+$ human population combining non-

classical and intermediate monocytes, translate to the purely non-classical $CD16^+$ population of the rat.

Despite this apparent non-classical monocyte phenotype reported in the literature, the experiments of Chapter IV failed to find any difference in inflammatory mediator expression, apart from *ccl2*, in the SHR stellate ganglion. Moreover, no differences in the levels of these mediators between the blood monocytes of SHR and Wistar rats were found, nor were there any differences between the pooled classical and non-classical cells, with the exception of *il10*, which, unlike in the literature, was expressed only by non-classical monocytes. These findings argue against the idea of an inflammatory reaction within the SHR sympathetic ganglia, although it is possible the monocyte-macrophages only start expressing substantial levels of these mediators once in the tissue. Unfortunately, it is almost impossible to FAC-sort sufficient levels of stellate monocyte-macrophages for qPCR analysis. It should be noted that with often <3 repeats per condition, the n numbers of these qPCR analyses were relatively low, for cost reasons, although no substantial trends towards higher SHR type 1 cytokine expression were present.

In the SHR stellate ganglia, there were higher relative numbers of neutrophils, an important inflammatory cell type, which are known to drive monocyte recruitment and polarisation towards an inflammatory phenotype (Soehnlein et al., 2017). Moreover, SHR neutrophils tend to produce higher levels of ROS (Schmidschonbein et al., 1991; Ohmori et al., 2000; Chatterjee et al., 2009), which tend to enhance inflammation. This certainly suggests some form of immunological reaction occurring in this tissue, but without any direct evidence of increased levels of mediators or oxidative stress markers, this leaves a weakness in this hypothesis. Further single cell RNA sequencing analysis of the stellate leukocytes could prove a useful tool in examining this further.

Application of cytokines TNF-α or IL-1β did not increase the responsiveness of Wistar or SHR stellate neurons to nicotinic or high $[K^+]_o$ stimulation (Chapter V). This suggests that these two inflammatory mediators would not cause peripheral sympathetic hyperactivity, but does not exclude others from being involved, such as IL-18 or leukaemia inhibitory factor, or the involvement of neuronal growth factors such as NGF, known to be produced by immune cells in some immune-neuronal interactions (Hasan et al., 2006; Wernli et al., 2009), or GDNF.

Very interestingly though, whole blood leukocytes in co-culture increase Wistar stellate neuron $[Ca^{2+}]_i$ transients, but not those from the SHR. Moreover, BMDMs of either strain increase Wistar neuron responsiveness to stimulation, while only SHR BMDMs increase that of SHR neurons. All co-culture results are summarised in Table 1. It seems unlikely that these macrophages or other leukocytes interact physically with the neurons, at least to any substantial extent, and therefore it is probable that these immune cells release a factor (or group of factors), which sensitises the sympathetic neurons. However, the multi-cytokine blockade experiment of Chapter V further suggests against TNF-α, IL-1β or IL-6, being involved. The observation that SHR neurons are unaffected by whole blood leukocytes, may imply they have already been exposed to a sensitising stimulus; or it could just be the case that leukocytes are sufficient, but not necessary for heightened sympathetic activity, without being the original cause in the SHR. Nevertheless, SHR BMDMs can still increase the activity of SHR stellate neurons (while those from Wistar rats cannot), suggesting a property specific to these SHR cells can promote the excitability of even these already hyperactive neurons. Taken together with the altered monocyte-macrophage composition of the SHR stellate ganglion, it is possible that macrophages play a role in SHR peripheral sympathetic hyperactivity. Macrophages in particular are implicated as only SHR concentration BMDMs, and not general leukocytes, could increase SHR stellate neuron nicotinic responsiveness. However, future work would need to confirm this *in vivo*, perhaps by cross-transplants of SHR and Wistar bone marrow.

Table 1| Summary of stellate neuronal $[Ca^{2+}]_i$ transient responsiveness to nicotinic stimulation in co-culture experiments. Wistar neurons in monoculture are taken as the baseline and all other permutations described relative to this.

		Control	Leukocytes		BMDMs		
			WST	SHR	WST	SHR	WST with TNF-α, IL-1β and IL-6 blockade
Stellate Neuron Strain	WST	Baseline	+	Baseline[9]	+	+	+
	SHR	+	+	+	+	++	Not tested

Additionally, one would need to identify the mediators responsible for neuronal sensitisation, if this effect is indeed real. The results of Chapter V suggest that the classic type 1 inflammatory triad of TNF-α, IL-1β and IL-6 are not involved as their blockade did not affect the increase in nicotinic responsiveness caused by BMDM co-culture. Mass spectrometry and isolation of any macrophage extracellular vesicles would be the next steps in finding the signal being transferred between the BMDMs and neurons.

[9] The nicotinic responsiveness of Wistar stellate neurons co-cultured with SHR leukocytes did not quite statistically significantly differ from baseline (p=0.080). For reasons discussed in Chapter V, it seems possible that this result was a type II error and that SHR leukocytes should increase Wistar neuron $[Ca^{2+}]_i$ transient responsiveness to stimulation. This is due to the observations that: 1) the nicotinic response of Wistar stellate neurons co-cultured with SHR leukocytes did not differ significantly from that of those cultured with Wistar leukocytes, which were themselves significantly different from baseline; 2) the responses of these two populations were much closer together in magnitude than that of the neurons cultured with SHR leukocytes compared to baseline; and 3) SHR leukocytes significantly increased the responsiveness of Wistar neurons to high $[K^+]_o$ depolarisation.

VI.4 Origin of the SHR's monocyte-macrophage subset shift

If the altered sympathetic ganglion monocyte-macrophage ratio in the SHR is indeed important to sympathetic hyperactivity, as suggested above, its cause would become important as a potential therapeutic target. The data of Chapter III point to this alteration of subset proportions being a systemic phenomenon, being present in the blood and kidneys, in addition to the sympathetic ganglia. It may seem therefore that the SHR has an inherent tendency to produce a higher proportion of non-classical monocytes, which then spread throughout the circulation and tissues. As non-classical monocytes derive from classical monocytes, this implies that once released from the bone marrow, SHR classical monocytes more frequently differentiate into non-classical cells. There are two main possibilities for this: either the SHR bone marrow-derived monocytes are inherently more likely to differentiate into the non-classical sub-type, or another factor in the SHR drives this process to a greater extent.

Interestingly, BMDMs cultured from Wistar and SHR bone marrow, expressed similar levels of both classical monocyte marker *ccr2*, and non-classical marker *cx3cr1* (Chapter IV), which could suggest against any inherent difference in differentiation potential arising from the bone marrow. However, this culture process involved using M-CSF (as an essential survival factor), a potent stimulus for the classical to non-classical monocyte transition, at a concentration of 20 ng/ml where the ED_{50} for proliferation listed on the manufacturer datasheet is ~2 ng/ml, so any innate differences could be masked. One cannot therefore exclude the possibility that SHR monocytes themselves tend to produce more non-classical cells. However, the only well-characterised mediator of this process is M-CSF (Weiner et al., 1994; Korkosz et al., 2012), whose levels have been shown higher in human hypertensive patients (Radaeva et al., 2019). Of course it is difficult to ascertain any direction of causality between M-CSF and hypertension, but if this were also present in the SHR, it could contribute to the altered

monocyte ratios. Anti-MCSF therapy may therefore be a way to reduce this shift in monocyte ratios.

The size of the monocyte ratio difference between the SHR and Wistar strains is much larger in the stellate and SCG than in the blood (Chapter III), which could perhaps suggest a difference in recruitment could also contribute to the observation within this tissue. The SHR stellate ganglia expressed ~4-fold higher levels of *ccl2*, which is interestingly the main chemokine mediating *classical* monocyte recruitment. If there is greater classical monocyte recruitment to the SHR stellate ganglion, this would suggest rapid trans-differentiation into non-classical cells and rapid turnover of these within the ganglionic tissue, where classical monocyte numbers are lowered, and non-classical cells slightly higher than in the Wistar. Future work to examine the dynamics of monocyte trafficking to and from the SHR stellate ganglion could therefore be useful to determine whether anti-CCL2 therapy could be beneficial.

VI.5 Conclusions & Future Directions

The SHR's form of hypertension appears to be characterised by a reduced classical/non-classical monocyte-macrophage ratio within their sympathetic ganglia, the blood and kidneys. This effect seems to be caused by an inherently higher differentiation of classical monocytes into the non-classical sub-type, which may be the result of higher M-CSF levels in the SHR. However, there is no evidence that this immunological phenotype is present within the blood of a small sample of human essential hypertensive patients.

The co-culture of whole blood leukocytes or BMDMs with Wistar stellate neurons seems to phenocopy the enhanced $[Ca^{2+}]_i$ transient responsiveness to nicotinic stimulation characterising those from the SHR, whereas the SHR neurons are generally unchanged by such interventions. Only SHR BMDMs are able to enhance the activity of neurons from this strain, suggesting that this strain's macrophage are more potent promoters of sympathetic neuron responsiveness to

stimulation. There was however, no evidence supporting a role for classic type 1 pro-inflammatory cytokines in the mechanism underlying this neuronal sensitisation.

Following on from the work of this thesis, owing to the robustness of the altered monocyte ratio finding in the SHR, and the ability of BMDMs (particularly those of the SHR) to increase sympathetic neuronal responsiveness, a potential human phenotype may merit further investigation, as the study reported in Chapter III here suffers from low n numbers, examining a subtly inflammatory and heterogeneous human disease of hypertension. Testing for this phenotype in other diseases of sympathetic hyperactivity may also be useful, to assess mechanistic similarity, knowledge of which could be helpful in improving therapy for a range of conditions. While BMDMs seem to promote stellate sympathetic hyperactivity, the mediators and mechanisms underlying this need to be determined, which, if this underlies human dysautonomia, could provide an important therapeutic target. Finally, it may be worth testing the potential role of higher SHR plasma M-CSF levels in causing the altered monocyte ratio, which could serve as another node of intervention to reverse this immunological phenotype.

References

AEBERLI, D., KAMGANG, R., BALANI, D., HOFSTETTER, W., VILLIGER, P. M. & SEITZ, M. 2016. Regulation of peripheral classical and non-classical monocytes on infliximab treatment in patients with rheumatoid arthritis and ankylosing spondylitis. *Rmd Open,* 2 (1), e000079.

AGHAEEPOUR, N., NIKOLIC, R., HOOS, H. H. & BRINKMAN, R. R. 2011. Rapid cell population identification in flow cytometry data. *Cytometry Part A*, 79 (1), 6-13.

AJIJOLA, O. A., HOOVER, D. B., SIMERLY, T. M., BROWN, T. C., YANAGAWA, J., BINIWALE, R. M., LEE, J. M., SADEGHI, A., KHANLOU, N., ARDELL, J. L. & SHIVKUMAR, K. 2017. Inflammation, oxidative stress, and glial cell activation characterize stellate ganglia from humans with electrical storm. *JCI Insight,* 2 (18), e94715.

AKIRA, S., UEMATSU, S. & TAKEUCHI, O. 2006. Pathogen recognition and innate immunity. *Cell,* 124 (4)**,** 783-801.

ANDRZEJCZAK, D., GORSKA, D. & CZARNECKA, E. 2006. Influence of amlodipine and atenolol on lipopolysaccharide (LPS)-induced serum concentrations of TNF-alpha, IL-1, IL-6 in spontaneously hypertensive rats (SHR). *Pharmacological Reports,* 58 (5)**,** 711-719.

ANNUNZIATO, F., ROMAGNANI, C. & ROMAGNANI, S. 2015. The 3 major types of innate and adaptive cell-mediated effector immunity. *Journal of Allergy and Clinical Immunology,* 135 (3)**,** 626-635.

ANNUNZIATO, L., PARMACCIONE, A., CATALDI, M., SECONDO, A., CASTALDO, P., DI RENZO, G. & TAGLIALATELA, M. 2002. Modulation of ion channels by reactive oxygen and nitrogen species: a pathophysiological role in brain aging? *Neurobiology of Aging,* 23 (5)**,** 819-834.

ARANTES, R. M. E., LOURENSSEN, S., MACHADO, C. R. S. & BLENNERHASSETT, M. G. 2000. Early damage of sympathetic neurons after co-culture with macrophages: a model of neuronal injury in vitro. *Neuroreport,* 11 (1)**,** 177-181.

AUFFRAY, C., FOGG, D., GARFA, M., ELAIN, G., JOIN-LAMBERT, O., KAYAL, S., SARNACKI, S., CUMANO, A., LAUVAU, G. & GEISSMANN, F. 2007. Monitoring of blood vessels and tissues by a population of monocytes with patrolling behavior. *Science,* 317 (5838)**,** 666-670.

BAETEN, D., DEMETTER, P., CUVELIER, C. A., KRUITHOF, E., VAN DAMME, N., DE VOS, M., VEYS, E. M. & DE KEYSER, F. 2002. Macrophages expressing the scavenger receptor CD163: a link between immune alterations of the gut and synovial inflammation in spondyloarthropathy. *Journal of Pathology,* 196 (3)**,** 343-350.

BARDSLEY, E. N., DAVIS, H., AJIJOLA, O. A., BUCKLER, K. J., ARDELL, J. L., SHIVKUMAR, K. & PATERSON, D. J. 2018a. RNA sequencing reveals novel transcripts from sympathetic stellate ganglia during cardiac sympathetic hyperactivity. *Scientific Reports,* 8, 8633.

BARDSLEY, E. N., DAVIS, H., BUCKLER, K. J. & PATERSON, D. J. 2018b. Neurotransmitter switching coupled to β-adrenergic signaling in sympathetic neurons in prehypertensive states. *Hypertension,* 71 (6)**,** 1226-1238.

BARNETT-VANES, A., SHARROCK, A., BIRRELL, M. A. & RANKIN, S. 2016. A single 9-colour flow cytometric method to characterise major leukocyte populations in the rat: validation in a model of LPS-induced pulmonary inflammation. *Plos One,* 11 (1), e0142520.

BAROUCH, R., KAZIMIRSKY, G., APPEL, E. & BRODIE, C. 2001. Nerve growth factor regulates TNF-alpha production in mouse macrophages via MAP kinase activation. *Journal of Leukocyte Biology,* 69 (6)**,** 1019-1026.

BAUER, J., BAUER, T. M., KALB, T., TAGA, T., LENGYEL, G., HIRANO, T., KISHIMOTO, T., ACS, G., MAYER, L. & GEROK, W. 1989. Regulation of interleukin-6 receptor expression in human monocytes and monocyte-derived macrophages. Comparison with the expression in human hepatocytes. *Journal of Experimental Medicine,* 170 (5)**,** 1537-1549.

BAUTISTA, L. E., VERA, L. M., ARENAS, I. A. & GAMARRA, G. 2005. Independent association between inflammatory markers (C-reactive protein, interleukin-6, and TNF-alpha) and essential hypertension. *Journal of Human Hypertension,* 19 (2)**,** 149-154.

BHATT, D. L., KANDZARI, D. E., O'NEILL, W. W., D'AGOSTINO, R., FLACK, J. M., KATZEN, B. T., LEON, M. B., LIU, M. L., MAURI, L., NEGOITA, M., COHEN, S. A., OPARIL, S.,

ROCHA-SINGH, K., TOWNSEND, R. R., BAKRIS, G. L. & INVESTIGATORS, S. H.-. 2014. A controlled trial of renal denervation for resistant hypertension. *New England Journal of Medicine,* 370 (15)**,** 1393-1401.

BLAKE, W. D., WEGRIA, R., WARD, H. P. & FRANK, C. W. 1950. Effect of renal arterial constriction on excretion of sodium and water. *American Journal of Physiology,* 163 (2)**,** 422-429.

BOHM, M., KARIO, K., KANDZARI, D. E., MAHFOUD, F., WEBER, M. A., SCHMIEDER, R. E., TSIOUFIS, K., POCOCK, S., KONSTANTINIDIS, D., CHOI, J. W., EAST, C., LEE, D. P., MA, A., EWEN, S., COHEN, D. L., WILENSKY, R., DEVIREDDY, C. M., LEA, J., SCHMID, A., WEIL, J., AGDIRLIOGLU, T., REEDUS, D., JEFFERSON, B. K., REYES, D., D'SOUZA, R., SHARP, A. S. P., SHARIF, F., FAHY, M., DEBRUIN, V., COHEN, S. A., BRAR, S., TOWNSEND, R. R. & THE SPYRAL HTN-OFF MED PIVOTAL INVESTIGATORS 2020. Efficacy of catheter-based renal denervation in the absence of antihypertensive medications (SPYRAL HTN-OFF MED Pivotal): a multicentre, randomised, sham-controlled trial. *Lancet,* 395 (10234)**,** 1444-1451.

BOYDEN, S. 1962. The chemotactic effect of mixtures of antibody and antigen on polymorphonuclear leucocytes. *Journal of Experimental Medicine,* 115 (3)**,** 453-466.

BOYETTE, L. B., MACEDO, C., HADI, K., ELINOFF, B. D., WALTERS, J. T., RAMASWAMIL, B., CHALASANI, G., TABOAS, J. M., LAKKIS, F. G. & METES, D. M. 2017. Phenotype, function, and differentiation potential of human monocyte subsets. *Plos One,* 12 (4), e0176460.

BRANDTZAEG, P. 1998. The increasing power of immunohistochemistry and immunocytochemistry. *Journal of Immunological Methods,* 216 (1-2)**,** 49-67.

BRUM, P. C., KOSEK, J., PATTERSON, A., BERNSTEIN, D. & KOBILKA, B. 2002. Abnormal cardiac function associated with sympathetic nervous system hyperactivity in mice. *American Journal of Physiology-Heart and Circulatory Physiology,* 283 (5)**,** H1838-H1845.

BRUNET, A., LEBEL, M., EGARNES, B., PAQUET-BOUCHARD, C., LESSARD, A. J., BROWN, J. P. & GOSSELIN, J. 2016. NR4A1-dependent $Ly6C^{low}$ monocytes contribute to reducing joint inflammation in arthritic mice through Treg cells. *European Journal of Immunology,* 46 (12)**,** 2789-2800.

BUFORD, T. W. 2016. Hypertension and aging. *Ageing Research Reviews,* 26**,** 96-111.

BURBA-ANCZEWSKA, I. 1978. Leukocyte system in spontaneously hypertensive rats. *Acta Physiologica Polonica,* 29 (4)**,** 353-358.

BURNIER, M. & EGAN, B. M. 2019. Adherence in hypertension. A review of prevalence, risk factors, impact, and management. *Circulation Research,* 124 (7)**,** 1124-1140.

BURNS, J., SIVANANTHAN, M. U., BALL, S. G., MACKINTOSH, A. F., MARY, D. A. S. G. & GREENWOOD, J. P. 2007. Relationship between central sympathetic drive and magnetic resonance imaging-determined left ventricular mass in essential hypertension. *Circulation,* 115 (15)**,** 1999-2005.

CAIRNS, A. P., CROCKARD, A. D. & BELL, A. L. 2002. The $CD14^{+}CD16^{+}$ monocyte subset in rheumatoid arthritis and systemic lupus erythematosus. *Rheumatology International,* 21 (5)**,** 189-192.

CECILIA ALVAREZ, M., CALDIZ, C., FANTINELLI, J. C., GARCIARENA, C. D., CONSOLE, G. M., CHIAPPE DE CINGOLANI, G. E. & MOSCA, S. M. 2008. Is cardiac hypertrophy in spontaneously hypertensive rats the cause or the consequence of oxidative stress? *Hypertension Research,* 31 (7)**,** 1465-1476.

CHAN, S. H. H., WU, K. L. H., CHANG, A. Y. W., TAI, M.-H. & CHAN, J. Y. H. 2009. Oxidative impairment of mitochondrial electron transport chain complexes in rostral ventrolateral medulla contributes to neurogenic hypertension. *Hypertension,* 53 (2)**,** 217-227.

CHAPLIN, D. D. 2010. Overview of the immune response. *Journal of Allergy and Clinical Immunology,* 125 (2 suppl. 2)**,** S3-S23.

CHATTERJEE, M., SALUJA, R., TEWARI, S., BARTHWAL, M. K., GOEL, S. K. & DIKSHIT, M. 2009. Augmented nitric oxide generation in neutrophils: oxidative and pro-inflammatory implications in hypertension. *Free Radical Research,* 43 (12)**,** 1195-1204.

CLAASSEN, I., VANROOIJEN, N. & CLAASSEN, E. 1990. A new method for removal of mononuclear phagocytes from heterogeneous cell populations *in vitro*, using the liposome-

mediated macrophage 'suicide' technique. *Journal of Immunological Methods,* 134 (2)**,** 153-161.

CLARKE, G. L., BHATTACHERJEE, A., TAGUE, S. E., HASAN, W. & SMITH, P. G. 2010. β-Adrenoceptor blockers increase cardiac sympathetic innervation by inhibiting autoreceptor suppression of axon growth. *Journal of Neuroscience,* 30 (37)**,** 12446-12454.

COHEN, J. B., LOTITO, M. J., TRIVEDI, U. K., DENKER, M. G., COHEN, D. L. & TOWNSEND, R. R. 2019. Cardiovascular events and mortality in white coat hypertension: a systematic review and meta-analysis. *Annals of Internal Medicine,* 170 (12)**,** 853-862.

COONS, A. H., CREECH, H. J., JONES, R. N. & BERLINER, E. 1942. The demonstration of pneumococcal antigen in tissues by the use of fluorescent antibody. *Journal of Immunology,* 45 (3)**,** 159-170.

COWLEY, A. W. & ROMAN, R. J. 1996. The role of the kidney in hypertension. *Journal of the American Medical Association,* 275 (20)**,** 1581-1589.

COWLEY, A. W., LIARD, J. F. & GUYTON, A. C. 1973. Role of the baroreceptor reflex in daily control of arterial blood pressure and other variables in dogs. *Circulation Research,* 32 (5)**,** 564-576.

CROS, J., CAGNARD, N., WOOLLARD, K., PATEY, N., ZHANG, S. Y., SENECHAL, B., PUEL, A., BISWAS, S. K., MOSHOUS, D., PICARD, C., JAIS, J. P., D'CRUZ, D., CASANOVA, J. L., TROUILLET, C. & GEISSMANN, F. 2010. Human $CD14^{dim}$ Monocytes Patrol and Sense Nucleic Acids and Viruses via TLR7 and TLR8 Receptors. *Immunity,* 33 (3)**,** 375-386.

CROWLEY, S. D. & COFFMAN, T. M. 2014. The inextricable role of the kidney in hypertension. *Journal of Clinical Investigation,* 124 (6)**,** 2341-2347.

CUDDY, S. R., SCHINLEVER, A. R., DOCHNAL, S., SEEGREN, P. V., SUZICH, J., KUNDU, P., DOWNS, T. K., FARAH, M., DESAI, B. N., BOUTELL, C. & CLIFFE, A. R. 2020. Neuronal hyperexcitability is a DLK-dependent trigger of herpes simplex virus reactivation that can be induced by IL-1. *Elife,* 9, e58037.

DALEKOS, G. N., ELISAF, M., BAIRAKTARI, E., TSOLAS, O. & SIAMOPOULOS, K. C. 1997. Increased serum levels of interleukin-1 beta in the systemic circulation of patients with essential hypertension: Additional risk factor for atherogenesis in hypertensive patients? *Journal of Laboratory and Clinical Medicine,* 129 (3)**,** 300-308.

DAVERN, P. J., NGUYEN-HUU, T. P., LA GRECA, L., ABDELKADER, A. & HEAD, G. A. 2009. Role of the sympathetic nervous system in Schlager genetically hypertensive mice. *Hypertension,* 54 (4)**,** 852-859.

DAVIS, H., BARDSLEY, E. N. & PATERSON, D. J. 2018. Transcriptional profiling of stellate ganglia from normotensive and spontaneously hypertensive rat strains. *Scientific Data,* 5, 180123.

DAVIS, H., HERRING, N. & PATERSON, D. J. 2020. Downregulation of M current is coupled to membrane excitability in sympathetic neurons before the onset of hypertension. *Hypertension,* 76 (6)**,** 1915-1923.

DIBONA, G. F. & ESLER, M. 2010. Translational medicine: the antihypertensive effect of renal denervation. *American Journal of Physiology-Regulatory Integrative and Comparative Physiology,* 298 (2)**,** R245-R253.

DIBONA, G. F. & KOPP, U. C. 1997. Neural control of renal function. *Physiological Reviews,* 77 (1)**,** 75-197.

DICKHOUT, J. G. & LEE, R. 1998. Blood pressure and heart rate development in young spontaneously hypertensive rats. *American Journal of Physiology-Heart and Circulatory Physiology,* 274 (3)**,** H794-H800.

DUFFY, M., GARLAND, J., ONDRUSCHKA, B., PATON, J. F. R., BARDSLEY, E. N., WONG, C. X., STABLES, S. & TSE, R. 2021. Stellate ganglionitis in sudden cardiac death: a case report. *Autonomic Neuroscience: Basic & Clinical,* 234, 102837.

EMS, R., GARG, A., OSTERGARD, T. A. & MILLER, J. P. 2019. Potential deep brain stimulation targets for the management of refractory hypertension. *Frontiers in Neuroscience,* 13, 19.

EPELMAN, S., LAVINE, K. J. & RANDOLPH, G. J. 2014. Origin and functions of tissue macrophages. *Immunity,* 41 (1)**,** 21-35.

ESLER, M. D., KRUM, H., SCHLAICH, M., SCHMIEDER, R. E., BOHM, M., SOBOTKA, P. A. & THE SYMPLICITY HTN-2 INVESTIGATORS 2012. Renal sympathetic denervation for

treatment of drug-resistant hypertension: one-year results from the Symplicity HTN-2 randomized, controlled trial. *Circulation,* 126 (25)**,** 2976-2982.

ESLER, M. D., KRUM, H., SOBOTKA, P. A., SCHLAICH, M. P., SCHMIEDER, R. E., BOEHM, M., MAHFOUD, F., SIEVERT, H., WUNDERLICH, N., RUMP, L. C., VONEND, O., UDER, M., LOBO, M., CAULFIELD, M., ERGLIS, A., AZIZI, M., SAPOVAL, M., THAMBAR, S., PERSU, A., RENKIN, J., SCHUNKERT, H., WEIL, J., HOPPE, U. C., WALTON, T., SCHEINERT, D., BINDER, T., JANUSZEWICZ, A., WITKOWSKI, A., RUILOPE, L. M., WHITBOURN, R., BRUCK, H., DOWNES, M., LUSCHER, T. F., JARDINE, A. G., WEBSTER, M. W., ZELLER, T., SADOWSKI, J., BARTUS, K., STRALEY, C. A., BARMAN, N. C., LEE, D. P., WITTELES, R. M., BHALLA, V., MASSARO, J. M. & THE SYMPLICITY HTN-2 INVESTIGATORS 2010. Renal sympathetic denervation in patients with treatment-resistant hypertension (The SYMPLICITY HTN-2 Trial): a randomised controlled trial. *Lancet,* 376 (9756)**,** 1903-1909.

ESLER, M., JENNINGS, G., KORNER, P., WILLETT, I., DUDLEY, F., HASKING, G., ANDERSON, W. & LAMBERT, G. 1988. Assessment of human sympathetic nervous system activity from measurements of norepinephrine turnover. *Hypertension,* 11 (1)**,** 3-20.

ESLER, M., LAMBERT, G. & JENNINGS, G. 1989. Regional norepinephrine turnover in human hypertension. *Clinical and Experimental Hypertension. Part A, Theory and Practice,* 11 (suppl. 1)**,** 75-89.

FARQUHAR, W. B., WENNER, M. M., DELANEY, E. P., PRETTYMAN, A. V. & STILLABOWER, M. E. 2006. Sympathetic neural responses to increased osmolality in humans. *American Journal of Physiology-Heart and Circulatory Physiology,* 291 (5)**,** H2181-H2186.

FERNANDEZ-REAL, J. M., VAYREDA, M., RICHART, C., GUTIERREZ, C., BROCH, M., VENDRELL, J. & RICART, W. 2001. Circulating interleukin 6 levels, blood pressure, and insulin sensitivity in apparently healthy men and women. *Journal of Clinical Endocrinology & Metabolism,* 86 (3)**,** 1154-1159.

FERRACINI, M., RIOS, F. J. O., PECENIN, M. & JANCAR, S. 2013. Clearance of apoptotic cells by macrophages induces regulatory phenotype and involves stimulation of CD36 and platelet-activating factor receptor. *Mediators of Inflammation,* 2013, 950273.

FERRIER, C., COX, H. & ESLER, M. 1993. Elevated total-body noradrenaline spillover in normotensive members of hypertensive families. *Clinical Science,* 84 (2)**,** 225-230.

FISHER, J. P., YOUNG, C. N. & FADEL, P. J. 2009. Central sympathetic overactivity: maladies and mechanisms. *Autonomic Neuroscience Basic & Clinical,* 148 (1-2)**,** 5-15.

FLORAS, J. S. & HARA, K. 1993. Sympathoneural and hemodynamic characteristics of young subjects with mild essential hypertension. *Journal of Hypertension,* 11 (6)**,** 647-655.

FLORAS, J. S. 2009. Sympathetic nervous system activation in human heart failure: clinical implications of an updated model. *Journal of the American College of Cardiology,* 54 (5)**,** 375-385.

FOLKOW, B. 1987. Structure and function of the arteries in hypertension. *American Heart Journal,* 114 (4 pt. 2)**,** 938-948.

FURBERG, C. D., WRIGHT, J. T., DAVIS, B. R., CUTLER, J. A., ALDERMAN, M., BLACK, H., CUSHMAN, W., GRIMM, R., HAYWOOD, L. J., LEENEN, F., OPARIL, S., PERRY, H. M., PROBSTFIELD, J., WHELTON, P., PAYNE, G., NWACHUKU, C., GORDON, D., PROSCHAN, M., FROMMER, P., EINHORN, P., HAWKINS, M., FORD, C., PRESSEL, S., PILLER, L., LUSK, C., BETTENCOURT, J., KIMMEL, B., GERACI, T., WALSH, S., RAHMAN, M., JURATOVAC, A., POSPISIL, R., BRENNAN, K., CARROLL, L., SULLIVAN, S., BARONE, G., CHRISTIAN, R., FELDMAN, S., LUCENTE, T., LEWIS, C. E., JENKINS, K., MCDOWELL, P., JOHNSON, J., KINGRY, C., LETTERER, R., MARGOLIS, K., HOLLAND, L., JAEGER-FOX, B., WILLIAMSON, J., LOUIS, G., RAGUSA, P., WILLIARD, A., FERGUSON, R. S., TANNER, J., ECKFELDT, J., CROW, R., PELOSI, J. & THE ALLHAT OFFICERS AND COORDINATORS 2000. Major cardiovascular events in hypertensive patients randomized to doxazosin vs chlorthalidone: the Antihypertensive and Lipid-Lowering Treatment to Prevent Heart Attack Trial (ALLHAT). *Journal of the American Medical Association,* 283 (15)**,** 1967-1975.

FURNESS, J. B. 2015. 'Peripheral Autonomic Nervous System' in PAXINOS, G. (editor) *The rat nervous system, 4th edition*. Cambridge, MA, US: Academic Press. 61-76.

GAGNÉ, F. 2014. *Biochemical ecotoxicology: principles and methods.* Cambridge, MA, US: Academic Press.

GALLA, S., CHAKRABORTY, S., CHENG, X., YEO, J., MELL, B., ZHANG, H., MATHEW, A. V., VIJAY-KUMAR, M. & JOE, B. 2018. Disparate effects of antibiotics on hypertension. *Physiological Genomics,* 50 (10)**,** 837-845.

GEISSMANN, F., JUNG, S. & LITTMAN, D. R. 2003. Blood monocytes consist of two principal subsets with distinct migratory properties. *Immunity,* 19 (1)**,** 71-82.

GELDSETZER, P., MANNE-GOEHLER, J., MARCUS, M. E., EBERT, C., ZHUMADILOV, Z., WESSEH, C. S., TSABEDZE, L., SUPIYEV, A., STURUA, L., BAHENDEKA, S. K., SIBAI, A. M., QUESNEL-CROOKS, S., NOROV, B., MWANGI, K. J., MWALIM, O., WONG-MCCLURE, R., MAYIGE, M. T., MARTINS, J. S., LUNET, N., LABADARIOS, D., KARKI, K. B., KAGARUKI, G. B., JORGENSEN, J. M. A., HWALLA, N. C., HOUINATO, D., HOUEHANOU, C., MSAIDIE, M., GUWATUDDE, D., GURUNG, M. S., GATHECHA, G., DOROBANTU, M., DAMASCENO, A., BOVET, P., BICABA, B. W., ARYAL, K. K., ANDALL-BRERETON, G., AGOUDAVI, K., STOKES, A., DAVIES, J. I., BARNIGHAUSEN, T., ATUN, R., VOLLMER, S. & JAACKS, L. M. 2019. The state of hypertension care in 44 low-income and middle-income countries: a cross-sectional study of nationally representative individual-level data from 1.1 million adults. *Lancet,* 394 (10199)**,** 652-662.

GINIATULLIN, R., NISTRI, A. & YAKEL, J. L. 2005. Desensitization of nicotinic ACh receptors: shaping cholinergic signaling. *Trends in Neurosciences,* 28 (7)**,** 371-378.

GOMES, P. M., SA, R. W. M., AGUIAR, G. L., PAES, M. H. S., ALZAMORA, A. C., LIMA, W. G., DE OLIVEIRA, L. B., STOCKER, S. D., ANTUNES, V. R. & CARDOSO, L. M. 2017. Chronic high-sodium diet intake after weaning lead to neurogenic hypertension in adult Wistar rats. *Scientific Reports,* 7, 5655.

GORDON, S. & TAYLOR, P. R. 2005. Monocyte and macrophage heterogeneity. *Nature Reviews Immunology,* 5 (12)**,** 953-964.

GRAHAM, L. N., SMITH, P. A., STOKER, J. B., MACKINTOSH, A. F. & MARY, D. 2002. Time course of sympathetic neural hyperactivity after uncomplicated acute myocardial infarction. *Circulation,* 106 (7)**,** 793-797.

GRASSI, G. 2009. Assessment of sympathetic cardiovascular drive in human hypertension: achievements and perspectives. *Hypertension,* 54 (4)**,** 690-697.

GRASSI, G. 2016. Sympathomodulatory effects of antihypertensive drug treatment. *American Journal of Hypertension,* 29 (6)**,** 665-675.

GRASSI, G., CATTANEO, B. M., SERAVALLE, G., LANFRANCHI, A. & MANCIA, G. 1998. Baroreflex control of sympathetic nerve activity in essential and secondary hypertension. *Hypertension,* 31 (1)**,** 68-72.

GRASSI, G., MARK, A. & ESLER, M. 2015. The sympathetic nervous system alterations in human hypertension. *Circulation Research,* 116 (6)**,** 976-990.

GRASSI, G., SERAVALLE, G. & QUARTI-TREVANO, F. 2010. The 'neuroadrenergic hypothesis' in hypertension: current evidence. *Experimental Physiology,* 95 (5)**,** 581-586.

GRASSI, G., SERAVALLE, G., BERTINIERI, G., TURRI, C., DELL'ORO, R., STELLA, M. L. & MANCIA, G. 2000. Sympathetic and reflex alterations in systo-diastolic and systolic hypertension of the elderly. *Journal of Hypertension,* 18 (5)**,** 587-593.

GREEN, A. L., WANG, S. Y., OWEN, S. L. F., XIE, K. N., LIU, X. G., PATERSON, D. J., STEIN, J. F., BAIN, P. G. & AZIZ, T. Z. 2005. Deep brain stimulation can regulate arterial blood pressure in awake humans. *Neuroreport,* 16 (16)**,** 1741-1745.

GREEN, A. L., WANG, S., BITTAR, R. G., OWEN, S. L. F., PATERSON, D. J., STEIN, J. F., BAIN, P. G., SHLUGMAN, D. & AZIZ, T. Z. 2007. Deep brain stimulation: a new treatment for hypertension? *Journal of Clinical Neuroscience,* 14 (6)**,** 592-595.

GREEN, A. L., HYAM, J. A., WILLIAMS, C., WANG, S. Y., SHLUGMAN, D., STEIN, J. F., PATERSON, D. J. & AZIZ, T. Z. 2010. Intra-operative deep brain stimulation of the

periaqueductal grey matter modulates blood pressure and heart rate variability in humans. *Neuromodulation,* 13 (3)**,** 174-181.

GREENE, L. A. 1977. Quantitative *in vitro* studies on nerve growth factor (NGF) requirement of neurons. I. Sympathetic neurons. *Developmental Biology,* 58 (1)**,** 96-105.

GROSSMAN, C., BORNSTEIN, G., LEIBOWITZ, A., BEN-ZVI, I. & GROSSMAN, E. 2017. Effect of tumor necrosis factor-α inhibitors on ambulatory 24-h blood pressure. *Blood Pressure,* 26 (1)**,** 24-29.

GRYNKIEWICZ, G., POENIE, M. & TSIEN, R. Y. 1985. A new generation of Ca^{2+} indicators with greatly improved fluorescence properties. *Journal of Biological Chemistry,* 260 (6)**,** 3440-3450.

GULL, W. W. & SUTTON, H. G. 1872. On the pathology of the morbid state commonly called chronic Bright's disease with contracted kidney, ("arterio-capillary fibrosis."). *Medico-chirurgical transactions,* 55**,** 273-330.

GUYTON, A. C. 1955. Determination of cardiac output by equating venous return curves with cardiac response curves. *Physiological Reviews,* 35 (1)**,** 123-129.

HALL, J. E., GUYTON, A. C., SMITH, M. J. & COLEMAN, T. G. 1980. Blood pressure and renal function during chronic changes in sodium intake: role of angiotensin. *American Journal of Physiology,* 239 (3)**,** F271-F280.

HALL, J. E., MIZELLE, H. L., HILDEBRANDT, D. A. & BRANDS, M. W. 1990. Abnormal pressure natriuresis. A cause or consequence of hypertension? *Hypertension,* 15 (6 pt. 1)**,** 547-559.

HAMEED, M. A. & DASGUPTA, I. 2019. Medication adherence and treatment-resistant hypertension: a review. *Drugs in context,* 8**,** 212560.

HARWANI, S. C., CHAPLEAU, M. W., LEGGE, K. L., BALLAS, Z. K. & ABBOUD, F. M. 2012. Neurohormonal modulation of the innate immune system is proinflammatory in the prehypertensive spontaneously hypertensive rat, a genetic model of essential hypertension. *Circulation Research,* 111 (9)**,** 1190-1197.

HASAN, W., JAMA, A., DONOHUE, T., WERNLI, G., ONYSZCHUK, G., AL-HAFEZ, B., BILGEN, M. & SMITH, P. G. 2006. Sympathetic hyperinnervation and inflammatory cell NGF synthesis following myocardial infarction in rats. *Brain Research,* 1124 (1)**,** 142-154.

HOPPE, U. C., BRANDT, M. C., WACHTER, R., BEIGE, J., RUMP, L. C., KROON, A. A., CATES, A. W., LOVETT, E. G. & HALLER, H. 2012. Minimally invasive system for baroreflex activation therapy chronically lowers blood pressure with pacemaker-like safety profile: results from the Barostim neo trial. *Journal of the American Society of Hypertension,* 6 (4)**,** 270-276.

IVY, J. R. & BAILEY, M. A. 2014. Pressure natriuresis and the renal control of arterial blood pressure. *Journal of Physiology,* 592 (18)**,** 3955-3967.

JACKSON, M. J. & MCARDLE, A. 2011. Age-related changes in skeletal muscle reactive oxygen species generation and adaptive responses to reactive oxygen species. *Journal of Physiology,* 589 (9)**,** 2139-2145.

JAKUBZICK, C. V., RANDOLPH, G. J. & HENSON, P. M. 2017. Monocyte differentiation and antigen-presenting functions. *Nature Reviews Immunology,* 17 (6)**,** 349-362.

JARDINE, D. L., CHARLES, C. J., ASHTON, R. K., BENNETT, S. I., WHITEHEAD, M., FRAMPTON, C. M. & NICHOLLS, M. G. 2005. Increased cardiac sympathetic nerve activity following acute myocardial infarction in a sheep model. *Journal of Physiology,* 565 (1)**,** 325-333.

JAYEDI, A., RAHIMI, K., BAUTISTA, L. E., NAZARZADEH, M., ZARGAR, M. S. & SHAB-BIDAR, S. 2019. Inflammation markers and risk of developing hypertension: a meta-analysis of cohort studies. *Heart,* 105 (9)**,** 686-692.

JIN, X. C. & GEREAU, R. W. 2006. Acute p38-mediated modulation of tetrodotoxin-resistant sodium channels in mouse sensory neurons by tumor necrosis factor-alpha. *Journal of Neuroscience,* 26 (1)**,** 246-255.

JULIUS, S. & VALENTINI, M. 1998. Consequences of the increased autonomic nervous drive in hypertension, heart failure and diabetes. *Blood pressure,* 7 (suppl. 3)**,** 5-13.

KALOYANIDES, G. J., DIBONA, G. F. & RASKIN, P. 1971. Pressure natriuresis in the isolated kidney. *American Journal of Physiology,* 220 (6)**,** 1660-1666.

KANDZARI, D. E., BHATT, D. L., BRAR, S., DEVIREDDY, C. M., ESLER, M., FAHY, M., FLACK, J. M., KATZEN, B. T., LEA, J., LEE, D. P., LEON, M. B., MA, A., MASSARO, J.,

MAURI, L., OPARIL, S., O'NEILL, W. W., PATEL, M. R., ROCHA-SINGH, K., SOBOTKA, P. A., SVETKEY, L., TOWNSEND, R. R. & BAKRIS, G. L. 2015. Predictors of blood pressure response in the SYMPLICITY HTN-3 trial. *European Heart Journal,* 36 (4)**,** 219-227.

KANDZARI, D. E., BOHM, M., MAHFOUD, F., TOWNSEND, R. R., WEBER, M. A., POCOCK, S., TSIOUFIS, K., TOUSOULIS, D., CHOI, J. W., EAST, C., BRAR, S., COHEN, S. A., FAHY, M., PILCHER, G., KARIO, K. & THE SPYRAL HTN-ON MED INVESTIGATORS 2018. Effect of renal denervation on blood pressure in the presence of antihypertensive drugs: 6-month efficacy and safety results from the SPYRAL HTN-ON MED proof-of-concept randomised trial. *Lancet,* 391 (10137)**,** 2346-2355.

KENNEY, M. J. & GANTA, C. K. 2014. Autonomic nervous system and immune system interactions. *Comprehensive Physiology,* 4 (3)**,** 1177-1200.

KING, D. E., EGAN, B. M., MAINOUS 3RD, A. G., & GEESEY, M. E. 2004. Elevation of C-reactive protein in people with prehypertension. *Journal of clinical hypertension (Greenwich, Conn.),* 6 (10)**,** 562-8.

KINTSURASHVILI, E., SHENOUDA, S., ONA, D., ONA, L., AHMAD, S., RAVID, K., GAVRAS, I. & GAVRAS, H. 2009. Hypertension in transgenic mice with brain-selective overexpression of the α_{2b}-adrenoceptor. *American Journal of Hypertension,* 22 (1)**,** 41-45.

KIRABO, A., FONTANA, V., DE FARIA, A. P. C., LOPERENA, R., GALINDO, C. L., WU, J., BIKINEYEVA, A. T., DIKALOV, S., XIAO, L., CHEN, W., SALEH, M. A., TROTT, D. W., ITANI, H. A., VINH, A., AMARNATH, V., AMARNATH, K., GUZIK, T. J., BERNSTEIN, K. E., SHEN, X. Z., SHYR, Y., CHEN, S. C., MERNAUGH, R. L., LAFFER, C. L., ELIJOVICH, F., DAVIES, S. S., MORENO, L. H., MADHUR, M. S., ROBERTS, J. & HARRISON, D. G. 2014. DC isoketal-modified proteins activate T cells and promote hypertension. *Journal of Clinical Investigation,* 124 (10)**,** 4642-4656.

KLARENBEEK, N. B., VAN DER KOOIJ, S. M., HUIZINGA, T. J. W., GOEKOOP-RUITERMAN, Y. P. M., HULSMANS, H. M. J., VAN KRUGTEN, M. V., SPEYER, I., DE VRIES-BOUWSTRA, J. K., KERSTENS, P. J. S. M., HUIZINGA, T. W. J., DIJKMANS, B. A. C. & ALLAART, C. F. 2010. Blood pressure changes in patients with recent-onset rheumatoid arthritis treated with four different treatment strategies: a post hoc analysis from the BeSt trial. *Annals of the Rheumatic Diseases,* 69 (7)**,** 1342-1345.

KORKOSZ, M., BUKOWSKA-STRAKOVA, K., SADIS, S., GRODZICKI, T. & SIEDLAR, M. 2012. Monoclonal antibodies against macrophage colony-stimulating factor diminish the number of circulating intermediate and nonclassical ($CD14^{++}CD16^{+}$/$CD14^{+}CD16^{++}$) monocytes in rheumatoid arthritis patient. *Blood,* 119 (22)**,** 5329-5330.

KRISTIANSEN, M., GRAVERSEN, J. H., JACOBSEN, C., SONNE, O., HOFFMAN, H. J., LAW, S. K. A. & MOESTRUP, S. K. 2001. Identification of the haemoglobin scavenger receptor. *Nature,* 409 (6817)**,** 198-201.

KRUM, H., SCHLAICH, M., WHITBOURN, R., SOBOTKA, P. A., SADOWSKI, J., BARTUS, K., KAPELAK, B., WALTON, A., SIEVERT, H., THAMBAR, S., ABRAHAM, W. T. & ESLER, M. 2009. Catheter-based renal sympathetic denervation for resistant hypertension: a multicentre safety and proof-of-principle cohort study. *Lancet,* 373 (9671)**,** 1275-1281.

LACERTE, P., BRUNET, A., EGARNES, B., DUCHENE, B., BROWN, J. P. & GOSSELIN, J. 2016. Overexpression of TLR2 and TLR9 on monocyte subsets of active rheumatoid arthritis patients contributes to enhance responsiveness to TLR agonists. *Arthritis Research & Therapy,* 18, 10.

LAKOSKI, S. G., CUSHMAN, M., SISCOVICK, D. S., BLUMENTHAL, R. S., PALMAS, W., BURKE, G. & HERRINGTON, D. M. 2011. The relationship between inflammation, obesity and risk for hypertension in the Multi-Ethnic Study of Atherosclerosis (MESA). *Journal of Human Hypertension,* 25 (2)**,** 73-79.

LARSEN, H. E., BARDSLEY, E. N., LEFKIMMIATIS, K. & PATERSON, D. J. 2016. Dysregulation of neuronal Ca^{2+} channel linked to heightened sympathetic phenotype in prohypertensive states. *Journal of Neuroscience,* 36 (33)**,** 8562-8573.

LEVICK, S. P., MURRAY, D. B., JANICKI, J. S. & BROWER, G. L. 2010. Sympathetic nervous system modulation of inflammation and remodeling in the hypertensive heart. *Hypertension,* 55 (2)**,** 270-276.

LI, D. & PATERSON, D. J. 2016. Cyclic nucleotide regulation of cardiac sympatho-vagal responsiveness. *Journal of Physiology,* 594 (14)**,** 3993-4008.

LI, D. & PATERSON, D. J. 2019. Pre-synaptic sympathetic calcium channels, cyclic nucleotide-coupled phosphodiesterases and cardiac excitability. *Seminars in Cell & Developmental Biology,* 94**,** 20-27.

LI, D., LEE, C. W., BUCKLER, K., PAREKH, A., HERRING, N. & PATERSON, D. J. 2012. Abnormal intracellular calcium homeostasis in sympathetic neurons from young prehypertensive rats. *Hypertension,* 59 (3)**,** 642-U282.

LI, D., NIKIFOROVA, N., LU, C. J., WANNOP, K., MCMENAMIN, M., LEE, C. W., BUCKLER, K. J. & PATERSON, D. J. 2013. Targeted neuronal nitric oxide synthase transgene delivery into stellate neurons reverses impaired intracellular calcium transients in prehypertensive rats. *Hypertension,* 61 (1)**,** 202-207.

LI, D., WANG, Q., ZHANG, Y., YANG, D. C., WEI, S. J., SU, L. A., YE, T. Q., ZHENG, X., PENG, K., ZHANG, L. P., ZHANG, Y. R., YANG, Y. J. & MA, S. T. 2016. A novel swine model of spontaneous hypertension with sympathetic hyperactivity responds well to renal denervation. *American Journal of Hypertension,* 29 (1)**,** 63-72.

LIM, S. S., VOS, T., FLAXMAN, A. D., DANAEI, G., SHIBUYA, K., ADAIR-ROHANI, H., AMANN, M., ANDERSON, H. R., ANDREWS, K. G., ARYEE, M., ATKINSON, C., BACCHUS, L. J., BAHALIM, A. N., BALAKRISHNAN, K., BALMES, J., BARKER-COLLO, S., BAXTER, A., BELL, M. L., BLORE, J. D., BLYTH, F., BONNER, C., BORGES, G., BOURNE, R., BOUSSINESQ, M., BRAUER, M., BROOKS, P., BRUCE, N. G., BRUNEKREEF, B., BRYAN-HANCOCK, C., BUCELLO, C., BUCHBINDER, R., BULL, F., BURNETT, R. T., BYERS, T. E., CALABRIA, B., CARAPETIS, J., CARNAHAN, E., CHAFE, Z., CHARLSON, F., CHEN, H., CHEN, J. S., CHENG, A. T.-A., CHILD, J. C., COHEN, A., COLSON, K. E., COWIE, B. C., DARBY, S., DARLING, S., DAVIS, A., DEGENHARDT, L., DENTENER, F., DES JARLAIS, D. C., DEVRIES, K., DHERANI, M., DING, E. L., DORSEY, E. R., DRISCOLL, T., EDMOND, K., ALI, S. E., ENGELL, R. E., ERWIN, P. J., FAHIMI, S., FALDER, G., FARZADFAR, F., FERRARI, A., FINUCANE, M. M., FLAXMAN, S., FOWKES, F. G. R., FREEDMAN, G., FREEMAN, M. K., GAKIDOU, E., GHOSH, S., GIOVANNUCCI, E., GMEL, G., GRAHAM, K., GRAINGER, R., GRANT, B., GUNNELL, D., GUTIERREZ, H. R., HALL, W., HOEK, H. W., HOGAN, A., HOSGOOD, H. D., III, HOY, D., HU, H., HUBBELL, B. J., HUTCHINGS, S. J., IBEANUSI, S. E., JACKLYN, G. L., JASRASARIA, R., JONAS, J. B., KAN, H., KANIS, J. A., KASSEBAUM, N., KAWAKAMI, N., KHANG, Y.-H., KHATIBZADEH, S., KHOO, J.-P., KOK, C., LADEN, F., et al. 2012. A comparative risk assessment of burden of disease and injury attributable to 67 risk factors and risk factor clusters in 21 regions, 1990-2010: a systematic analysis for the Global Burden of Disease Study 2010. *Lancet,* 380 (9859)**,** 2224-2260.

LIN, W. J., SHEN, P., SONG, Y. Q., HUANG, Y. & TU, S. H. 2021. Reactive oxygen species in autoimmune cells: function, differentiation, and metabolism. *Frontiers in Immunology,* 12, 635021.

LIU, B. Y., DHANDA, A., HIRANI, S., WILLIAMS, E. L., SEN, H. N., ESTRADA, F. M., LING, D., THOMPSON, I., CASADY, M., LI, Z. Y., SI, H., TUCKER, W., WEI, L., JAWAD, S., SURA, A., DAILEY, J., HANNES, S., CHEN, P., CHIEN, J. L., GORDON, S., LEE, R. W. J. & NUSSENBLATT, R. B. 2015. $CD14^{++}CD16^{+}$ monocytes are enriched by glucocorticoid treatment and are functionally attenuated in driving effector T Cell responses. *Journal of Immunology,* 194 (11)**,** 5150-5160.

LOHMEIER, T. E. & ILIESCU, R. 2015. The baroreflex as a long-term controller of arterial pressure. *Physiology,* 30 (2)**,** 148-158.

LOHMEIER, T. E., ILIESCU, R., DWYER, T. M., IRWIN, E. D., CATES, A. W. & ROSSING, M. A. 2010. Sustained suppression of sympathetic activity and arterial pressure during chronic activation of the carotid baroreflex. *American Journal of Physiology-Heart and Circulatory Physiology,* 299 (2)**,** H402-H409.

LOWN, B. & VERRIER, R. L. 1976. Neural activity and ventricular fibrillation. *New England Journal of Medicine,* 294 (21)**,** 1165-1170.

LU, C. J., HAO, G. L., NIKIFOROVA, N., LARSEN, H. E., LIU, K., CRABTREE, M. J., LI, D., HERRING, N. & PATERSON, D. J. 2015. CAPON modulates neuronal calcium handling and cardiac sympathetic neurotransmission during dysautonomia in hypertension. *Hypertension,* 65 (5)**,** 1288-1297.

MANCIA, G. & GRASSI, G. 2014. The autonomic nervous system and hypertension. *Circulation Research,* 114 (11)**,** 1804-1814.

MANCIA, G., DE BACKER, G., DOMINICZAK, A., CIFKOVA, R., FAGARD, R., GERMANO, G., GRASSI, G., HEAGERTY, A. M., KJELDSEN, S. E., LAURENT, S., NARKIEWICZ, K., RUILOPE, L., RYNKIEWICZ, A., SCHMIEDER, R. E., STRUIJKER BOUDIER, H. A. J., ZANCHETTI, A., VAHANIAN, A., CAMM, J., DE CATERINA, R., DEAN, V., DICKSTEIN, K., FILIPPATOS, G., FUNCK-BRENTANO, C., HELLEMANS, I., KRISTENSEN, S. D., MCGREGOR, K., SECHTEM, U., SILBER, S., TENDERA, M., WIDIMSKY, P., ZAMORANO, J. L., ERDINE, S., KIOWSKI, W., AGABITI-ROSEI, E., AMBROSIONI, E., LINDHOLM, L. H., MANOLIS, A., NILSSON, P. M., REDON, J., STRUIJKER-BOUDIER, H. A. J., VIIGIMAA, M., ADAMOPOULOS, S., BERTOMEU, V., CLEMENT, D., FARSANG, C., GAITA, D., LIP, G., MALLION, J. M., MANOLIS, A. J., O'BRIEN, E., PONIKOWSKI, P., RUSCHITZKA, F., TAMARGO, J., VAN ZWIETEN, P., WAEBER, B., WILLIAMS, B., THE EUROPEAN SOCITY OF HYPERTENSION & THE EUROPEAN SOCIETY OF CARDIOLOGY 2007. 2007 Guidelines for the management of arterial hypertension - The task force for the management of arterial hypertension of the European society of hypertension (ESH) and of the European society of cardiology (ESC). *European Heart Journal,* 28 (5)**,** 1462-1536.

MARZ, P., CHENG, J. G., GADIENT, R. A., PATTERSON, P. H., STOYAN, T., OTTEN, U. & ROSE-JOHN, S. 1998. Sympathetic neurons can produce and respond to interleukin 6. *Proceedings of the National Academy of Sciences of the United States of America,* 95 (6)**,** 3251-3256.

MASUO, K., MIKAMI, H., OGIHARA, T. & TUCK, M. L. 1997. Sympathetic nerve hyperactivity precedes hyperinsulinemia and blood pressure elevation in a young, nonobese Japanese population. *American Journal of Hypertension,* 10 (1)**,** 77-83.

MCCUBBIN, J. W., GREEN, J. H. & PAGE, I. H. 1956. Baroceptor function in chronic renal hypertension. *Circulation Research,* 4 (2)**,** 205-210.

MEHAFFEY, E. & MAJID, D. S. A. 2017. Tumor necrosis factor-α, kidney function, and hypertension. *American Journal of Physiology-Renal Physiology,* 313 (4)**,** F1005-F1008.

MERAH-MOURAH, F., COHEN, S. O., CHARRON, D., MOONEY, N. & HAZIOT, A. 2020. Identification of novel human monocyte subsets and evidence for phenotypic groups defined by interindividual variations of expression of adhesion molecules. *Scientific Reports,* 10, 4397.

MILDNER, A., SCHONHEIT, J., GILADI, A., DAVID, E., LARA-ASTIASO, D., LORENZO-VIVAS, E., PAUL, F., CHAPPELL-MAOR, L., PRILLER, J., LEUTZ, A., AMIT, I. & JUNG, S. 2017. Genomic characterization of murine monocytes reveals C/EBPβ transcription factor dependence of Ly6C$^-$ cells. *Immunity,* 46 (5)**,** 849-862.

MISHARIN, A. V., CUDA, C. M., SABER, R., TURNER, J. D., GIERUT, A. K., HAINES, G. K., BERDNIKOVS, S., FILER, A., CLARK, A. R., BUCKLEY, C. D., MUTLU, G. M., BUDINGER, G. R. S. & PERLMAN, H. 2014. Nonclassical Ly6C$^-$ monocytes drive the development of inflammatory arthritis in mice. *Cell Reports,* 9 (2)**,** 591-604.

MONTGOMERY, A. B., HOMAN, P. J., WINTER, D. & PERLMAN, H. R. 2019. Novel subclass of non-classical monocytes are crtical for inflammation. *Annals of the Rheumatic Diseases,* 78 (suppl. 1)**,** A36-A36.

MOREIRA, H. G., LAGE, R. L., MARTINEZ, D. G., FERREIRA-SANTOS, L., RONDON, M., NEGRAO, C. E. & NICOLAU, J. C. 2017. Sympathetic nervous activity in patients with acute coronary syndrome: a comparative study of inflammatory biomarkers. *Clinical Science,* 131 (9)**,** 883-895.

MUKHERJEE, R., BARMAN, P. K., THATOI, P. K., TRIPATHY, R., DAS, B. K. & RAVINDRAN, B. 2015. Non-Classical monocytes display inflammatory features: validation in sepsis and systemic lupus erythematous. *Scientific Reports,* 5, 13886.

MURRAY, P. J. 2017. Macrophage Polarization. *Annual Review of Physiology,* 79**,** 541-566.

MUSCHTER, D., GOTTL, C., VOGEL, M., GRIFKA, J., STRAUB, R. H. & GRASSEL, S. 2015. Reactivity of rat bone marrow-derived macrophages to neurotransmitter stimulation in the context of collagen II-induced arthritis. *Arthritis Research & Therapy,* 17, 169.

NARASIMHAN, P. B., MARCOVECCHIO, P., HAMERS, A. A. J. & HEDRICK, C. C. 2019. Nonclassical Monocytes in Health and Disease. *Annual Review of Immunology,* 37**,** 439-456.

NAZARETH, N., MAGRO, F., SILVA, J., DURO, M., GRACIO, D., COELHO, R., APPELBERG, R., MACEDO, G. & SARMENTO, A. 2014. Infliximab therapy increases the frequency of circulating $CD16^+$ monocytes and modifies macrophage cytokine response to bacterial infection. *Clinical and Experimental Immunology,* 177 (3)**,** 703-711.

NETEA, M. G., DOMINGUEZ-ANDRES, J., BARREIRO, L. B., CHAVAKIS, T., DIVANGAHI, M., FUCHS, E., JOOSTEN, L. A. B., VAN DER MEER, J. W. M., MHLANGA, M. M., MULDER, W. J. M., RIKSEN, N. P., SCHLITZER, A., SCHULTZE, J. L., BENN, C. S., SUN, J. S. C., XAVIER, R. J. & LATZ, E. 2020. Defining trained immunity and its role in health and disease. *Nature Reviews Immunology,* 20 (6)**,** 375-388.

NEWCOMBE, C. P., SHUCKSMITH, H. S. & SUFFERN, W. S. 1959. Sympathectomy for hypertension: follow-up of 212 pateints. *British Medical Journal,* 1 (5115)**,** 142-144.

National Insitute for Health and Care Excellence (NICE) 2019. Hypertension in adults: diagnosis and management [NICE Guideline No. 136]. Available at: https://www.nice.org.uk/guidance/ng136 [Accessed 01 June 2021].

NISHI, E. E., BERGAMASCHI, C. T. & CAMPOS, R. R. 2015. The crosstalk between the kidney and the central nervous system: the role of renal nerves in blood pressure regulation. *Experimental Physiology,* 100 (5)**,** 479-484.

NOMURA, K., HIYAMA, T. Y., SAKUTA, H., MATSUDA, T., LIN, C. H., KOBAYASHI, K., KUWAKI, T., TAKAHASHI, K., MATSUI, S. & NODA, M. 2019. $[Na^+]$ increases in body fluids sensed by central Na_x induce sympathetically mediated blood pressure elevations via H^+-dependent activation of ASIC1a. *Neuron,* 101 (1)**,** 60-75.

NOUBIAP, J. J., NANSSEU, J. R., NYAGA, U. F., SIME, P. S., FRANCIS, I. & BIGNA, J. J. 2019. Global prevalence of resistant hypertension: a meta-analysis of data from 3.2 million patients. *Heart,* 105 (2)**,** 98-105.

O'CALLAGHAN, E. L., HART, E. C., SIMS-WILLIAMS, H., JAVED, S., BURCHELL, A. E., PAPOUCHADO, M., TANK, J., HEUSSER, K., JORDAN, J., MENNE, J., HALLER, H., NIGHTINGALE, A. K., PATON, J. F. R. & PATEL, N. K. 2017. Chronic deep brain stimulation decreases blood pressure and sympathetic nerve activity in a drug- and device-resistant hypertensive patient. *Hypertension,* 69 (4)**,** 522-528.

OHMORI, M., KITOH, Y., HARADA, K., SUGIMOTO, K. & FUJIMURA, A. 2000. Polymorphonuclear leukocytes (PMNs) functions in SHR, L-NAME- and DOCA/salt-induced hypertensive rats. *Journal of Hypertension,* 18 (6)**,** 703-707.

OKAMOTO, K. & AOKI, K. 1963. Development of a strain of spontaneously hypertensive rats. *Japanese Circulation Journal,* 27**,** 282-293.

OKAMOTO, K., YAMORI, Y. & NAGAOKA, A. 1974. Establishment of stroke-prone spontaneously hypertensive rat (SHR). *Circulation Research,* 34/35**,** 143-153.

ONG, S.-M., HADADI, E., DANG, T.-M., YEAP, W.-H., TAN, C. T.-Y., NG, T.-P., LARBI, A. & WONG, S.-C. 2018. The pro-inflammatory phenotype of the human non-classical monocyte subset is attributed to senescence. *Cell Death & Disease,* 9, 266.

PATEL, A. A., ZHANG, Y., FULLERTON, J. N., BOELEN, L., RONGVAUX, A., MAINI, A. A., BIGLEY, V., FLAVELL, R. A., GILROY, D. W., ASQUITH, B., MACALLAN, D. & YONA, S. 2017. The fate and lifespan of human monocyte subsets in steady state and systemic inflammation. *Journal of Experimental Medicine,* 214 (7)**,** 1913-1923.

PATTERSON, S. W., PIPER, H. & STARLING, E. H. 1914. The regulation of the heart beat. *Journal of Physiology,* 48 (6)**,** 465-513.

PFEIFER, M. A., WEINBERG, C. R., COOK, D., BEST, J. D., REENAN, A. & HALTER, J. B. 1983. Differential changes of autonomic nervous system function with age in man. *American Journal of Medicine,* 75 (2)**,** 249-258.

PIENTA, K. J., MACHIELS, J. P., SCHRIJVERS, D., ALEKSEEV, B., SHKOLNIK, M., CRABB, S. J., LI, S., SEETHARAM, S., PUCHALSKI, T. A., TAKIMOTO, C., ELSAYED, Y.,

DAWKINS, F. & DE BONO, J. S. 2013. Phase 2 study of carlumab (CNTO 888), a human monoclonal antibody against CC-chemokine ligand 2 (CCL2), in metastatic castration-resistant prostate cancer. *Investigational New Drugs,* 31 (3)**,** 760-768.

PIRZGALSKA, R. M., SEIXAS, E., SEIDMAN, J. S., LINK, V. M., SANCHEZ, N. M., MAHU, I., MENDES, R., GRES, V., KUBASOVA, N., MORRIS, I., ARUS, B. A., LARABEE, C. M., VASQUES, M., TORTOSA, F., SOUSA, A. L., ANANDAN, S., TRANFIELD, E., HAHN, M. K., IANNACONE, M., SPANN, N. J., GLASS, C. K. & DOMINGOS, A. I. 2017. Sympathetic neuron-associated macrophages contribute to obesity by importing and metabolizing norepinephrine. *Nature Medicine,* 23 (11)**,** 1309-1318.

POITOU, C., DALMAS, E., RENOVATO, M., BENHAMO, V., HAJDUCH, F., ABDENNOUR, M., KAHN, J. F., VEYRIE, N., RIZKALLA, S., FRIDMAN, W. H., SAUTES-FRIDMAN, C., CLEMENT, K. & CREMER, I. 2011. $CD14^{dim}CD16^{+}$ and $CD14^{+}CD16^{+}$ Monocytes in Obesity and During Weight Loss Relationships With Fat Mass and Subclinical Atherosclerosis. *Arteriosclerosis Thrombosis and Vascular Biology,* 31 (10)**,** 2322-2330.

POWER, C. P., WANG, J. H., MANNING, B., KELL, M. R., AHERNE, N. F., WU, Q. D. & REDMOND, H. P. 2004. Bacterial lipoprotein delays apoptosis in human neutrophils through inhibition of caspase-3 activity: Regulatory roles for CD14 and TLR-2. *Journal of Immunology,* 173 (8)**,** 5229-5237.

PUCHNER, A., SAFERDING, V., BONELLI, M., MIKAMI, Y., HOFMANN, M., BRUNNER, J. S., CALDERA, M., GONCALVES-ALVES, E., BINDER, N. B., FISCHER, A., SIMADER, E., STEINER, C.-W., LEISS, H., HAYER, S., NIEDERREITER, B., KARONITSCH, T., KOENDERS, M. I., PODESSER, B. K., O'SHEA, J. J., MENCHE, J., SMOLEN, J. S., REDLICH, K. & BLUEML, S. 2018. Non-classical monocytes as mediators of tissue destruction in arthritis. *Annals of the Rheumatic Diseases,* 77 (10)**,** 1490-1497.

QI, Y., KIM, S., LEACH, D. D., LONG, S. J., HANDBERG, E. M., RODRIGUEZ, V., MANDLOI, A., RAIZADA, M. K. & PEPINE, C. J. 2016. Antihypertensive effects of minocycline are associated with improvement of inflammatory status in patients with treatment resistant hypertension. *Circulation,* 134 (suppl. 1).

QU, C. F., EDWARDS, E. W., TACKE, F., ANGELI, V., LLODRA, J., SANCHEZ-SCHMITZ, G., GARIN, A., HAQUE, N. S., PETERS, W., VAN ROOIJEN, N., SANCHEZ-TORRES, C., BROMBERG, J., CHARO, I. F., JUNG, S., LIRA, S. A. & RANDOLPH, G. J. 2004. Role of CCR8 and other chemokine pathways in the migration of monocyte-derived dendritic cells to lymph nodes. *Journal of Experimental Medicine,* 200 (10)**,** 1231-1241.

RADAEVA , O. A., SIMBIRTSEV, A. S. & KOSTINA, J. A. 2019. The change in the circadian rhythm of macrophage colony-stimulating factor content in the blood of patients with essential hypertension. *Cytokine X,* 1 (3) 100010.

RAMER, M. S., MURPHY, P. G., RICHARDSON, P. M. & BISBY, M. A. 1998. Spinal nerve lesion-induced mechanoallodynia and adrenergic sprouting in sensory ganglia are attenuated in interleukin-6 knockout mice. *Pain,* 78 (2)**,** 115-121.

REED, J. P. & HENDLEY, E. D. 1994. Blood cell changes in spontaneously hypertensive rats are not all associated with the hypertensive phenotype. *Journal of Hypertension,* 12 (4)**,** 391-399.

RIMOLDI, S. F., SCHERRER, U. & MESSERLI, F. H. 2014. Secondary arterial hypertension: when, who, and how to screen? *European Heart Journal,* 35 (19)**,** 1245-1254.

RIZZO, S., BASSO, C., TROOST, D., ARONICA, E., FRIGO, A. C., DRIESSEN, A. H. G., THIENE, G., WILDE, A. A. M. & VAN DER WAL, A. C. 2014. T-cell-mediated inflammatory activity in the stellate ganglia of patients with ion-channel disease and severe ventricular arrhythmias. *Circulation: Arrhythmia and Electrophysiology,* 7 (2)**,** 224-229.

RODRIGO, R., LIBUY, M., FELIU, F. & HASSON, D. 2013. Oxidative stress-related biomarkers in essential hypertension and ischemia-reperfusion myocardial damage. *Disease Markers***,** 35 (6), 773-790.

RODRIGUEZ-ITURBE, B., PONS, H. & JOHNSON, R. J. 2017. Role of the immune system in hypertension. *Physiological Reviews,* 97 (3)**,** 1127-1164.

ROEDERER , M. 2002. Compensation in flow cytometry. *Current Protocols in Cytometry***,** 22 (1), 1.14.1-1.14.20.

ROSSOL, M., KRAUS, S., PIERER, M., BAERWALD, C. & WAGNER, U. 2012. The $CD14^{bright}CD16^{+}$ monocyte subset is expanded in rheumatoid arthritis and promotes expansion of the Th17 cell population. *Arthritis and Rheumatism,* 64 (3)**,** 671-677.

ROSZER, T. 2015. Understanding the mysterious M2 macrophage through activation markers and effector mechanisms. *Mediators of Inflammation,* 2015, 816460.

ROTHMAN, A. M. K., MACFADYEN, J., THUREN, T., WEBB, A., HARRISON, D. G., GUZIK, T. J., LIBBY, P., GLYNN, R. J. & RIDKER, P. M. 2020. Effects of interleukin-1β inhibition on blood pressure, incident hypertension, and residual inflammatory risk: a secondary analysis of CANTOS. *Hypertension,* 75 (2)**,** 477-482.

RUBIO-NAVARRO, A., GUERRERO-HUE, M., MARTN-FERNANDEZ, B., CORTEGANO, I., OLIVARES-ALVARO, E., HERAS, N. D. L., ALIA, M., DE ANDRES, B., GASPAR, M. L., EGIDO, J. & MORENO, J. A. 2016. Phenotypic characterization of macrophages from rat kidney by flow cytometry. *Journal of Visualized Experiments*, 18 (116), 54599.

SAGVOLDEN, T., JOHANSEN, E. B., WOIEN, G., WALAAS, S. I., STORM-MATHISEN, J., BERGERSEN, L. H., HVALBY, O., JENSEN, V., AASE, H., RUSSELL, V. A., KILLEEN, P. R., DASBANERJEE, T., MIDDLETON, F. A. & FARAONE, S. V. 2009. The spontaneously hypertensive rat model of ADHD – the importance of selecting the appropriate reference strain. *Neuropharmacology,* 57 (7-8)**,** 619-626.

SAKATA, K., SHIROTANI, M., YOSHIDA, H. & KURATA, C. 1999. Cardiac sympathetic nervous system in early essential hypertension assessed by I-123-MIBG. *Journal of Nuclear Medicine,* 40 (1)**,** 6-11.

SANDOO, A., PANOULAS, V. F., TOMS, T. E., SMITH, J. P., STAVROPOULOS-KALINOGLOU, A., METSIOS, G. S., GASPARYAN, A. Y., CARROLL, D., VAN ZANTEN, J. J. C. S. V. & KITAS, G. D. 2011. Anti-TNF alpha therapy may lead to blood pressure reductions through improved endothelium-dependent microvascular function in patients with rheumatoid arthritis. *Journal of Human Hypertension,* 25 (11)**,** 699-702.

SANTISTEBAN, M. M., AHMARI, N., CARVAJAL, J. M., ZINGLER, M. B., QI, Y. F., KIM, S., JOSEPH, J., GARCIA-PEREIRA, F., JOHNSON, R. D., SHENOY, V., RAIZADA, M. K. & ZUBCEVIC, J. 2015. Involvement of bone marrow cells and neuroinflammation in hypertension. *Circulation Research,* 117 (2)**,** 178-191.

SCHEFFERS, I. J. M., KROON, A. A., SCHMIDLI, J., JORDAN, J., TORDOIR, J. J. M., MOHAUPT, M. G., LUFT, F. C., HALLER, H., MENNE, J., ENGELI, S., CERAL, J., ECKERT, S., ERGLIS, A., NARKIEWICZ, K., PHILIPP, T. & DE LEEUW, P. W. 2010. Novel Baroreflex Activation Therapy in Resistant Hypertension Results of a European Multi-Center Feasibility Study. *Journal of the American College of Cardiology,* 56 (15)**,** 1254-1258.

SCHEIERMANN, C., KUNISAKI, Y., LUCAS, D., CHOW, A., JANG, J. E., ZHANG, D., HASHIMOTO, D., MERAD, M. & FRENETTE, P. S. 2012. Adrenergic nerves govern circadian leukocyte recruitment to tissues. *Immunity,* 37 (2)**,** 290-301.

SCHLAGER, G. & SIDES, J. 1997. Characterization of hypertensive and hypotensive inbred strains of mice. *Laboratory Animal Science,* 47 (3)**,** 288-292.

SCHMIDSCHONBEIN, G. W., SEIFFGE, D., DELANO, F. A., SHEN, K. & ZWEIFACH, B. W. 1991. Leukocyte counts and activation in spontanesouly hypertensive and normotensive rats. *Hypertension,* 17 (3)**,** 323-330.

SCHOLZ, J. & WOOLF, C. J. 2007. The neuropathic pain triad: neurons, immune cells and glia. *Nature Neuroscience,* 10 (11)**,** 1361-1368.

SENGUPTA, P., 2013. The laboratory rat: relating its age with human's. *International Journal of Preventative Medicine*, 4 (6), 624-630.

SESSO, H. D., BURING, J. E., RIFAI, N., BLAKE, G. J., GAZIANO, J. M. & RIDKER, P. M. 2003. C-reactive protein and the risk of developing hypertension. *Journal of the American Medical Association,* 290 (22)**,** 2945-2951.

SHANKS, J., HERRING, N., JOHNSON, E., LIU, K., LI, D. & PATERSON, D. J. 2017. Overexpression of sarcoendoplasmic reticulum calcium ATPase 2a promotes cardiac sympathetic neurotransmission via abnormal endoplasmic reticulum and mitochondria Ca^{2+} regulation. *Hypertension,* 69 (4)**,** 625-632.

SHANKS, J., MANE, S., RYAN, R. & PATERSON, D. J. 2013a. Ganglion-specific impairment of the norepinephrine transporter in the hypertensive rat. *Hypertension,* 61 (1)**,** 187-193.

SHANKS, J., MANOU-STATHOPOULOU, S., LU, C. J., LI, D., PATERSON, D. J. & HERRING, N. 2013b. Cardiac sympathetic dysfunction in the prehypertensive spontaneously hypertensive rat. *American Journal of Physiology-Heart and Circulatory Physiology,* 305 (7)**,** H980-H986.

SHAPIRO, H. M. 2003. *Practical Flow Cytometry, 4th edition*. Hoboken, NJ, US: John Wiley & Sons Inc.

SHI, C. & PAMER, E. G. 2011. Monocyte recruitment during infection and inflammation. *Nature Reviews Immunology,* 11 (11)**,** 762-774.

SHI, H. K., GUO, H. C., LIU, H. Y., ZHANG, Z. L., HU, M. Y., ZHANG, Y. & LI, Q. 2020. Cannabinoid type 2 receptor agonist JWH133 decreases blood pressure of spontaneously hypertensive rats through relieving inflammation in the rostral ventrolateral medulla of the brain. *Journal of Hypertension,* 38 (5)**,** 886-895.

SHI, P., GROBE, J. L., DESLAND, F. A., ZHOU, G. N., SHEN, X. Z., SHAN, Z. Y., LIU, M., RAIZADA, M. K. & SUMNERS, C. 2014. Direct pro-inflammatory effects of prorenin on microglia. *Plos One,* 9 (10), e92937.

SHI, Z., GAN, X. B., FAN, Z. D., ZHANG, F., ZHOU, Y. B., GAO, X. Y., DE, W. & ZHU, G. Q. 2011. Inflammatory cytokines in paraventricular nucleus modulate sympathetic activity and cardiac sympathetic afferent reflex in rats. *Acta Physiologica,* 203 (2)**,** 289-297.

SINGH, B., MOODLEY, J., ALLOPI, L. & CASSIMJEE, H. M. 2006. Horner syndrome after sympathectomy in the thoracoscopic era. *Surgical Laparoscopy Endoscopy & Percutaneous Techniques,* 16 (4)**,** 222-225.

SINGH, M. V., CHAPLEAU, M. W., HARWANI, S. C. & ABBOUD, F. M. 2014. The immune system and hypertension. *Immunologic Research,* 59 (1-3)**,** 243-253.

SMILJANOVIC, B., RADZIKOWSKA, A., KUCA-WARNAWIN, E., KUROWSKA, W., GRUN, J. R., STUHLMULLER, B., BONIN, M., SCHULTE-WREDE, U., SORENSEN, T., KYOGOKU, C., BRUNS, A., HERMANN, S., OHRNDORF, S., AUPPERLE, K., BACKHAUS, M., BURMESTER, G. R., RADBRUCH, A., GRUTZKAU, A., MASLINSKI, W. & HAUPL, T. 2018. Monocyte alterations in rheumatoid arthritis are dominated by preterm release from bone marrow and prominent triggering in the joint. *Annals of the Rheumatic Diseases,* 77 (2)**,** 300-308.

SMITH, G. D., LAWLOR, D. A., HARBORD, R., TIMPSON, N., RUMLEY, A., LOWE, G. D. O., DAY, I. N. M. & EBRAHIM, S. 2005. Association of C-reactive protein with blood pressure and hypertension: life course confounding and Mendelian randomization tests of causality. *Arteriosclerosis Thrombosis and Vascular Biology,* 25 (5)**,** 1051-1056.

SMITH, P. A., GRAHAM, L. N., MACKINTOSH, A. F., STOKER, J. B. & MARY, D. 2004. Relationship between central sympathetic activity and stages of human hypertension. *American Journal of Hypertension,* 17 (3)**,** 217-222.

SOEHNLEIN, O., STEFFENS, S., HIDALGO, A. & WEBER, C. 2017. Neutrophils as protagonists and targets in chronic inflammation. *Nature Reviews Immunology,* 17 (4)**,** 248-261.

SOLAK, Y., AFSAR, B., VAZIRI, N. D., ASLAN, G., YALCIN, C. E., COVIC, A. & KANBAY, M. 2016. Hypertension as an autoimmune and inflammatory disease. *Hypertension Research,* 39 (8)**,** 567-573.

SPITS, H., ARTIS, D., COLONNA, M., DIEFENBACH, A., DI SANTO, J. P., EBERL, G., KOYASU, S., LOCKSLEY, R. M., MCKENZIE, A. N. J., MEBIUS, R. E., POWRIE, F. & VIVIER, E. 2013. Innate lymphoid cells – a proposal for uniform nomenclature. *Nature Reviews Immunology,* 13 (2)**,** 145-149.

STRAUB, R. H., STEBNER, K., HARLE, P., KEES, F., FALK, W. & SCHOLMERICH, J. 2005. Key role of the sympathetic microenvironment for the interplay of tumour necrosis factor and interleukin 6 in normal but not in inflamed mouse colon mucosa. *Gut,* 54 (8)**,** 1098-1106.

SUN, L., GAO, Y.-H., TIAN, D.-K., ZHENG, J.-P., ZHU, C.-Y., KE, Y. & BIAN, K. 2006. Inflammation of different tissues in spontaneously hypertensive rat. *Acta Physiologica Sinica,* 58 (4)**,** 318-323.

SVERRISDOTTIR, Y. B., MARTIN, S. C., HADJIPAVLOU, G., KENT, A. R., PATERSON, D. J., FITZGERALD, J. J. & GREEN, A. L. 2020. Human dorsal root ganglion stimulation reduces

sympathetic outflow and long-term blood pressure. *JACC: Basic to Translational Science,* 5 (10)**,** 973-985.

TAK, T., DRYLEWICZ, J., CONEMANS, L., DE BOER, R. J., KOENDERMAN, L., BORGHANS, J. A. M. & TESSELAAR, K. 2017. Circulatory and maturation kinetics of human monocyte subsets *in vivo*. *Blood,* 130 (12)**,** 1474-1477.

TAK, T., VAN GROENENDAEL, R., PICKKERS, P. & KOENDERMAN, L. 2017. Monocyte subsets are differentially lost from the circulation during acute inflammation induced by human experimental endotoxemia. *Journal of Innate Immunity,* 9 (5)**,** 464-474.

TAKESUE, K., KISHI, T., HIROOKA, Y. & SUNAGAWA, K. 2017. Activation of microglia within paraventricular nucleus of hypothalamus is NOT involved in maintenance of established hypertension. *Journal of Cardiology,* 69 (1)**,** 84-88.

TAN, X., JIAO, P. L., WANG, Y. K., WU, Z. T., ZENG, X. R., LI, M. L. & WANG, W. Z. 2017. The phosphoinositide-3 kinase signaling is involved in neuroinflammation in hypertensive rats. *CNS Neuroscience & Therapeutics,* 23 (4)**,** 350-359.

THIESEN, S., JANCIAUSKIENE, S., URONEN-HANSSON, H., AGACE, W., HOGERKORP, C. M., SPEE, P., HAKANSSON, K. & GRIP, O. 2014. $CD14^{hi}$ $HLA\text{-}DR^{dim}$ macrophages, with a resemblance to classical blood monocytes, dominate inflamed mucosa in Crohn's disease. *Journal of Leukocyte Biology,* 95 (3)**,** 531-541.

TIAN, Y., WITTWER, E. D., KAPA, S., MCLEOD, C. J., XIAO, P. L., NOSEWORTHY, P. A., MULPURU, S. K., DESHMUKH, A. J., LEE, H. C., ACKERMAN, M. J., ASIRVATHAM, S. J., MUNGER, T. M., LIU, X. P., FRIEDMAN, P. A. & CHA, Y. M. 2019. Effective use of percutaneous stellate ganglion blockade in patients with electrical storm. *Circulation: Arrhythmia and Electrophysiology,* 12 (9), e007118.

TSIEN, R. Y. 1981. A non-disruptive technique for loading calcium buffers and indicators into cells. *Nature,* 290 (5806)**,** 527-528.

UEYAMA, T., HAMADA, M., HANO, T., NISHIO, I., MASUYAMA, Y. & FURUKAWA, S. 1992. Increased nerve growth factor levels in spontaneously hypertensive rats. *Journal of Hypertension,* 10 (3)**,** 215-219.

VAN RHEE, F., CASPER, C., VOORHEES, P. M., FAYAD, L. E., DE VELDE, H. V., VERMEULEN, J., QIN, X., QI, M., TROMP, B. & KURZROCK, R. 2015. A phase 2, open-label, multicenter study of the long-term safety of siltuximab (an anti-interleukin-6 monoclonal antibody) in patients with multicentric Castleman disease. *Oncotarget,* 6 (30)**,** 30408-30419.

VASEGHI, M., SALAVATIAN, S., RAJENDRAN, P. S., YAGISHITA, D., WOODWARD, W. R., HAMON, D., YAMAKAWA, K., IRIE, T., HABECKER, B. A. & SHIVKUMAR, K. 2017. Parasympathetic dysfunction and antiarrhythmic effect of vagal nerve stimulation following myocardial infarction. *JCI Insight*, 2 (16), e86715.

VONGPATANASIN, W., KARIO, K., ATLAS, S. A. & VICTOR, R. G. 2011. Central sympatholytic drugs. *Journal of Clinical Hypertension,* 13 (9)**,** 658-661.

WAKI, H., GOURAUD, S. S., MAEDA, M. & PATON, J. F. R. 2010. Evidence of specific inflammatory condition in nucleus tractus solitarii of spontaneously hypertensive rats. *Experimental Physiology,* 95 (5)**,** 595-600.

WANG, Y. Z., ZHAO, M., LIU, S. Y., GUO, J., LU, Y. R., CHENG, J. Q. & LIU, J. P. 2020. Macrophage-derived extracellular vesicles: diverse mediators of pathology and therapeutics in multiple diseases. *Cell Death & Disease,* 11 (10), 924.

WEINER, L. M., LI, W., HOLMES, M., CATALANO, R. B., DOVNARSKY, M., PADAVIC, K. & ALPAUGH, R. K. 1994. Phase I trial of recombinant macrophage-colony stimulating factor and recombinant gamma-interferon: toxicity, monocytosis, and clinical effects. *Cancer Research,* 54 (15)**,** 4084-4090.

WERNLI, G., HASAN, W., BHATTACHERJEE, A., VAN ROOIJEN, N. & SMITH, P. G. 2009. Macrophage depletion suppresses sympathetic hyperinnervation following myocardial infarction. *Basic Research in Cardiology,* 104 (6)**,** 681-693.

WILLIAMS, B., LACY, P. S., THOM, S. M., CRUICKSHANK, K., STANTON, A., COLLIER, D., HUGHES, A. D., THURSTON, H., THE CAFE INVESTIGATORS & THE CAFE STEERING COMMITTEE AND WRITING COMMITTEE 2006. Differential impact of blood pressure-lowering drugs on central aortic pressure and clinical outcomes: principal

results of the Conduit Artery Function Evaluation (CAFE) study. *Circulation,* 113 (9)**,** 1213-1225.

WIYSONGE, C. S., BRADLEY, H. A., VOLMINK, J., MAYOSI, B. M. & OPIE, L. H. 2017. Beta-blockers for hypertension. *Cochrane Database of Systematic Reviews*, 1 (1), CD002003.

WOFFORD, M. R., ANDERSON, D. C., BROWN, C. A., JONES, D. W., MILLER, M. E. & HALL, J. E. 2001. Antihypertensive effect of alpha- and beta-adrenergic blockade in obese and lean hypertensive subjects. *American Journal of Hypertension,* 14 (7 pt. 1)**,** 694-698.

WOLF, A. A., YANEZ, A., BARMAN, P. K. & GOODRIDGE, H. S. 2019. The ontogeny of monocyte subsets. *Frontiers in Immunology,* 10, 1642.

WONG, K. L., TAI, J. J. Y., WONG, W. C., HAN, H., SEM, X., YEAP, W. H., KOURILSKY, P. & WONG, S. C. 2011. Gene expression profiling reveals the defining features of the classical, intermediate, and nonclassical human monocyte subsets. *Blood,* 118 (5)**,** e15-e30.

WORLD HEALTH ORGANIZATION 2014. Global status report on noncommunicable diseases 2014. WHO Press: Geneva, Switzerland.

WU, K. L. H., CHAN, S. H. H. & CHAN, J. Y. H. 2012. Neuroinflammation and oxidative stress in rostral ventrolateral medulla contribute to neurogenic hypertension induced by systemic inflammation. *Journal of Neuroinflammation,* 9, 212.

XIA, Y., HU, H. Z., LIU, S. M., REN, J., ZAFIROV, D. H. & WOOD, J. D. 1999. IL-1β and IL-6 excite neurons and suppress nicotinic and noradrenergic neurotransmission in guinea pig enteric nervous system. *Journal of Clinical Investigation,* 103 (9)**,** 1309-1316.

YAMADA, Y., MIYAJIMA, E., TOCHIKUBO, O., MATSUKAWA, T., SHIONOIRI, H., ISHII, M. & KANEKO, Y. 1988. Impaired baroreflex changes in muscle sympathetic nerve activity in adolescents who have a family history of essential hypertension. *Journal of Hypertension,* 6 (4)**,** S525-S528.

YOON, B. R., YOO, S. J., CHOI, Y. H., CHUNG, Y. H., KIM, J., YOO, I. S., KANG, S. W. & LEE, W. W. 2014. Functional phenotype of synovial monocytes modulating inflammatory T-cell responses in rheumatoid arthritis (RA). *Plos One,* 9 (10), e109775.

YOSHIDA, S., TAKEUCHI, T., KOTANI, T., YAMAMOTO, N., HATA, K., NAGAI, K., SHODA, T., TAKAI, S., MAKINO, S. & HANAFUSA, T. 2014. Infliximab, a TNF-α inhibitor, reduces 24-h ambulatory blood pressure in rheumatoid arthritis patients. *Journal of Human Hypertension,* 28 (3), 165-169.

YRLID, U., JENKINS, C. D. & MACPHERSON, G. G. 2006. Relationships between distinct blood monocyte subsets and migrating intestinal lymph dendritic cells in vivo under steady-state conditions. *Journal of Immunology,* 176 (7)**,** 4155-4162.

YU, X., YANG, Z. & YU, M. L. 2010. Correlation of tumor necrosis factor alpha and interleukin 6 with hypertensive renal damage. *Renal Failure,* 32 (4)**,** 475-479.

ZALBA, G., BEAUMONT, F. J., SAN JOSE, G., FORTUNO, A., FORTUNO, M. A., ETAYO, J. C. & DIEZ, J. 2000. Vascular NADH/NADPH oxidase is involved in enhanced superoxide production in spontaneously hypertensive rats. *Hypertension,* 35 (5)**,** 1055-1061.

ZHAO, Q. W., HONG, D. S., ZHANG, Y., SANG, Y. L., YANG, Z. H. & ZHANG, X. G. 2015. Association between anti-TNF therapy for rheumatoid arthritis and hypertension: a meta-analysis of randomized controlled trials. *Medicine,* 94 (14), e731.

ZHOU, B., DANAEI, G., STEVENS, G. A., BIXBY, H., TADDEI, C., CARRILLO-LARCO, R. M., SOLOMON, B., RILEY, L. M., DI CESARE, M., IURILLI, M. L. C., RODRIGUEZ-MARTINEZ, A., ZHU, A., HAJIFATHALIAN, K., AMUZU, A., BANEGAS, J. R., BENNETT, J. E., CAMERON, C., CHO, Y., CLARKE, J., CRAIG, C. L., CRUZ, J. J., GATES, L., GIAMPAOLI, S., GREGG, E. W., HARDY, R., HAYES, A. J., IKEDA, N., JACKSON, R. T., JENNINGS, G., JOFFRES, M., KHANG, Y.-H., KOSKINEN, S., KUH, D., KUJALA, U. M., LAATIKAINEN, T., LEHTIMAKI, T., LOPEZ-GARCIA, E., LUNDQVIST, A., MAGGI, S., MAGLIANO, D. J., MANN, J. I., MCLEAN, R. M., MCLEAN, S. B., MILLER, J. C., MORGAN, K., NEUHAUSER, H. K., NIIRANEN, T. J., NOALE, M., OH, K., PALMIERI, L., PANZA, F., PARNELL, W. R., PELTONEN, M., RAITAKARI, O., RODRIGUEZ-ARTALEJO, F., ROY, J. G. R., SALOMAA, V., SARGANAS, G., SERVAIS, J., SHAW, J. E., SHIBUYA, K., SOLFRIZZI, V., STAVRESKI, B., TAN, E. J., TURLEY, M. L., VANUZZO, D., VIIKARI-JUNTURA, E.,

WEERASEKERA, D., EZZATI, M. & THE NCD RISK FACTOR COLLABORATION 2019. Long-term and recent trends in hypertension awareness, treatment, and control in 12 high-income countries: an analysis of 123 nationally representative surveys. *Lancet,* 394 (10199)**,** 639-651.

ZHOU, R., YAZDI, A. S., MENU, P. & TSCHOPP, J. 2011. A role for mitochondria in NLRP3 inflammasome activation. *Nature,* 469 (7329)**,** 221-225.

ZHOU, S. M., CHEN, L. S., MIYAUCHI, Y., MIYAUCHI, M., KAR, S., KANGAVARI, S., FISHBEIN, M. C., SHARIFI, B. & CHEN, P. S. 2004. Mechanisms of cardiac nerve sprouting after myocardial infarction in dogs. *Circulation Research,* 95 (1)**,** 76-83.

ZHU, H. Q., HU, F. L., SUN, X. L., ZHANG, X. Y., ZHU, L., LIU, X., LI, X., XU, L. L., SHI, L. J., GAN, Y. Z. & SU, Y. 2016. $CD16^{+}$ monocyte subset was enriched and functionally exacerbated in driving T-cell activation and B-cell response in systemic lupus erythematosus. *Frontiers in Immunology,* 7, 512.

ZUBCEVIC, J., JUN, J. Y., KIM, S., PEREZ, P. D., AFZAL, A., SHAN, Z., LI, W., SANTISTEBAN, M. M., YUAN, W., FEBO, M., MOCCO, J., FENG, Y., SCOTT, E., BAEKEY, D. M. & RAIZADA, M. K. 2014. Altered inflammatory response is associated with an impaired autonomic input to the bone marrow in the spontaneously hypertensive rat. *Hypertension,* 63 (3)**,** 542-550.